A geophysical survey (TEM; ERT) of the Punata alluvial fan, Bolivia

Joakim Mårdh

**Dissertations in Geology at Lund University,
Master's thesis, no 496
(45 hp/ECTS credits)**

**Department of Geology
Lund University
2017**

This study has been carried out within the framework of the Minor Field Studies (MFS) Scholarship Programme, which is funded by the Swedish International Development Cooperation Agency, Sida.

The MFS Scholarship Programme offers Swedish university students an opportunity to carry out two months' field work in a developing country resulting in a graduation thesis work, a Master's dissertation or a similar in-depth study. These studies are primarily conducted within subject areas that are important from an international development perspective and in a country supported by Swedish international development assistance.

The main purpose of the MFS Programme is to enhance Swedish university students' knowledge and understanding of developing countries and their problems. An MFS should provide the student with initial experience of conditions in such a country. A further purpose is to widen the human resource base for recruitment into international co-operation. Further information can be reached at the following internet address: http://www.tg.lth.se/mfs

The responsibility for the accuracy of the information presented in this MFS report rests entirely with the authors and their supervisors.

Gerhard Barmen
Local MFS Programme Officer

A geophysical survey (TEM; ERT) of the Punata alluvial fan, Bolivia

Master's thesis
Joakim Mårdh

Department of Geology
Lund University
2017

Contents

Cover Picture: Picture taken on a typical sunny day in the field taken while waiting for the measurement to finish

A geophysical survey (TEM; ERT) of the Punata alluvial fan, Bolivia

JOAKIM MÅRDH

Abstract:
The Punata alluvial fan, situated in central Bolivia (Valle Alto) between the Altiplano and the lowlands, is an important aquifer for the local rural population. Due to rapid development and population growth in the area, the demand for fresh water has increased in recent year. In combination with decreasing annual rainfall, in the already semi-arid climate, the groundwater level is steadily sinking and thus depleting shallow wells. The current solution is to drill new, deeper, wells and continue to overexploit the reservoir in an unsustainable manner. In order to map the aquifer geometry this paper presents a TEM (Transient Electromagnetic Method) survey with the aim to find the sediment – bedrock boundary, which is thought be at >300 m depth. The survey acts as a complement to the previously conducted ERT (Electrical Resistivity Tomography) surveys in the area.

Valle Alto is a tectonic basin, in the department of Cochabamba, with predominantly Palaeozoic sedimentary bedrock (Ordovician and Silurian) and minor Mesozoic formations from the late Cretaceous. The lithology varies between shales, siltstones and sandstones, deposited in a marine environment during the Palaeozoic and in a continental rift basin during the Mesozoic. Valle Alto is the result of tectonic activity during the Pliocene, which yielded an enclosed lake in the area. An unquantified amount of lacustrine clay was deposited in the basin before the lake was drained due to renewed tectonic activity. On top of the clay there is interfingering alluvial fans and colluvial deposits of different generations, with the Punata alluvial fan being one of them.

In an attempt to achieve adequate depth of penetration, TEM was used in this survey. The method utilizes the fact that an electrical field always yields a proportional magnetic field and vice versa. In short, an electrical pulse is sent through transmitter loop and then abruptly turned off. This induces an electromotive force which propagate into the ground and in turn induces currents proportional to the resistivity. The currents yield a secondary magnetic field which can be measured by receiver coils, and then used to create resistivity models of the subsurface.

Unfortunately, the lacustrine clay restricted the depth penetration to 90 – 200 m and the models did not reach the bedrock boundary. The survey did however present a few other interesting features such as a distinct thin layer with very low resistivity, interpreted to be brine, on top of the alluvium – clay boundary. There might also be a fault line beneath the fan, but the results of the survey are inconclusive and further studies of the tectonic regime necessary in order to verify or disregard the hypothesis.

Joakim Mårdh, Department of Geology, Lund University, Sölvegatan 12, SE-223 62 Lund, Sweden. E-mail: ada10jm1@student.lu.se

En geofysisk undersökning (TEM; ERT) av Punata alluvialkon, Bolivia

JOAKIM MÅRDH

Sammanfattning:
Punata alluvialkon ligger i centrala Bolivia (Valle Alto) i ett område mellan Altiplanot och lågländerna. Det är en viktig grundvattenreservoar för den lokala landsortsbefolkningen och pga. utveckling samt befolkningsökning i området har efterfrågan på färskvatten ökat de senaste åren. Tillsammans med minskande årlig nederbörd, i ett redan halvtorrt (semi-arid) klimat, sjunker grundvattennivån stadigt och torrlägger grunda brunnar. Den nuvarande lösningen är att borra nya, djupare brunnar och sedan fortsätta att överexploatera grundvattentillgången på ett ohållbart vis. För att få en bild av akvifärens geometri presenterar denna uppsats en TEM-undersökning (Transient Elektromagnetisk Metod), med målet att kartlägga gränsen mellan lösa sediment och berggrund som tros ligga på >300 m djup. Undersökningen är ämnad att komplettera tidigare ERT-undersökningar (Elektrisk Resistivitetstomografi) i området.

Valle Alto är en tektonisk bassäng i "department of Cochabamba", med främst paleozoisk sedimentär berggrund (Ordovicium and Silur) och sporadiska mesozoiska formationer från sen Krita. Litologin varierar mellan lerskiffer, siltsten och sandsten, som är avsatta i en marin miljö under Paleozoikum och i en kontinental riftbassäng under Mesozoikum. Valle Alto uppkom under Pliocen pga. tektonisk aktivitet under Pliocen och en sluten sjö bildades i bassängen. En okänd mängd lakustrin lera avsattes i området innan sjön tappades som resultat av ny tektonisk aktivitet. Ovanpå leran ligger olika generationer alluvialkoner och kolluviala sediment om vartannat, där Punata alluvialkon är en av dem.

I ett försök att uppnå tillräckligt penetrationsdjup har TEM används i denna undersökning. Metoden använder sig av det faktum att elektriska fält alltid förekommer tillsammans med ett proportionellt magnetiskt fält och vice versa. Metoden bygger i korthet på att en kort elektrisk puls skickas i en sändarslinga och sedan abrupts stängs av. Det resulterar i en elektromotorisk kraft som sprider sig i marken och inducerar en ström som är proportionell mot resistiviteten. Strömmen ger i sin tur ett sekundärt magnetfält som kan mätas med hjälp av mottagarslingor, och sedan användas för att skapa resistivitetsmodeller av marken.

Den lakustrina leran begränsade tyvärr djupnedträngningen till 90 – 200 m och modellerna nådde inte berggrundsytan. Undersökningen påvisade däremot ett par andra intressanta saker, såsom ett tydligt tunt lager med väldigt låg resistivitet, vilket är tolkat som saltlake ovanpå alluvium – lergränsen. Där finns även indikationer på en förkastning under konen, men resultaten från undersökningen är inte tillräckliga för en säker slutsats och fortsatta studier av den tektoniska historien i området är nödvändig för att verifiera eller förkasta hypotesen.

Joakim Mårdh, Geologiska institutionen, Lunds Universitet, Sölvegatan 12, 223 62 Lund, Sverige. E-post: ada10jm1@student.lu.se

1 Introduction

This paper is written as a master's thesis at the Department of Geology, in collaboration with Engineering Geology at Lund University. It is a part of a larger PhD project by Andres Gonzales, which aims to map the aquifer properties of the Punata alluvial fan in Valle Alto, Bolivia. In this particular survey the objective was to find the depth of the sediment – bedrock boundary in the fan, using a Transient Electromagnetic Method (TEM). The depth is currently unknown but according to GEOBOL (1983), which is the geological survey of Bolivia (Servicio Geológico de Bolivia), it is presumed to be >300 m. It is imperative to know the vertical location of the basement in order to accurately evaluate the hydrogeological properties of the aquifer. As the area is dominated by a rural population that are dependent on the groundwater from the reservoir, for irrigation of their farmland, a proper hydrogeological model of the fan is important in order to achieve sustainable water management. Previous studies in the area include VES (Vertical Electrical Sounding) by UNDP-GEOBOL (1978), regional Landsat TM imaging for mapping of salinity-alkalinity of soil surfaces by Metternicht & Zinck (1996), borehole inventory by Centro Agua (2012) and ERT (Electrical Resistivity Tomography) and hydrochemistry surveys by Gonzales et al. (2016;2017a). Renner & Velasco (2000) has made a detailed geologic description of Valle Central (Central Valley) which is an adjacent valley, where the Cochabamba urban area is situated, and which belongs to the same tectonic regime.

The ERT surveys, as carried out in the area, do not have adequate depth of penetration to find the bedrock surface which is why the method used in this survey is TEM. In short it is a method that utilize short pulses of electrical currents, in a closed loop, to induce a magnetic field and an electromotive force, which propagates in the subsurface and induces eddy currents proportional to the resistivity. The eddy currents induce a proportional secondary magnetic field which can be measured using receiver coils and the decay time of the signal depends on the geological properties in the ground. Modelling of the subsurface is possible by running numerical inversions on the retrieved signal data. Compared to ERT, a TEM sounding usually has great depth of investigation, also referred to as DOI, but it varies depending on geologic material. Another advantage of TEM is that it is point based, instead of requiring long profile layouts, which makes it fast to deploy and a measurement usually do not take more than ~10 minutes. The point based methodology allows for great flexibility in the survey setup, whether the aim is to make profiles or grids over larger areas.

1.1 Background

Since the 1970's the population and agricultural growth in the Punata-Cliza valley has been rapid, resulting in an increased demand for fresh water. Most of the water is needed for irrigation during the dry season, as the valley has a semi-arid climate, but also for human consumption. This has led to a rampant development of new wells being bored in the Punata alluvial fan. An inventory of known wells was made by Centro Agua (2012) and in 1998 there were 108 boreholes in the area. In 2012 the number had inflated to 310 boreholes (Fig 1) with an estimation of roughly 100 new boreholes being made every 5 years. There is no more recent inventory but in 2015 the estimated amount of boreholes was 355 (Gonzales et al., 2016). This overexploitation has consequently lead to continuous lowering of the groundwater level and when a shallow well runs dry the response has predominantly been to drill a new deeper one close by. Over the last decades Centro Agua (2012) recorded a trend of increasing depths with newer wells reaching as deep as 140 m. This type of uncontrolled drilling is a big issue in the relatively poor rural community of Punata,
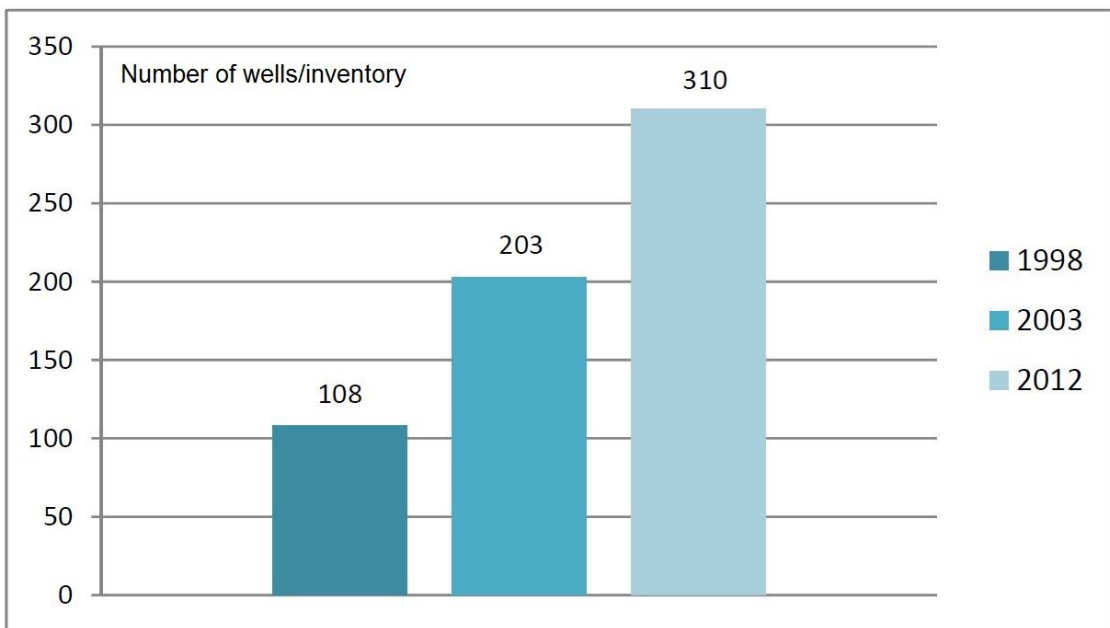

Fig 1. Histogram of well count by Centro Agua at University Mayor de San Simon (Modified from Centro Agua, 2012).
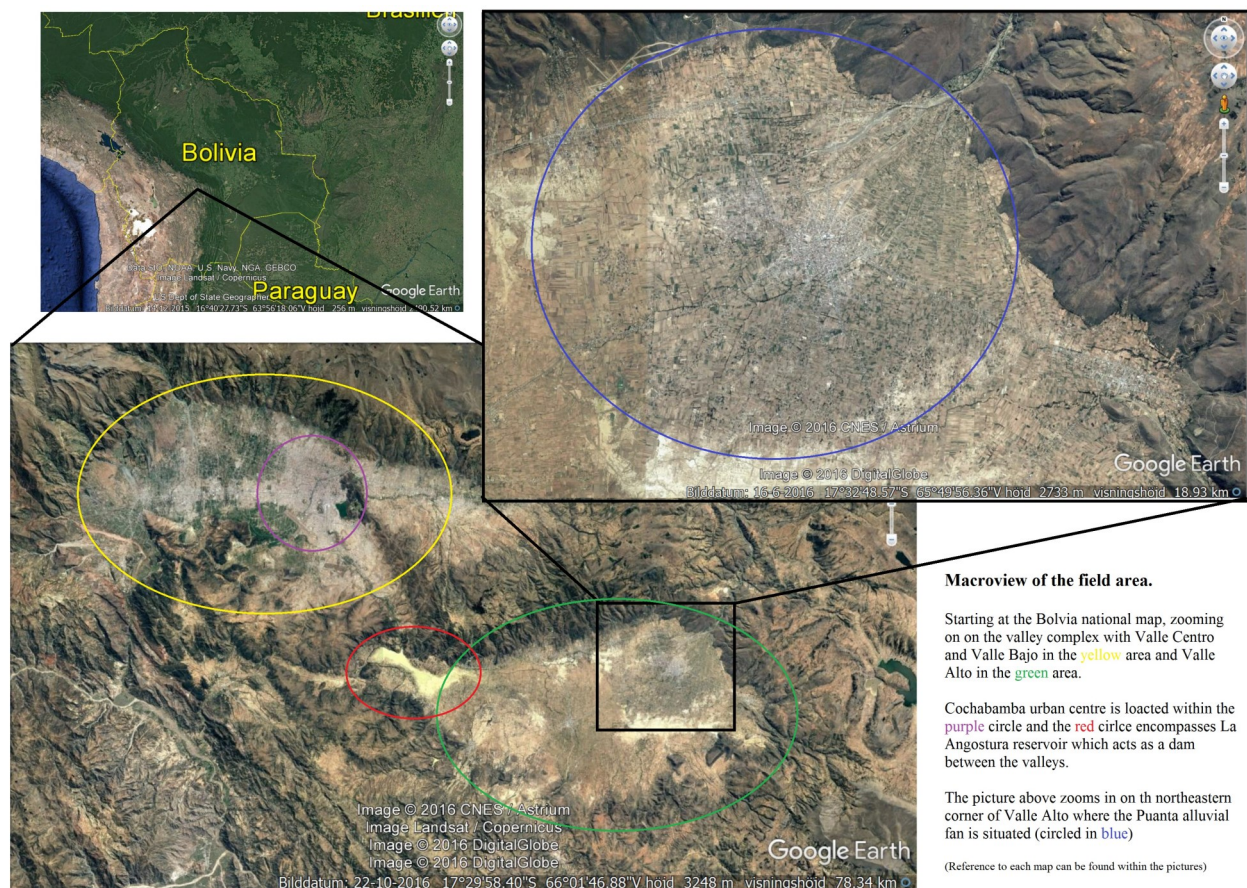
Fig 2. Maps of the area in different scales with important features marked in different colours.

Macroview of the field area.

Starting at the Bolvia national map, zooming on on the valley complex with Valle Centro and Valle Bajo in the yellow area and Valle Alto in the green area.

Cochabamba urban centre is loacted within the purple circle and the red cirlce encompasses La Angostura reservoir which acts as a dam between the valleys.

The picture above zooms in on th northeastern corner of Valle Alto where the Puanta alluvial fan is situated (circled in blue)

(Reference to each map can be found within the pictures)

where the locals are completely dependent on their agricultural activities. A local farmer from Area B said that he had to drill a new well as his current one was near depletion, but unfortunately when the well reached ~70 m the water became saline and unfit for irrigation. The water rights in many parts of the Andes is a complex socioeconomic matter, with aspects of traditional inheritance rules and demographic structures, trumping the physical parameters of reasonable water distribution. This leads to reoccurring disputes over benefits and water management, where the losing party usually are the indigenous agricultural peasant communities. Access to water is also a geographical issue where the communities downstream tend to receive less water than the upstream communities (Saldías et al., 2013)

The recent development has led to a wide range of well logs from the area with varying credibility and accessibility. Most drilling companies do not release their logs, and other have made mud logs without care for detail. Some wells do however have wire-line resistivity logs.

2 Study area
2.1 Geography
The study area is situated in the central part of Bolivia in the so-called Zone of the Valleys, a transitional zone between the Bolivian Altiplano and the lowlands (Renner & Velasco, 2000), at latitude 17.59°S – 17.49°S and longitude 65.90°W – 65.78°W (Fig 2). It belongs to the department of Cochabamba and the

Punata alluvial fan is located in the north eastern part of Valle Alto (High Valley; also referred to as Punata-Cliza valley) which is a tectonic basin, filled with Quaternary lacustrine and alluvial/colluvial sediments (SERGEOTECMIN, 2011). Valle Alto is part of a larger basin complex running in a NW – SE direction which is limited by the Tunari mountain massif in the north (Renner & Velasco, 2000). The basin complex is subdivided in Valle Bajo (Low Valley) in the west, Valle Centro (Central Valley) in the middle and Valle Alto (High Valley) in the east. Valle Alto, as the name suggest lies at the highest altitude, averaging at roughly 2700 m.a.s.l (Gonzales et al., 2016). This is slightly higher than Cochabamba in Valle Centro which lies at an average elevation of 2600 m.a.s.l. Valle Centro and Valle Alto are separated by a body of water called La Angostura reservoir, which is dammed up by a bedrock threshold (Velasco & Renner, 2000).

The fan in question has an altitude ranging from ~2800 – 2700 m.a.s.l, with a gentle NE – SW dip, and covers an approximate area of 90 km^2 (Gonzales et al., 2016). In the north-eastern part of the fan, the Pucara river flume enters the basin and is responsible for the alluvium deposition. It is an ephemeral river which only holds water during the rainy season in November – March/April. The mean annual rainfall is 350 mm/yr (Montenegro & Rojas, 2007) and the majority (80 %) falls during December-February, which makes the area semi-arid (Metternicht & Zinck, 2010). High potential evapotranspiration of >800 mm/yr (Montenegro & Rojas, 2007) makes the soils slightly – highly saline (depending on the sediment type) during the dry sea-
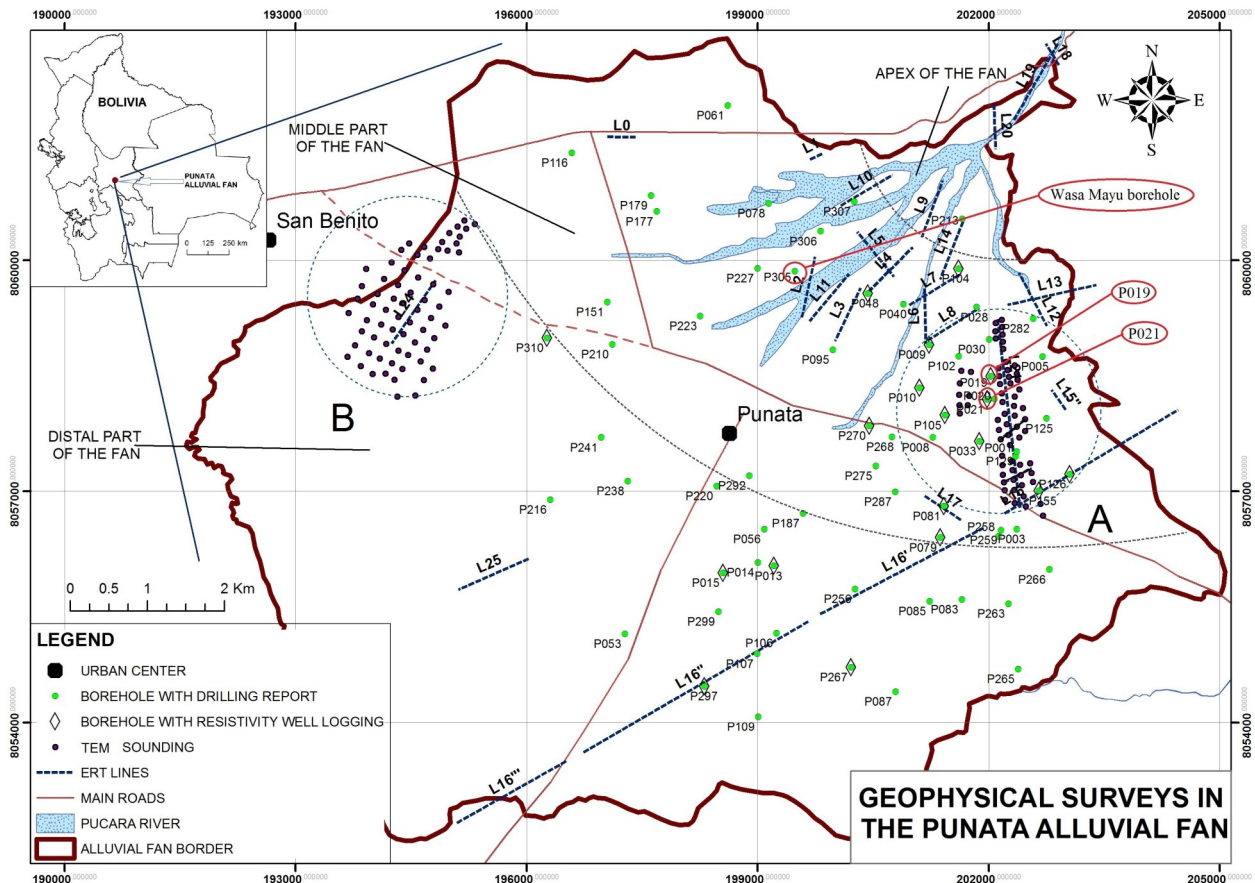
Fig 3. An overview of the field area with previous geophysical surveys marked as well as borehole with well logs. The studied areas in this paper are marked with A and B along with the locations for each sounding. The fan border is solely based on visible clay fringe and varies somewhat between different literature. (Modified from Gonzales, 2017b).

son and the natural local flora is often halophytic and xenomorphic (Metternicht & Zinck, 2010). However, the fertile soils of the Punata alluvial fan makes it suitable for irrigated agriculture and the majority of the area is dominated by farmland, with the exception of the Punata urban area situated in the centre of the fan. Grown crops include maize, alfalfa, onions, potatoes, various vegetables and a wide variety of fruits (Saldías et al., 2013; Renner & Velasco, 2000).

Originally the plan was to conduct TEM-soundings in profiles that cross-cut the entire fan, but due to spatial restrictions, irrigation patterns and urban interference this was not possible. Instead the soundings where concentrated in two different areas of the fan (Fig 3).

Area A in the eastern part of the fan, close to the Tunari massif, is dominated by farmland, divided into small patches, where flood irrigation is common (Fig 4). Irrigated areas could in some cases be under ~0.2 m of water which made the setup of soundings difficult. The sparse natural vegetation is generally low, with only a few trees. Close proximity to anthropogenic structures further restricted the spatial distribution of soundings.

Area B is situated close to the fan border in the western part of the fan. In this area the land is not divided into patches in the same way as area A, and it is not irrigated during the dry season. The flatness and absence of vegetation and anthropogenic structures (except for the northernmost part) made it suitable for TEM soundings (fig 5). The area is crisscrossed with

wide (2-5 m), dug ditches which are used to redirect river water during the rainy season, however they were easily avoided.

There are no bedrock outcrops in the study area and all geological interpretation associated with the basement had to be made based on the macro-structure of the valley mentioned in the literature.

2.2 Bedrock geology

The study area is situated in a tectonic graben on the eastern side of the Cordillera del Tunari. In Valle Centro the graben is delimited by normal faults in the north and south, which makes it likely that so is the case in Valle Alto, as they belong to the same basin complex. North of the basin the Tunari mountain range reaches an altitude of >5000 m.a.s.l at its highest peak, while the southern range is substantially lower (maximum altitude of 4000 m.a.s.l) due to extensive denudation (Renner & Velasco, 2000). The majority of the bedrock is Palaeozoic sedimentary rocks with Ordovician origin. There are a few occurrences of Silurian formations and a Mesozoic formation from the late Cretaceous (SERGEOTECMIN, 2011).

The lowermost formation is the Anzaldo Fm. which was deposited in a distal – middle shelf shallow marine setting with transgressive and regressive episodes (Fig 6). It consists of mainly bluish grey siltstones and some light brown medium – coarse grained sandstones. There is an abundant fossil content in different levels within the formation (GEOBOL, 1983; Renner & Velasco, 2000; SERGEOTECMIN, 2011).

Fig 4. Typical use of flood irrigation in area A, which made soundings difficult. The water depth is estimated to be at least 0.2 m

Fig 5. Area B was well suited for TEM soundings, with flat topography, no flood irrigation or high vegetation.

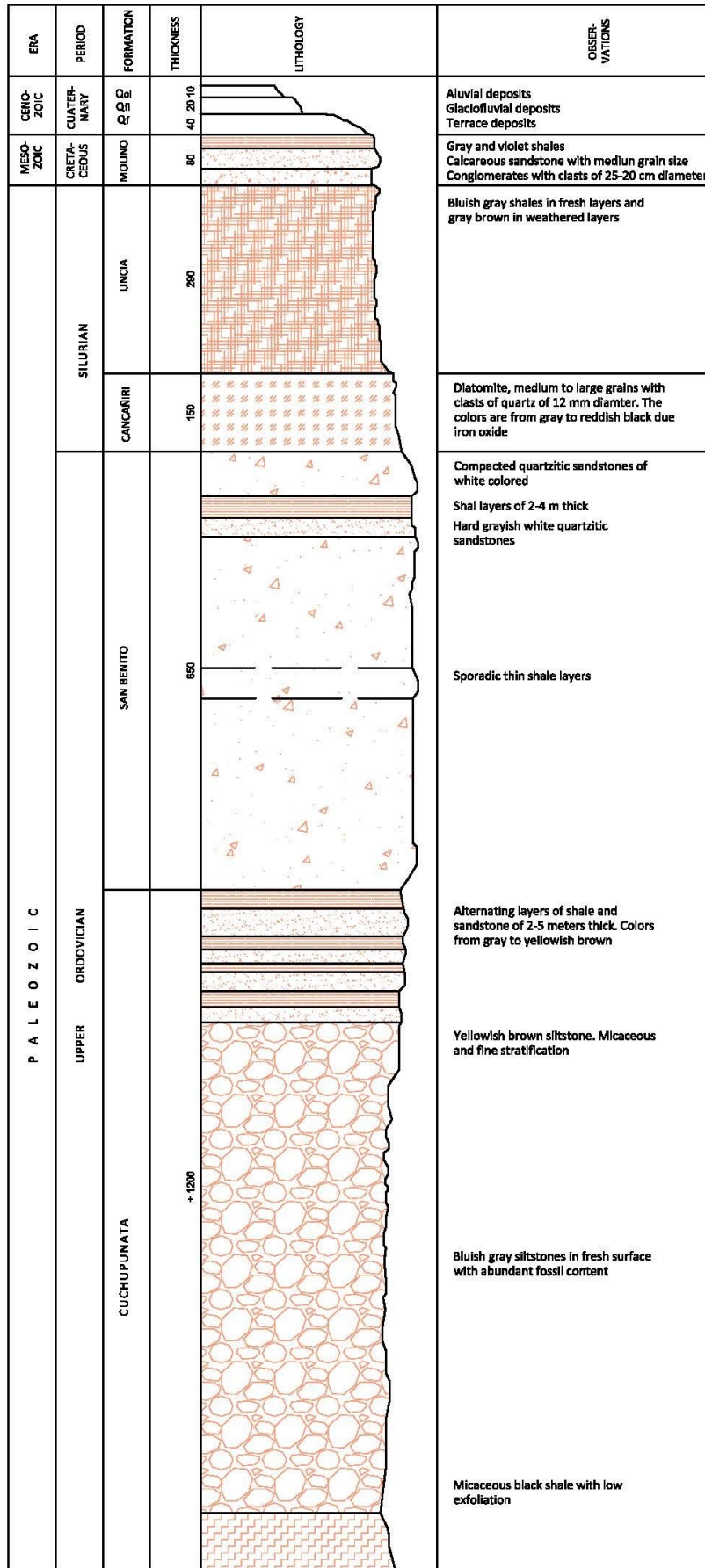| ERA	PERIOD	FORMATION	THICKNESS	LITHOLOGY	OBSERVATIONS
CENO-ZOIC	CUATER-NARY	Qt Qg Qal	40 20 10		Aluvial deposits / Glaciofluvial deposits / Terrace deposits
MESO-ZOIC	CRETA-CEOUS	MOLINO	80		Gray and violet shales / Calcareous sandstone with medium grain size / Conglomerates with clasts of 25-20 cm diameter
PALEOZOIC	SILURIAN	UNCIA	290		Bluish gray shales in fresh layers and gray brown in weathered layers
		CANCAÑIRI	150		Diatomite, medium to large grains with clasts of quartz of 12 mm diameter. The colors are from gray to reddish black due iron oxide
	UPPER ORDOVICIAN	SAN BENITO	650		Compacted quartzitic sandstones of white colored / Shal layers of 2-4 m thick / Hard grayish white quartzitic sandstones / Sporadic thin shale layers
		CUCHUPUNATA	+ 1200		Alternating layers of shale and sandstone of 2-5 meters thick. Colors from gray to yellowish brown / Yellowish brown siltstone. Micaceous and fine stratification / Bluish gray siltstones in fresh surface with abundant fossil content / Micaceous black shale with low exfoliation

Fig 6. Stratigraphy of the field area from Palaeozoic rock to Quaternary sediments. The region has experienced extensive deformation due to the Andean orogeny. Cuchupunata Fm. is the collective name of Anzaldo Fm. and Amutara Fm. This stratigraphy was made by GEOBOL (1983).

There are no outcrops of the lower part of the formation and its thickness is therefore disputed. According to SERGEOTEMIN (2011) it has a thickness of ~2000 m. GEOBOL (1983) on the other hand refers to both the Anzaldo Fm. and overlying Amutara Fm. as a single entity called the Cuchupunata Fm. and claim a collective thickness of >1200 m.

The Amutara Fm. overlies the Anzaldo Fm. concordantly. It is roughly 500 m thick with siliceous sandstone and intercalated greenish-grey shales with abundant fossils and bioturbation. Deposition of the sediments occurred in a coastal setting with transgressive episodes and transitions into overlying San Benito Fm. The boundary is marked by a transgressive event (SERGEOTECMIN, 2011).

In the San Benito Fm. the depositional pattern changes to a regressive setting which resembles fore shore and back shore sediments. The lithology is mainly light coloured quartzitic sandstones, which become increasingly micaceous towards the top, with sporadic thin layers of shale. SERGEOTEMIN (2011) states that the formation is ~1000 m thick, while GEOBOL (1983) says ~650 m but it is assumed that the discrepancy is due to where the thickness was measured.

All of the above mentioned formations were deposited during Ordovician, while the following, Cancañiri Fm, is the first Silurian deposit. Silurian deposits are scarce and only found at the bottom of some synclines. According to Renner & Velasco (2000) the formation boundary is concordant, while SERGEOTECMIN (2011) claim it is discordant. Either way the formation is quite thin (~30 – 150 m) and consists of glacio-marine diamictite with sporadic lateral variations that include thin layers of quartzitic sandstone and shale. These variations are attributed to the transgressions and regressions associated with the glaciation during the time of deposition (GEOBOL 1983; Renner & Velasco, 2000; SERGEOTECMIN, 2011).

Just as for the Cancañiri Fm., the thickness of the overlying Uncía Fm. differs between GEOBOL (1983), which claim ~200 m, and SERGEOTEMIN (2011) which claim it is ~500 m. The Uncía Fm. is discordant to Cancañiri and consist almost entirely of brittle shale deposited on a subsiding marine shelf (SERGEOTECMIN, 2011; Renner & Velasco, 2000)

The deposition of Palaeozoic marine shelf sediments was discontinued by the uplift associated with the Andean orogeny in the Early Jurassic. During the orogeny the strata experienced extensive deformation linked to the movements of two mega faults. The first one is the Mean Andean Thrust which is responsible for the macrostructures in the NNW – SSE direction and the other is the transpressive sinistral fault of Cochabamba. The latter caused a clockwise rotation of a local tectonic block, but the main structures were imposed by the Bolivian Orocline (SERGEOTECMIN, 2011), which is also responsible for the bending of the south American west coast.

The regional geology also includes sparse Mesozoic rocks from the upper Cretaceous. These include the Toro Toro Fm. and the El Molino Fm. Renner & Velasco (2000) describes the Toro Toro Fm. as a polymictic conglomerate which in GEOBOL (1983) is included in the bottom of the El Molino Fm., while SERGEOTECMIN (2011) describes the Toro Toro Fm. as predominantly sandstone deposited in a continental rift basin. Renner & Velasco (2000) and GEOBOL (1983) do however agree that the El Molino Fm. consists of calcareous sandstone. SERGEOTECMIN (2011) makes no mention of the El Molino Fm. at all.

2.3 Unconsolidated sediments

During the Neogene (Pliocene) renewed tectonic movements produced the graben structure in which the study area is situated. Due to a damming effect of the movements a closed lake, with calm sedimentation, formed in the basin during the Pleistocene or possibly during late Pliocene. This resulted in deposition of lacustrine and fluvio-lacustrine clay and silt with high organic content. Along with a calm reductive environment, caused by low water circulation, the sedimentation was possibly sapropelic. The draining of the lake is thought to have been caused by fault movements which lowered a ridge that acted as a dam. Which ridge caused the drain and when it occurred is currently unknown, but it is thought to have been during the Pleistocene (Renner & Velasco, 2000).

The high relief of the surrounding mountains and the latest glaciation has produced piedmont structures with intersecting alluvial, glacio-fluvial and colluvial sediments along the edges of the basin, which overlays the lacustrine clays from the former lake (Metternicht & Zinck, 2010). The general sedimentary succession of the Punata fan can be seen in (Fig 7) which is a well log from the Wasa Mayu borehole (P305) at the fan apex. Lithological accuracy of the log cannot be verified, but judging from the deposition pattern it is reasonable. The layer boundaries are presumed to be accurate. There are also evidence of some remnant terrace deposits at the fringes of the river mouths. The dominant landform on top of the lacustrine clay, in the Punata-Cliza valley, are different generations of alluvial fans (SERGEOTECMIN, 2011).

Alluvial fans form when a river, cutting into e.g. a mountain, reach an area with low relief and no lateral restrictions. This causes the flow velocity to decrease, which allows the suspended sediments to settle in a fan shape. Coarse sediments are first to fall out of suspension, and therefore the general morphology of an alluvial fan is sand/gravel (occasionally boulders) at its apex and with increasing amount of clay and silt in the distal parts of the fan. As the fan genesis proceeds the build-up of sediments will eventually be so great that the river starts cutting into the previously deposited sediments. Shifting streams cause reworking of the upper sediments of the alluvial fans over time (Huggett, 2011).

The conceptual model of the Punata fan in particular has ~100 m thick coarse material, ranging from sparse boulders, gravel and sand before reaching the lacustrine clay (Fig 8). This boundary can be seen in the Wasa Mayu borehole where the silty sand transitions to clayey sand (UNDP-GEOBOL, 1978). The thickness of the coarse alluvial material varies laterally and the distal parts have significantly less alluvium in accordance with typical fan morphology. Presence of boulders in the fan would suggest that the deposition has been linked to torrential river events.

As mentioned earlier a semi-arid climate has high evapotranspiration compared to precipitation, which
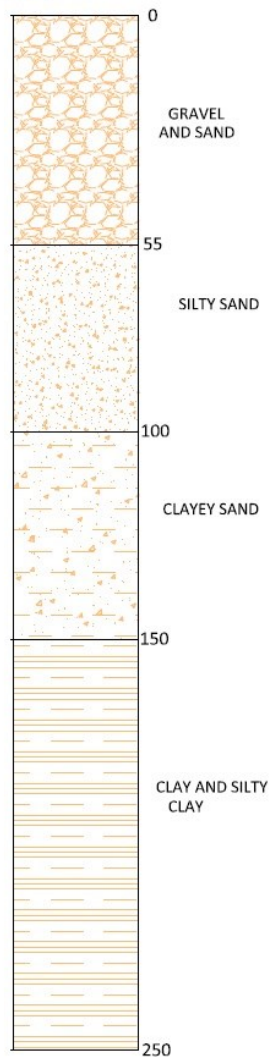
LITHOLOGY IN WASAMAYU BOREHOLE

Fig 7. Stratigraphy of the Wasa Mayu borehole (See location in fig 2) with important layer boundaries. The accuracy of the lithology cannot be verified, but judging from the geologic background with alluvium on top of lacustrine clays, it is reasonable (modified from GEOBOL, 1983).

results in high salinity/alkalinity in the top soils during the dry season. Metternicht & Zinck (2010) found that coarse material is less sensitive to this phenomenon while fine-grained areas display significantly higher salinity/alkalinity. The spatial distribution of salinity and alkalinity in the valley can be found in appendix A. The legend and colour scale is somewhat confusing which makes it hard to interpret, but it shows that the coarse material of the Punata Alluvial fan is largely unaffected. This clearly marks a clay fringe around the fan which can be used to estimate the location of the fan border.

2.4 Hydrogeology

The Punata alluvial fan constitutes an, for the most part, unconfined aquifer. It is possible that some areas of the fan are semiconfined due to increasing amount of clay in the upper part of the subsurface. Groundwater levels vary between 35-40 m below surface at the apex to 10-15 m in the distal parts of the fan. The lacustrine clay that underlies the fan is an aquiclude or at least a potent aquitard, and acts as the bottom limitation of the aquifer (Gonzales, 2016). Surveys that penetrate the thick clay layer currently do not yet exist and it is not possible to know whether there is an underlying confined aquifer or not. The geologic records indicate that it is unlikely as the Pleistocene lacustrine sediments are believed to be the first unconsolidated material to be deposited in the basin (Renner & Velasco, 2000). Recharge of the aquifer is attributed to the Pucara River which funnels the water from the Pucara and Chullku Basin watershed into the alluvial fan in Punata-Cliza valley during the rainy season (Fig 9) (Montenegro & Rojas, 2009). The influence on the recharge by rainfall, secondary streams and bedrock fractures is debated, but a recent hydrogeochemical study by Gonzales (2017a) suggest that the streams north and northwest of the fan do not contribute to the recharge. He also found that the Pocoata River, coming from the southeast through Arani, provides an unquantified addition to the recharge and that the general groundwater flow is from northeast and southeast (which correspond with the river mouths) with a westward direction. The flow direction is confirmed by former springs in the western distal parts of the fan (UNDP-GEOBOL, 1978), however the springs are no
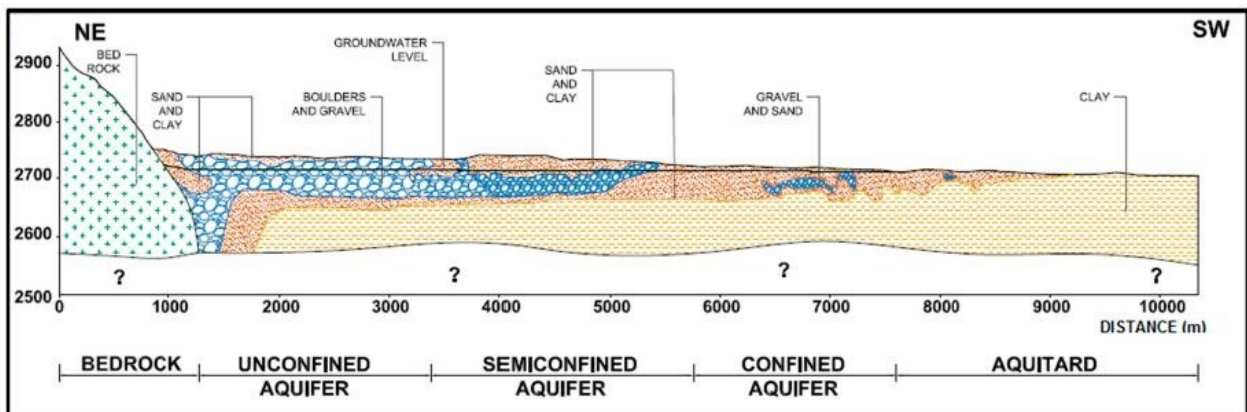

Fig 8. The figure illustrates a refined model of the fan and underlying lacustrine clay, based on ERT measurements in 2015 by Gonzales et al. This indicates that some parts of the aquifer might be semiconfined by clay rich sediments. Comparing with the Wasa Mayu borehole, in the fan apex (see Fig 2.), the alluvial sediments should be gravel and sand instead of boulders and gravel, however lateral variations are possible (Gonzales et al., 2016a).
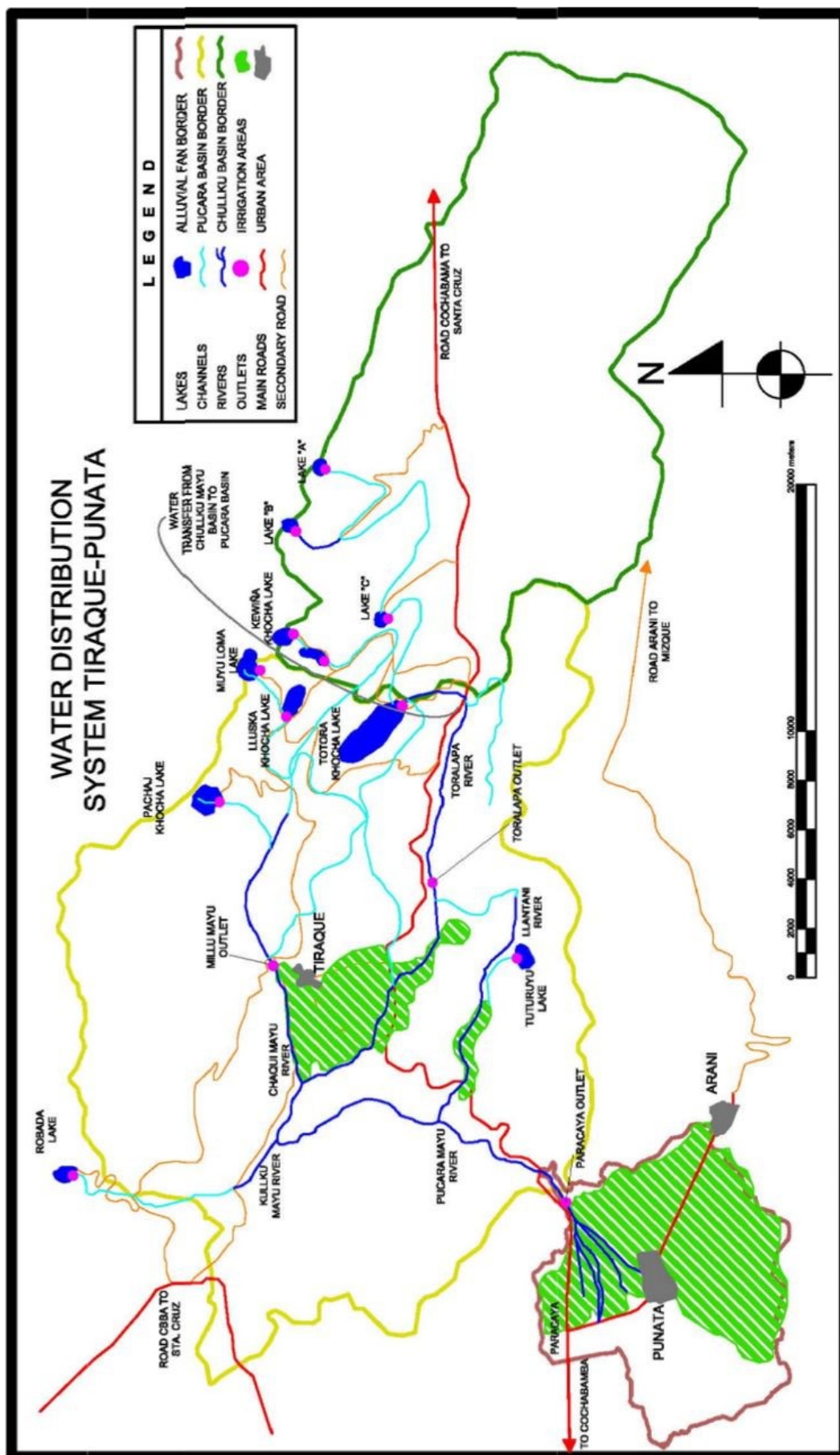
WATER DISTRIBUTION SYSTEM TIRAQUE-PUNATA

LEGEND

	ALLUVIAL FAN BORDER	
	PUCARA BASIN BORDER	
	CHULLKU BASIN BORDER	
	IRRIGATION AREAS	
	URBAN AREA	
LAKES		
CHANNELS		
RIVERS		
OUTLETS		
MAIN ROADS		
SECONDARY ROAD		

WATER TRANSFER FROM CHULLKU MAYU BASIN TO PUCARA BASIN

LAKE "A"

LAKE "B"

KEWIÑA KHOCHA LAKE

LAKE "C"

MUYU LOMA LAKE

LLUSKA KHOCHA LAKE

TOTORA KHOCHA LAKE

PACHAJ KHOCHA LAKE

ROBADA LAKE

MILLU MAYU OUTLET

TIRAQUE

CHAQUI MAYU RIVER

KULLKU MAYU RIVER

LLANTANI RIVER

TUTURUYU LAKE

TORALAPA RIVER

TORALAPA OUTLET

PUCARA MAYU RIVER

PARACAYA OUTLET

PARACAYA

PUNATA

ARANI

ROAD CBBA TO STA. CRUZ

TO COCHABAMBA

ROAD COCHABAMA TO SANTA CRUZ

ROAD ARANI TO MIZQUE

N

0 2000 4000 6000 8000 10000 20000 metres

Fig 9. This is a schematic map of the Pucara and Chullku basin catchment areas which feed the Pucara river and are responsible for most of the Punata aquifer recharge (modified from Montenegro & Rojas, 2007).

16

longer there due to overexploitation and a trend of decreasing annual rainfall. A decade ago the Pucara river was a perennial river with greatly reduced flow (~10 l/s compared ~8000 l/s in the rainy season) during the dry season (Montenegro & Rojas, 2007), but has now turned into an ephemeral river with ever decreasing annual water quantities. The exact time when the river transitioned from perennial to ephemeral is not recorded and the estimation is based on hearsay.

In the hydrogeochemical study, Gonzales (2017a) also studied the stable $\delta^{18}O$ and $\delta^{2}H$ isotopic ratios of the groundwater. The samples from the Punata aquifer were consistently depleted in the heavy isotope compared to the general rainfall samples. Normal/light rainfall preferentially precipitates ^{18}O and ^{2}H which gives it high $\delta^{18}O$ and $\delta^{2}H$. During a heavy rainfall all the water in the air is precipitated regardless of isotopic composition which depletes the $\delta^{18}O$ and $\delta^{2}H$ ratios. Such events are commonly associated with flash floods and the fact that the groundwater in Punata is depleted, suggests that recharge from rainfall is not a big factor. The main recharge of the aquifer occurs during the heaviest storms that create flash floods (Gonzales, 2017a).

3 Method
(Modified and translated from Mårdh (2016))

3.1 Electromagnetic methods
3.1.1 Time domain electromagnetic methods

Electromagnetic methods are divided into two categories, induction methods and reflection methods. Reflection methods, such as ground penetrating radar (GPR/Georadar), utilize pulses of electromagnetic waves with high frequency (1 MHz – 1 GHz) that are reflected back at layer boundaries. Induction methods on the other hand measure induced secondary magnetic fields from low frequency waves (1 – 100 000 Hz). These methods can in turn be divided into frequency domain methods (FEM) and time domain methods (TEM) depending on which type of electromagnetic wave is being used. In FEM, the amplitude of a periodic wave at a specific frequency is measured, while TEM measures the decay of the amplitude as a function of time on a transient wave. (Fig. 10). The decay time is directly proportional to the conductivity/resistivity in the ground (Reynolds, 2011).

TEM is a relatively young method compared to FEM and has essentially been developed since the middle of the 1980's. Part of the reason for the late development is the data-processing power required to interpret TEM-data, which is 50-100 times greater than that required for FEM. In past decades when the computers had limited processing power, this was a major issue. With modern computers the hardware restrictions are no longer a problem, but 3d-inversions are still rarely performed due to the sheer amount of data that needs to be collected and processed in order to produce adequate results (Christiansen et al., 2009). It is worth noting that making a 3d-inversion refers to a 3-dimensional view of a single sounding and is not to be confused with combining multiple 1d-inversions, and extrapolating the results in a grid. The soundings in this survey are exclusively 1 dimensional.
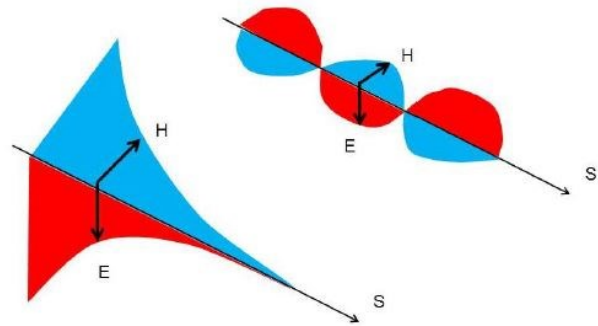

Fig 10. A transient electromagnetic wave (left), where the amplitude is a function of time compared to a periodic wave (right) with a constant amplitude at a specific frequency (Jeppson, 2015). S indicates the direction of wave propagation, E represents the electrical component and H is the associated magnetic component, which is perpendicular to the electric field.

A TEM-survey generally results in vertical profiles, consisting of multiple soundings, which display the resistivity in the ground. It is also possible to present the resistivity at a specific depth over larger areas in an aerial view of several soundings. Resistivity is the physical parameter of a material's ability to not conduct electricity and is the inverse of conductivity. Resistivity is presented in Ωm (Ohm meter). As the resistivity in geologic materials vary with lithology and composition, a resistivity profile can often be used to distinguish important layer boundaries, groundwater surfaces, sulphide ores etc. In some cases, it can also be used to trace pollutants in the ground, given that the pollutant yields a marked increase or decrease in resistivity (McNeil, 1980). High salinity, pore water and clay fraction reduces the resistivity as the amount of free ions increase. Lower salinity in the pore water consequently increase the resistivity, as do a high degree of compaction (less pore water) and lithification. There are of course exceptions to these general trends. Massive igneous rock such as granite and basalt tend to have high resistivity while sulphide ores are very conductive. As the molecular composition of these rocks may vary greatly there is no specific resistivity attributed to each rock type, but rather a span in which they usually occur (Fig. 11). Since these spans overlap in many cases, there is an equivalence problem and it is not possible to tell from only resistivity profile which material there is, whereby it is important to consider what is geologically feasible. When considering unconsolidated sediments, larger fractions (sand and gravel) have higher resistivity than small fractions (silt and clay) unless there is interference from saline pore water (Unsworth, 2014).

FEM and TEM are both highly sensitive to conductive formations with resistivity <100 Ωm, but are unsuitable for distinguishing high resistivity. FEM also struggles to penetrate thick highly resistive formations even if there is an underlying low resistivity formation. TEM does not encounter this problem but it does have trouble penetrating thick layers of conductive clay (Christiansen et al., 2009).
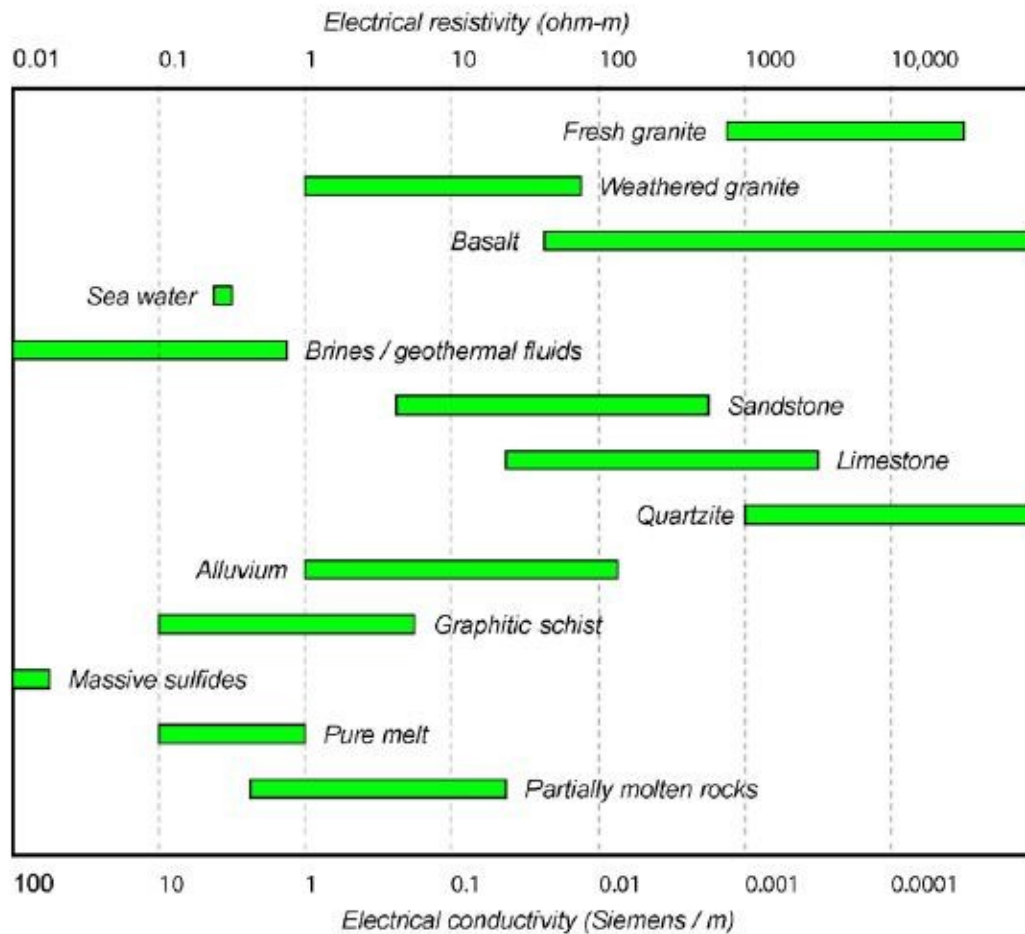
Fig 11. Chart of generalized resistivity values for different geological materials (Unsworth, 2014)

3.1.2 Theory

The basic principles of electromagnetic waves are explained by Maxwell's equations, which stipulate that an electric field will always produce a proportional, but phase shifted, magnetic field. The magnetic field will in turn create a new electric field and so on (Christiansen et al., 2009). When the field strength of a magnetic field changes, it induces an electromotive force (emf) which will disperse away from the source. The magnitude of the emf depends on the rate of change in the magnetic field. A fast change in the magnetic field will yield a greater emf than a slow change of the same magnitude. As the emf disperses in the ground, it will induce eddy currents within the geologic formations, propagating downwards and outwards at a 30° angle from the source (Fig. 12). The electrical currents are proportional to the resistivity in the ground and will produce a secondary magnetic field. Depending on the resistivity in the ground, the currents will abate at different rates. Highly resistive materials will lose their charge much faster than low resistive materials (Fig. 13). Consequently, the magnetic field will also abate with time. Low resistive materials will display magnetic fields with low initial amplitude and slow decay while high resistive materials yield high initial amplitude and rapid decay (McNeil, 1980). By placing a receiver coil on the ground, in which a proportional electrical current is induced by the secondary magnetic field, one can indirectly measure the field strength (B) as a function of time (dB/dt) (Christiansen et al., 2009). The time derivative can then be translated into apparent resistivity (Rhoa). Note that the apparent resistivity is a normalized value and do not necessarily represent the geological layering.

The information about high resistive layers is sparse are as the signal dissipates rapidly in these settings and TEM can rarely distinguish between two adjacent high resistivity formations. If the data gathering is perfect, there will be no equivalence problem (several models yielding the same apparent resistivity) and in theory only one model can fit the measured data. However, in practice this is not the case as data gathering is never perfect due to background noise. Therefore, all measurements are assigned an uncertainty (Christiansen et al., 2009).

3.1.3 Signal transmission and reception

A typical WalkTEM sounding uses a transmitter loop, placed in a square shape on the ground, and one or two receiver loops in either central or off-set configuration (see data acquisition for details). By transmitting a square waveform current through the transmitter loop, and then abruptly switching it off, the previously described emf is induced. One pulse (transient) consists of 50 – 200 μs turn-on ramp, 1 – 40 ms on-time, 1 –
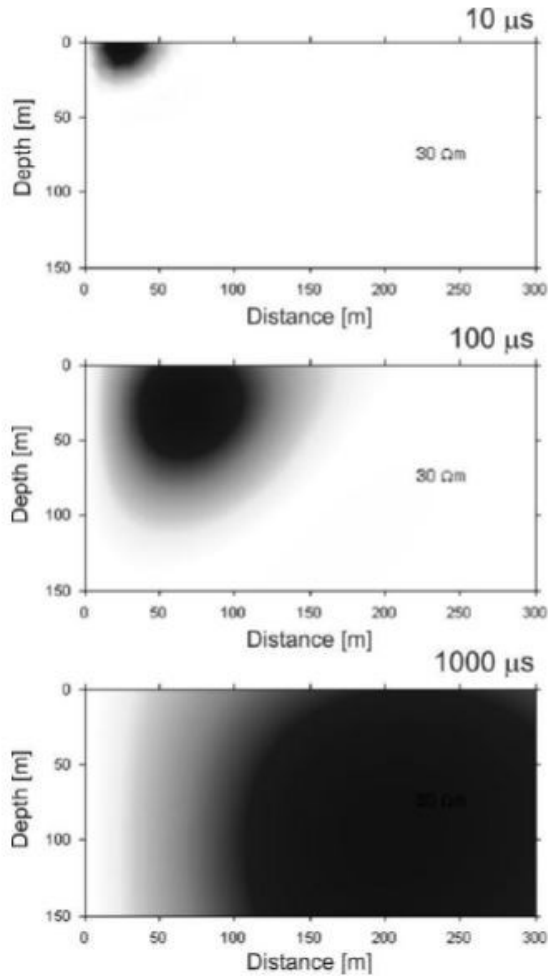
Fig 12. Conceptual model of the current density dispersion in a homogenous halfspace, at 10, 100 and 1000 μs after transmitter turn-off (Christiansen et al., 2009).
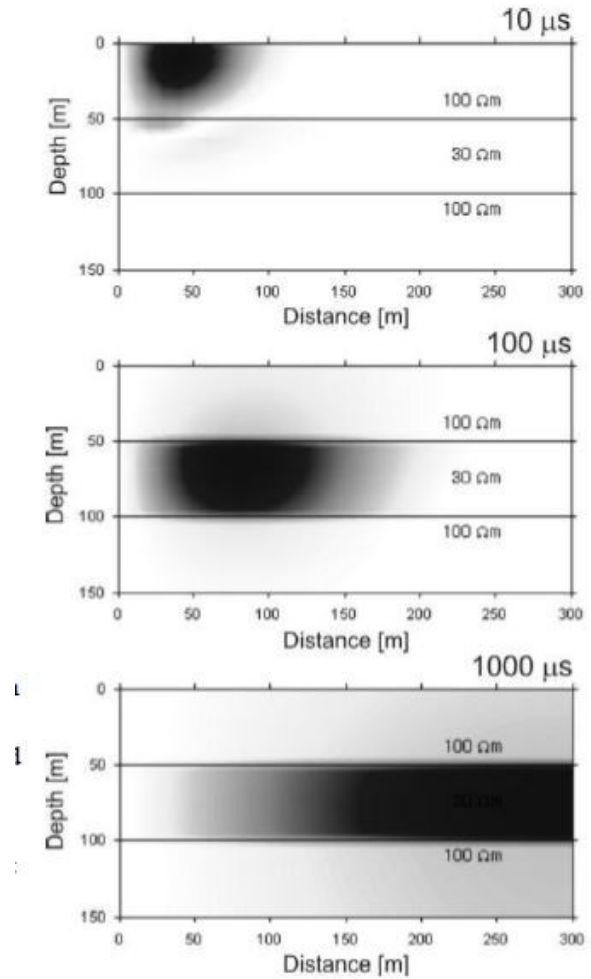

Fig 13. Conceptual model of the current density in a heterogeneous halfspace. Formations with low resistivity are more susceptible to electrical currents which makes the current density linger (Christiansen et al., 2009)

30 μs turn-off ramp and 1 – 40 ms off-time (Fig 14). The turn-on ramp is the time it takes from the initiation of the current until it reaches its maximum value. During the turn on ramp an initial emf is induced which creates an associated magnetic field. The current in the transmitter loop has to be turned on long enough for the emf to disappear and only a static magnetic field (primary) around the transmitter loop remains. When the transmitter current is turned off a new emf is induced. Just as the turn-on is not instantaneous, neither is the turn-off. The time it takes for the current to completely disappear is the turn-off ramp. Since the magnitude of the emf is proportional to the rate of change in the magnetic field strength the turn-off has to be as abrupt as possible to get a good signal. When the primary magnetic field from the transmitter loop has dissipated, it is possible to measure the change in the secondary magnetic field which has been induced by the eddy currents. This happens during off-time and is done in so called gates. The gates are time windows that are logarithmically distributed throughout the off-time (Christiansen et al., 2009). The early gates are narrow in order to register the rapid initial changes in the magnetic field which yield information about layers close to the surface. As the signal rapidly grows weaker, the later gates are wider in order to minimize interference from background noise. The narrow early gates do not register any information from greater depths as the signal needs time to reach the surface. The wide late gates contain information from greater depth but are not as reliable as the early gates in the shallow layers (McNeil, 1994).

As TEM register signals from a wide frequency span, each individual measurement (a transient) is sensitive to natural background noise such as lightning storms, radio antennas and the local power grid etc. Power grids tend to have a constant frequency at 50 or 60 Hz, which the instrument can take in consideration and effectively supress (McNeil, 1994). In order to minimize the effect of background noise, a sounding (the full measurement in one spot) usually consists of 1000 – 10 000 transients which are stacked to create a mean signal (Fig 15). As the noise has an irregular pattern compared to the signal, the stacking will minimize the noise and amplify the signal. The signal-to-noise ratio (s/n) is proportional to $\sqrt{N}$, where N is the amount of transients that have been stacked (Christiansen et al., 2009).
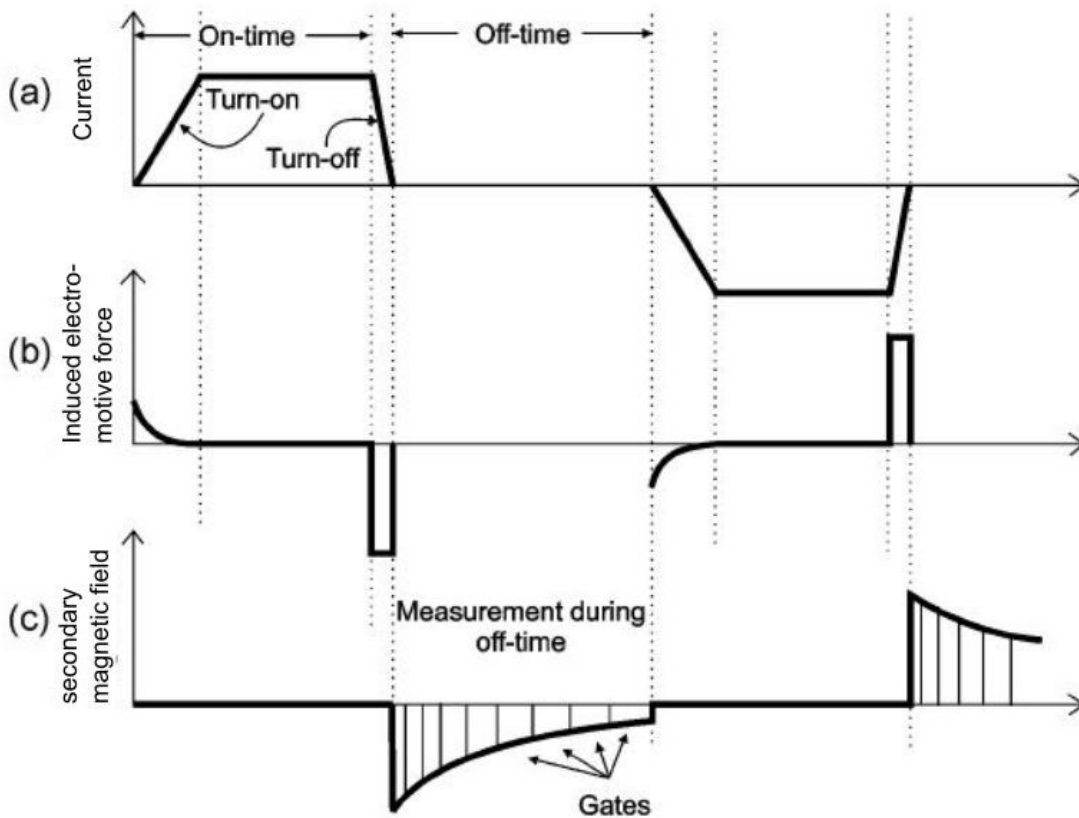
19

Fig 14. a) Illustration of the square wave in the transmitter cable. Turn-on is the time it takes for the current to reach its maximum potential. Turn-off is the time it takes for the current to completely disappear. Fast turn-off results in greater emf. b) The induced emf from the turn-off. During the turn-on an initial emf is induced which must be allowed time to decay before the measurement. c) During off-time, the secondary magnetic field strength is measured in logarithmically divided time gates. (modified from Christiansen et al., 2009)
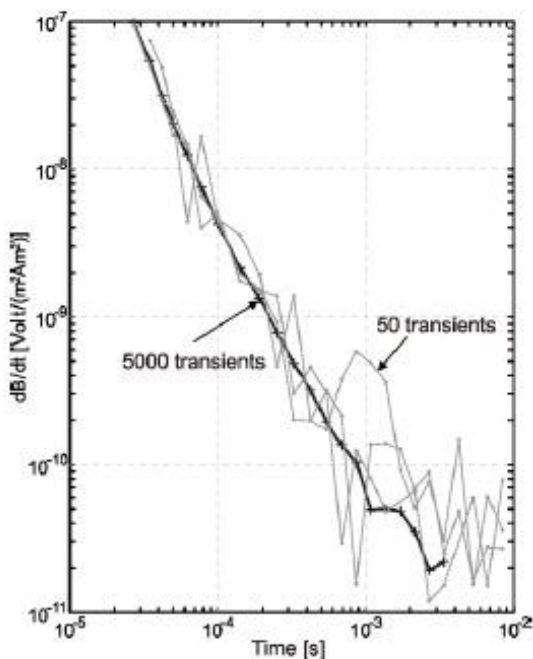
Fig 15. A comparison between a signal that has been stacked 50 times compared to 5000 times. The signal gets a smoother appearance with increased number of stackings and deviating data points lose their influence (Christiansen et al., 2009)

The influence of background noise can also be suppressed by transmitting at a higher moment (stronger current) whereby the signal becomes significantly stronger than the noise (Christiansen et al., 2009). By using a 24V power supply instead of 12V, the moment can be effectively increased from 8 A to 16 A. A higher moment will however result in a longer turn-off time. If the current does not completely dissipate during the turn-off ramp, it could result in so called 'ringing' which presents itself as an oscillating signal in early gates (pers. com. Foged, April 2016). The ringing effect can partly be reduced by using a dampening resistor with lower resistance (ABEM Instruments, 2012). To further avoid the problem, soundings consist of transients from both a high (HM) and a low moment (LM). During a measurement with a 24 V power supply, the low moment only transmits a current at 2 A (1 A if 12 V is used) which allows for a quick turn off and the ringing effect is minimized. The backside is that the induced emf from the LM will be weak and quickly disappear, which in turn leads to poor depth penetration. During the transmission of HM, the current is 16 A and the induced emf will be substantially stronger which allows for greater depth penetration but poor signal quality in early gates. By combining data from the late gates of the HM and early gates of the LM reliable data from throughout the

stratigraphic succession can be acquired (Christiansen et al., 2009).

The effective penetration depth of a sounding is limited to the point where the signal drowns in background noise. There are three factors that influence the penetration depth; the moment of the current, conductivity in the ground and the amount of background noise. If the ground contains highly conductive layers the signal will not be able to pass through and the depth of penetration will be limited. Calculating the effective depth of penetration is very hard, but the following equation can be used to calculate an estimation:

$$Z_d = 0.551 \; x \; (\frac{M}{\sigma \; x \; V_{noise}})^{\frac{1}{5}}$$

where Z_d = depth of penetration, M = moment, σ =the product of the conductivity and V_{noise} = noise level (Christiansen et al., 2009).

3.1.4 Coupling

Besides background noise, coupling with conductive objects can cause disturbances in a TEM-investigation. The types of couplings that can distort the data are divided into capacitive coupling and galvanic coupling (Christiansen et al., 2009).

3.1.4.1 Capacitive coupling

Capacitive coupling occurs when a current is induced in an ungrounded conductive object such as cars, isolated cables, railways, and metal fences. How much these objects affect the results depends on the size and shape of the object as well as the distance to the transmitter loop (Danielsen et al., 2003). The safety distance required depends on the loop size but in general at least 100 m from known metallic objects is adviced. Fortunately, capacitive coupling is easy to identify in a measurement as it causes an oscillating signal and the data will have an irregular, jagged shape (Fig. 16). In case of capacitive coupling the data should generally not be used (Christiansen et al., 2009), however if the coupling is limited it is possible to discard the affected gates (+2-3 succeeding gates) and use the remaining data for inversion. This type of data refining should be made with great care and the interpretation of the result must account for the missing data points (pers. com. Foged, April 2016).

3.1.4.2 Galvanic coupling

As opposed to capacitive coupling, galvanic coupling occurs in grounded conductors such as power lines and electric fences. This type of coupling skews the data in a way that it indicates lower resistivity than it should (Fig. 17). It does not cause any oscillations as those seen during capacitive coupling, which makes it hard to identify. The only way to discern whether a sounding was coupled or not is to compare the data to adjacent soundings that are expected to have similar data curves. When trying to single out soundings with galvanic coupling it is important to be careful as lower
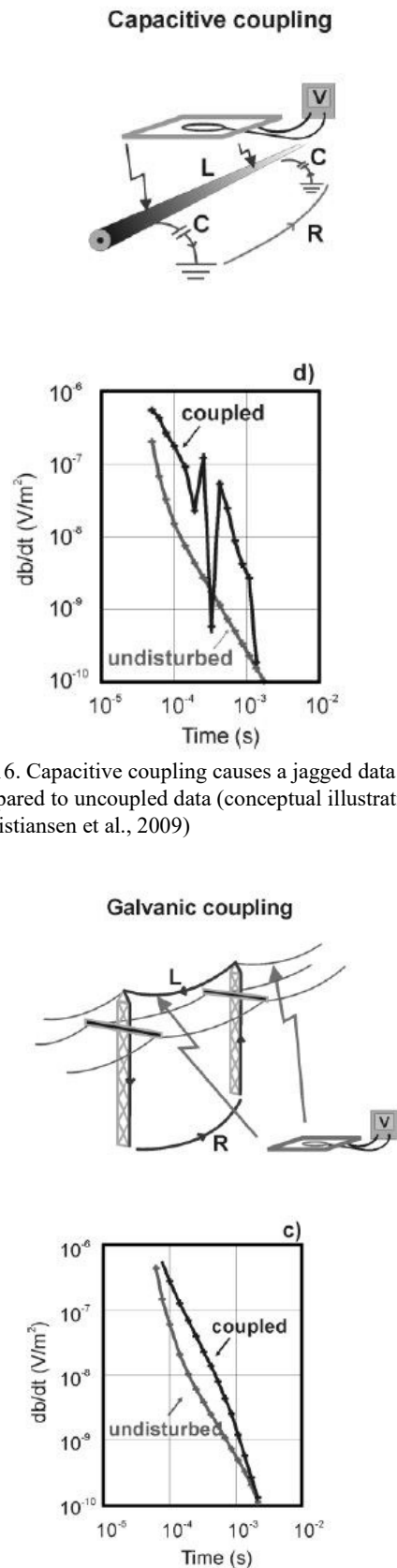
Capacitive coupling

Fig 16. Capacitive coupling causes a jagged data curve compared to uncoupled data (conceptual illustration) (Christiansen et al., 2009)

Galvanic coupling

Fig 17. Galvanic coupling is harder to detect as it skews the data without causing any oscillating effect. This type of coupling can only be detected by comparing it with adjacent soundings and evaluate whether the anomaly is geological or disturbed (Christiansen et al., 2009)

resistivity might be due to a local highly conductive feature in the ground. Before dismissing a galvanic coupling as a natural variation it is very important to consider what is geologically reasonable. If you suspect that galvanic coupling has occurred, the data are unusable and the whole sounding should be discarded (Christiansen et al., 2009).

3.2 Field methodology

This chapter describes the practical steps from gathering data in the field, to data processing and modelling. The field methodology is intertwined with relevant theory aspects to provide a better understanding of each step.

3.2.1 Equipment

The field study was carried out with WalkTEM from ABEM Instrument AB. The instrument was developed in a collaboration between ABEM instrument AB, HydroGeophysics Group at Aarhus University and SkyTEM Survey ApS, and is basically a miniaturized version of the airborne SkyTEM instrument (Nilsson, 2013). The equipment used in the field consisted of the following parts:

- WalkTEM instrument, with built in Windows XP operating system, GPS and 2 internal batteries (one of the internal batteries is automatically disabled when an external power source is present and the other powers the RC-5 receiver).
- 2 transmitter loops (AWG12), 200 m (50x50 m). (in order to setup next point while measuring).
- 2 receiver loops, RC-5 (0.59x0.59 m) and RC-200 (10x10 m) with 5 m^2 and 200 m^2 effective area respectively (20 laps in the RC-5 and 2 laps in the RC-200).
- 3 m extension cord.
- 330 Ohm dampening resistor.
- 2 x 12V car batteries with necessary cables and chargers.

3.2.2 Data acquisition

Deployment and measuring with a WalkTEM is fairly simple and straightforward in a flat terrain without high vegetation or other obstacles. There are two main configurations in which the instrument can be set up; central loop and off-set loop. In the off-set loop configuration the receiver is placed outside the transmitter loop which makes it more sensitive to lateral changes than central loop configuration. This is useful for mineral exploration where you are trying to pinpoint the position of ores. If two receivers are in use it is possible to place the RC-5 in the centre of the transmitter loop and the RC-200 outside the loop. Central loop configuration has the receivers placed in the centre of the transmitter loop and is not sensitive to lateral variation in the ground. It also yields a more accurate layer-

ing than off-set loop which makes it suitable for groundwater surveys. However, if two receivers are used in a central loop configuration there is a possibility of interference. The RC-5 has a higher band width than the RC-200. If the RC-5 is placed within the RC-200, the RC-200 will superimpose its lower band width on the RC-5 which would slow down the response. The consequence will be that the resistivity in early gates (near surface layers) will appear lower than they actually are. The RC-5 will not have any adverse effect on the RC-200 (pers. com. Sørensen, August 2016). The initial plan was to use the off-set configuration but due to lateral space restrictions in the field area along with farmland irrigation patterns (flood irrigation) we had to use the central loop configuration. When the survey commenced the instrument was set up in accordance with step 1 - 8 below, however when the super imposed band width issue was discovered the RC-200 was removed and the remaining soundings only used RC-5. Unfortunately, the majority of the soundings where already done by the time.

1) Place the RC-5 in a spot with as flat terrain and low vegetation as possible. This point will be the midpoint of the sounding.
2) Place the instrument 35.35 m from the midpoint in a straight line through 2 RC-5 corners (Fig. 18).
3) Starting from the position of the instrument, roll out the transmitter loop. At 50 m there is a marking that should be 35.35 m from the midpoint in the next corner. Make sure the cable is straight and properly stretched. Attach the corner in a spike or have someone hold it in place while rolling out the next side of the transmitter loop. Repeat until you are back at the instrument.
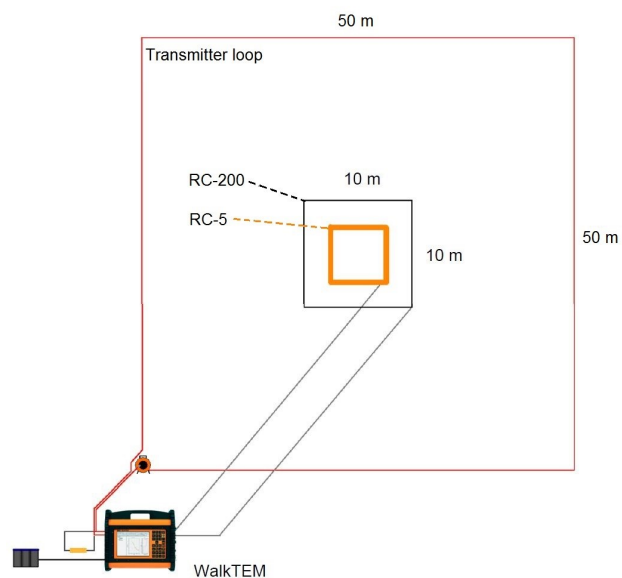

Fig 18. Conceptual depiction of the deployment in double central loop configuration (Modified from ABEM Instrument AB, 2014)

4) Place the RC-200 around the RC-5. The first corner should be ~7.1 m from the midpoint.

5) Roll out the cables of the receivers and connect them to the instrument. Make sure the cables cross the transmitter loop in a 90° angle to minimize any possible interference. The Rc-5 should be connected to input A and RC-200 to input B. Use the 3 m extension cord to make sure the instrument is placed away from the transmitter loop and connect the dampening resistor. When connecting the power cables to the transmitter loop, make sure the current direction is always the same as the direction of the receivers. This is easily managed by always setting up in a clockwise manner.

6) Connect the external power source. If you are using double batteries, connect them in series.

7) Make sure no cables are folded and place conductive objects as far away from the site as possible. Start the instrument to commence measurements.

8) While the instrument is measuring, pick the midpoint of the next sounding and start rolling out the second transmitter loop for increased efficiency. When the first measurement is done, move the receivers loops to the next transmitter and do a new measurement and then repeat. The distance between the soundings depends on a compromise between the resolution you wish to achieve and the area you like to cover. In area A of this survey the distance between the soundings varied between 100 – 130 m and in area B between 180 – 200 m.

This methodology is fast and efficient if you have plenty of manpower. In case the survey is carried out by only two people other methodologies for setting up might be more efficient. It is also a matter of personal preference. This particular methodology is a modified version of the one used by Nilsson (2013).

When the instrument is started, the WalkTEMUI will open automatically. WalkTEMUI is a user interface which makes it easy to manage settings and get an in-field view of the measured data. The first thing to do is to create a project where all the soundings (called stations for all processing purposes) will be stored. Next order of business is choosing which script to use. The script contains measurement instructions for the instrument such as how many transients should be measured and stacked, which frequency span should be used, gate durations and ramp times etc. In this survey we used a custom made 10 ms/37 gate script made by HydroGeophysics group at Aarhus university as well as a 50 x 50 m transmitter loop setting with 24V power source. Before starting the measurements, it is important to input the frequency of the local power grid in order to minimize noise. In Bolivia the power grid runs on 50 Hz. When the settings are done the measurement can commence. During the measurements the data for each receiver and moment will be plotted separately on the display. This way it is easy to spot capacitive coupling while working in the field. Galvanic coupling is harder to recognize and requires extensive data comparison which is not possible in the field (Aarhus Geosoftware, 2015). With the 10ms/37gates script a measurement takes approximately 10-12 minutes and when it is done the instrument automatically updates the station number. All settings will be saved so that you only need to press start at the next station.

During the campaign some issues were encountered as the instrument sporadically rebooted itself mid measurement. The problems were initially thought to be due to overheating whereby the instrument was kept in the shade under an umbrella at all times. This lowered the frequency at which reboots occurred but did not solve the issue. An investigation as to why this occurred was undertaken during the following fall, and it seems that the problem was caused by lower resistance in the transmitter cable than intended. This allowed a HM current of 18 – 20 A instead of 16, which consequently lead to instrument protecting its circuits by rebooting.

3.2.3 Data processing and modelling

The gathered data were processed and inverted in ViewTEM/SPIA. They are essentially the same program and WalkTEM is the commercial version, marketed by ABEM Instruments AB, of SPIA which is developed by HydroGeophysics group. After processing and inversion, the acquired models were imported into Aarhus Workbench for visualization. Workbench is also developed by the HydroGeophysics group and is a GIS-program where it is possible to combine the models in profiles or grids and illustrate them on a map.

Inversion of data is a mathematical process of creating a model that would yield a model response similar to the measured data, through iteration. The models become more reliable when the data residual is low, which indicates a good fit between the model response and the data. As the measured data are seldom perfect, several models might yield equal fit, which is known as an equivalence problem (Fig 19). By adding model parameters, the models can be refined to make sure they are geologically feasible. The opposite of inversion is forward theory, where a model is created from known parameters and then used to predict the data such a model would result in (Loke, 2013).

3.2.3.1 ViewTEM/SPIA

When the data is exported from the instrument, the information of each station is gathered in a GERDA database file (.gdb). By opening this file in ViewTEM/SPIA the station data is uploaded to an SQL-database. In the program interface the data for each station is presented in a single window or subdivided for each of the 6 channels (high moment, low moment and noise for each receiver). It is possible to view the stacked and unstacked data as both dB/dt and Rhoa (Fig 20, 21). Each curve is presented with automatically calculated standard deviations, but it is possible to change it manually if need be. The program can also mark the coordinates from the built in GPS for each station on the map. As the GPS is inside the instrument and not in the centre of the loop all the coordinates will be somewhat skewed. In this particular instrument there was a GPS malfunction so all the coordinates had to be added manually, from a separate GPS, and therefore all the stations are in the right place.
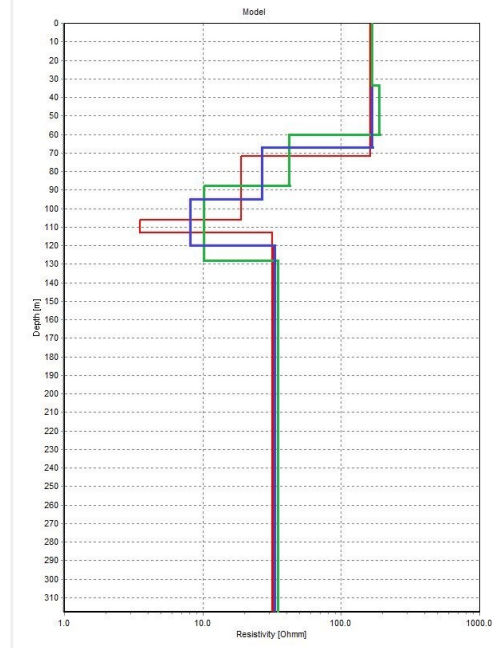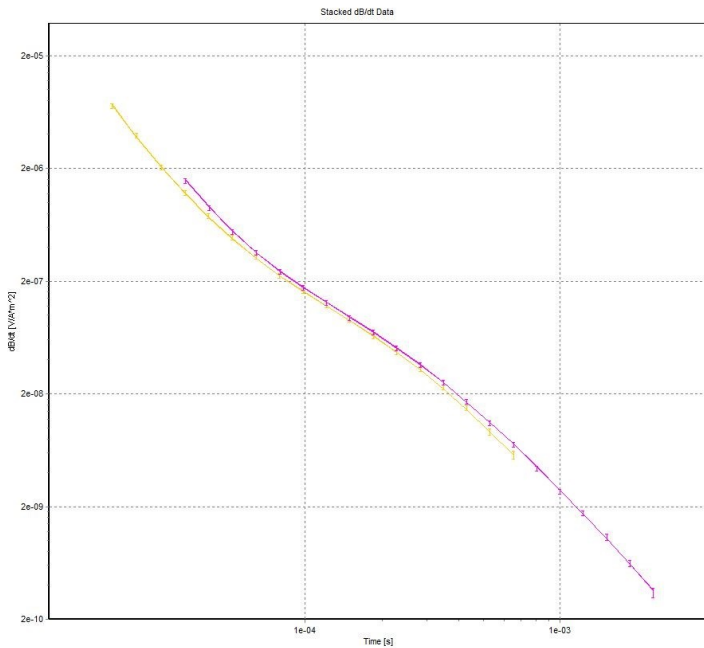
Fig 19. Due to imperfect data gathering, several models can have equal fit to measured data. The 3 models (red, blue and green) all have a data residual of 0.40 and are based on the same sounding. A thin low resistivity layer and a thicker layer with slightly higher resistivity are equally plausible, from a pure model perspective.

In order to perform an inversion it is necessary to select which data points should be used. This can be done in either viewing mode and is just a matter of preference (Aarhus Geosoftware, 2015). Data processing for this survey was done in the stacked dB/dt mode as it makes it slightly easier to evaluate when the data drowns in background noise. When performing the inversions, the general mode of operation is to use the LM from RC-5 and the HM from RC-200. The reason is that RC-5 is generally more precise when measuring near surface signals than the RC-200, while the RC-200 has a much greater effective area which allows it to detect weaker signals from greater depths (pers. com. Foged, April 2016). When transmitting the HM there is a risk of saturating the amplifier in the RC-5 and therefore the data is disabled. The LM data from the RC-200 is also disabled. However, due to the newly recognized adverse effect on the RC-5 by the RC-200 in a double receiver central loop configuration, the inversions have been made with the RC-200 data alone (station 41-68 in area B was measured with only RC-5 after the discovery). The use of RC-200 LM data causes a slight loss of resolution at shallow depths, but that is not a big issue as the near surface geology is not particularly important for this survey. Late measurements with only the RC-5 could result in slightly lower depth penetration, but as can be seen in the results such differences appear negligible.

Ideally all the data points in a data curve can be used, but is usually not the case due to ringing effects. The easiest way to discern which points can be used is to look at the data curve in stacked dB/dt and see if the late gates overlap with the noise. If the signal has been stacked so that there is a clear discrepancy in the slope angle between the sounding and the noise, all of the late gates can be used (Fig 22). Should the measured data start to follow the noise trend however, there is reason to believe that the data might be unreliable. In case it is not possible to separate the data trend from the noise trend these gates should be disgarded (pers. com. Foged, September 2016). Furthermore, the early gates of both the LM and HM should be disabled if there is a ringing effect in the data. At this point it is a good idea to perform a simple inversion and look at the forward response. If the spatial separation between the HM and LM in the forward response is the same as that of the data it is possible to move on the advanced inversions to refine the models, if not more data needs to be disabled. As the early gates are more reliable in the LM it is possible to disable the corresponding gates in the HM without losing any data. Conversely the late gates are more reliable in the HM and the corresponding gates in LM can be disabled. This will make the forward response easier to fit to the measured data. If the late gates are difficult to fit it is possible to raise the uncertainty of the last gates. In the data set acquired in this study, the first 2-3 gates in both HM and LM has been systematically disabled due to minor ringing. These gates only provide information about the upper most part of the ground which is not of interest either way.

When performing a simple inversion, the program runs an inversion algorithm which creates two 1-dimensional models that would fit the measured data. The first one is a layered model which is designed to minimize the amount of layers. It usually calculates 4-5 layers. The second model is a 'smooth model' and has a fixed amount (20) of layers with predetermined thicknesses, which increase with depth due to lower signal in late gates. Further, the resistivity between two adjacent layers in a smooth model cannot vary with more than a factor of 4, 2 or 1,5 depending if you choose low, normal or high smoothness. This will grant a model with a smooth appearance and high vertical resolution of minor variations in the strata. However, it will not be able to discern an abrupt, major
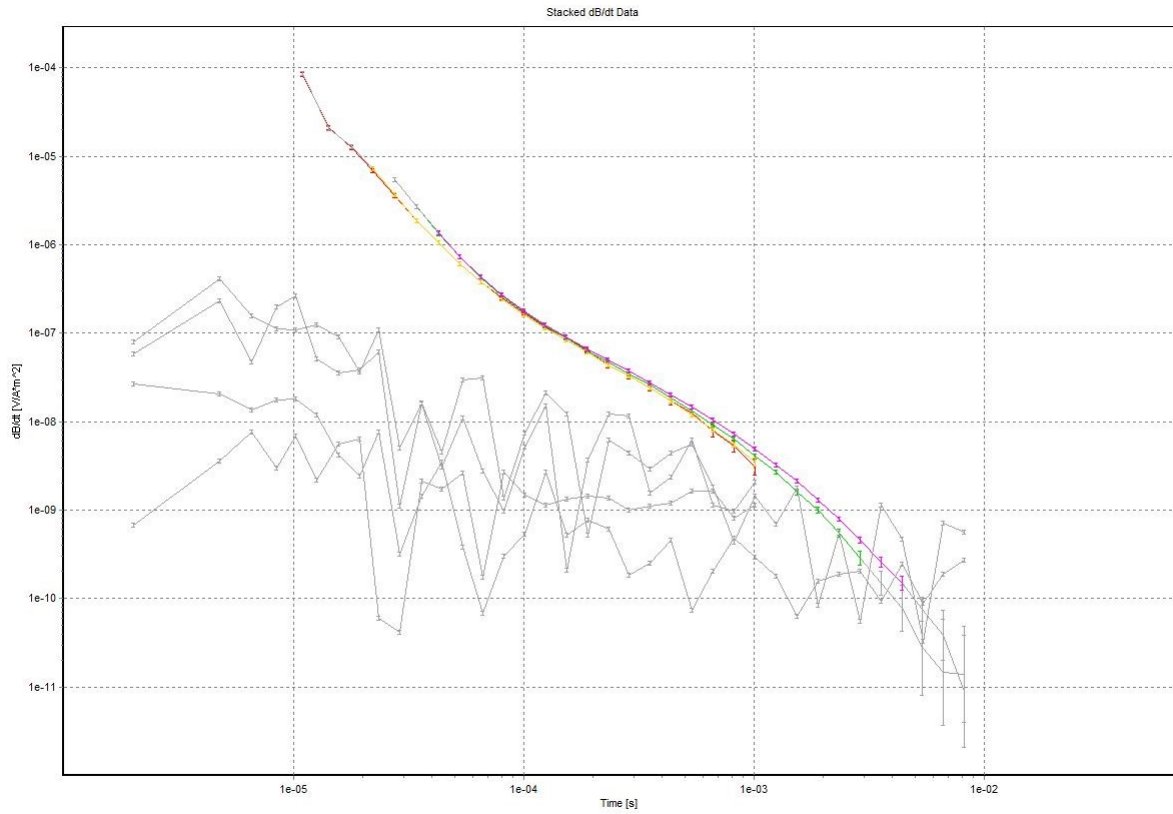
Fig 20. Example of sounding data with corresponding background noise in stacked dB/dt view (sounding 21 in area A). The four coloured curves represents the LM and HM for each receiver and the grey jagged curves are noise.
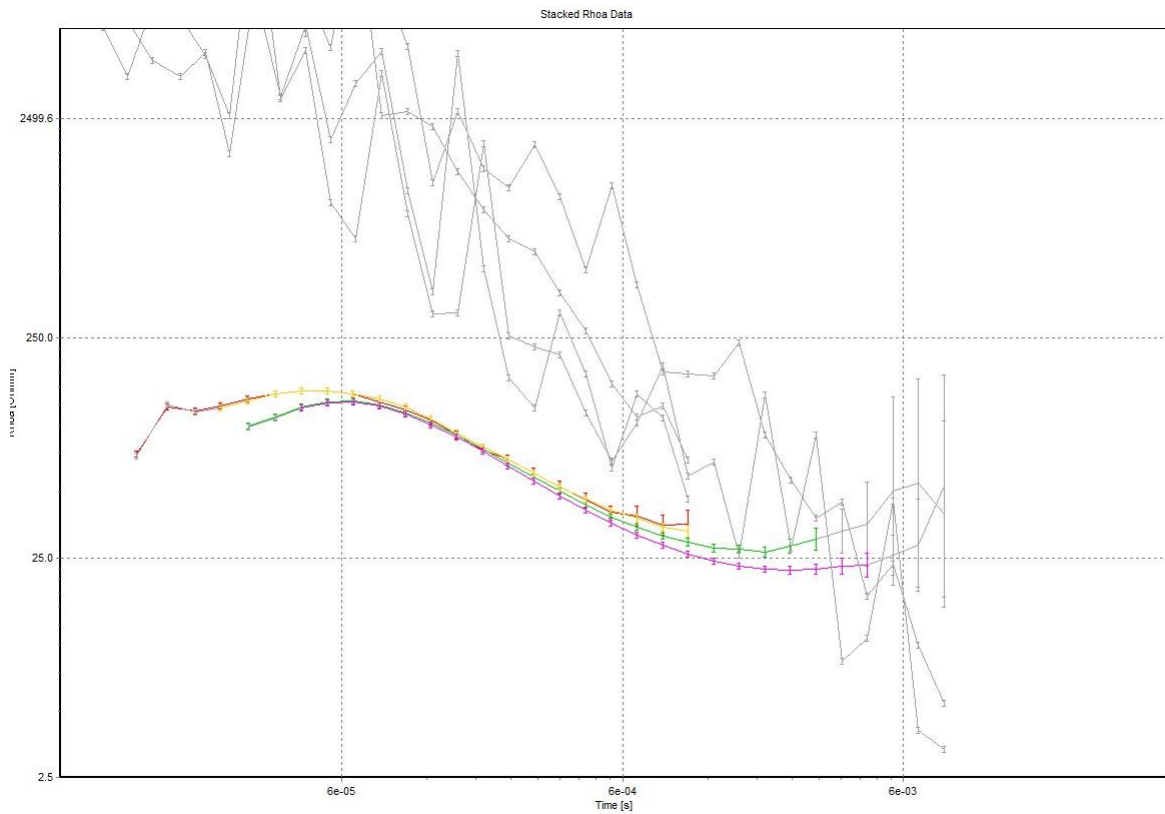

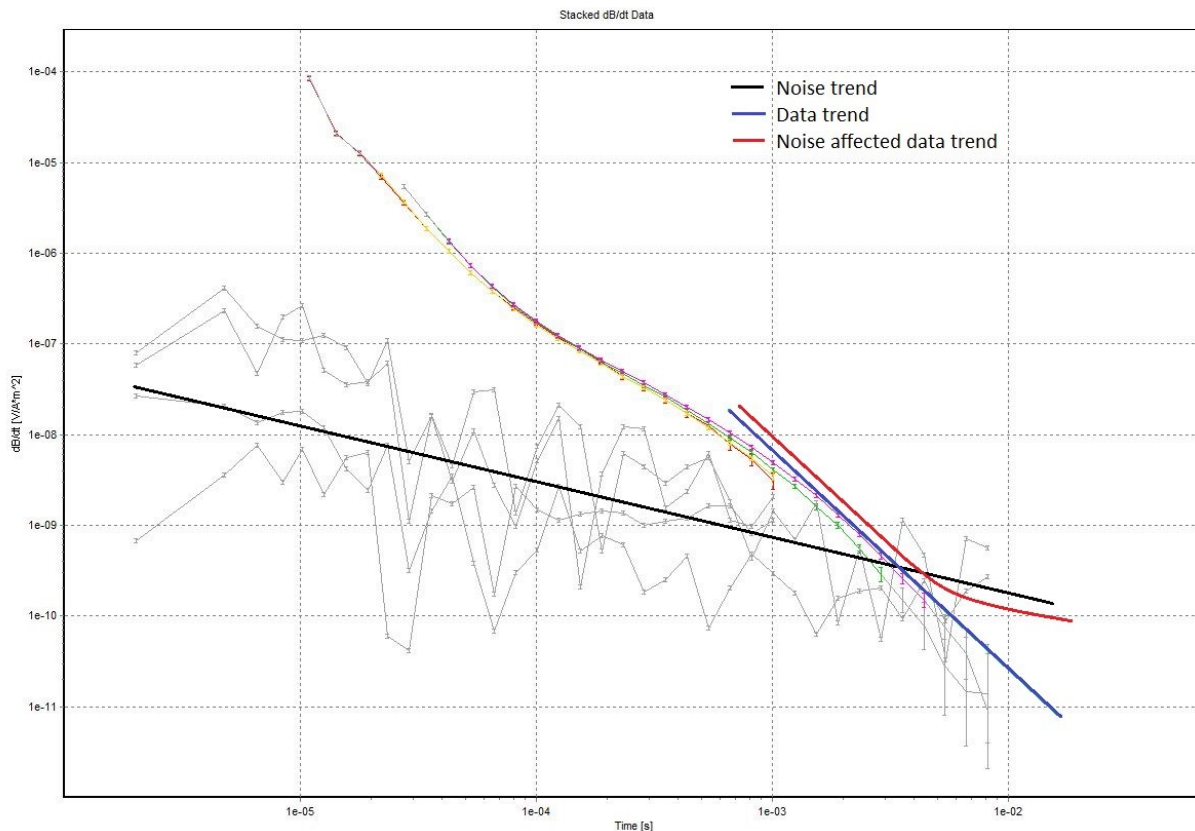Fig 21. Example of the same data as in fig 11 in the stacked Rhoa view.

Fig 22. In this particular data set the data set continues along the blue trend even after the signal decayed to the noise level. Therefore, the signal is unaffected by the noise and the data is reliable. If the data curve would have turned and followed the red trend after reaching the noise level, there is cause for concern and the data is most likely affected by the noise.

increase or decrease in resistivity and a sharp layer boundary may in worst case be modelled as a gradual change. The layered model has no restrictions concerning thickness and resistivity which allows it to accurately pinpoint sharp transitions, but will not detect minor variations as it uses fewer layers. Smooth models can be very useful, but are over parameterized and in accordance with Occam's razor, the solution with the fewest assumptions are more likely to be correct. Therefore, a layered model is probably closer to the true layering.

After the simple inversion the models can be modified in an advanced inversion. The advanced inversion allows the user to lock specific layer boundary depths and resistivity values in case there is previously known information at hand. It is however advised to let the data speak for themselves and try to avoid being biased by what results background studies might make you expect. By modifying the starting model and running consecutive advanced inversions until the data residual is as low as possible, one can produce the most reliable model. The aim is to have a data residual that is at least less than 1, which is considered a good fit (pers. com. Foged & Auken, August 2016).

3.2.3.2 Aarhus Workbench
ViewTEM/SPIA is a great tool for inverting models from TEM-data, but it is not suitable for visualization as all the models are 1-dimensional and can only be viewed as such. It is possible to place several models on top of each other, which is useful for comparing individual soundings, but it will not provide much insight of spatial variations. Therefore, the inverted models are imported into Aarhus Workbench where they can be combined into profiles of grids. The pro-

gram is ideal for handling the models. By opening the '.gdb'-file in Workbench, the chosen models are automatically available and plotted at their corresponding coordinates in a GIS-interface. This allows the user to draw and add the models to profiles or create grids. The grids visualize the mean resistivity over a certain depth interval for each model from an aerial perspective.

Aarhus Workbench is not solely designed to visualize TEM-data, but support a range of other geophysical methods and can also act as an inversion tool. The reason ViewTEM/SPIA was used for the inversions is that the program is designed specifically for inversion of WalkTEM-data.

3.3 Additional Information
The TEM survey was complimented by additional ERT surveys (instrument borrowed from Centro Agua of University Mayor de San Simon) following the same profiles to use for comparison. This data was processed and inverted by A. Gonzales while the TEM data was processed and modelled by J. Mårdh.

Measurements in the Punata alluvial fan were carried out during an 8-week period by J. Mårdh and A. Gonzales, from mid-July to mid-September of 2016. To optimize time efficiency local bachelor students Angeles Moron, Delia Aguilar, Gerson Salamanca and Tomas Gutierrez from UMSS (University Mayor de San Simon) were recruited as field assistants. A pickup truck, with associated driver Nestor Quisbert, was borrowed from the university to facilitate the transportation of staff and equipment to and from the field area. Transportation between soundings was carried out by foot.

4 Results

Data were collected from 128 different points and were inverted with varying results. In Area A only a few soundings demonstrate signs of capacitive coupling and are excluded. No soundings displayed any apparent galvanic coupling, but as such disturbances are hard to identify there is a reservation for unidentified occurrences. There are no identified cases of galvanic coupling in area B either, but the occurrences of capacitive coupling are greater than in Area A. The disturbed soundings are concentrated in the northern part of the investigated area and directly south of the small country road connecting Punata and San Benito.

In area A, the layered models generally have a better fit than the smooth models, with data residuals ranging from 0.3 – 0.6 with a few anomalies between 0.8 – 1.0, indicating a good model fit. The smooth models have good fit in the centre of the area, with residuals of 0.3 – 0.5, and poorer fit (0.8 – 1.2) in the north and south parts of the area.

The model fit in area B varies more than in Area A. Layered models generally have a good fit (0.4 – 0.8), with the lowest data residuals in soundings from the southern part of the area. Some soundings deviate from the average trend with data residuals of 0.3 and 1.1. The smooth models have a slightly better average fit (0.3 – 0.5), with some anomalies reaching 0.8, than the layered models in the south part. However, north of the Punata – San Benito road, the smooth models have data residuals >1.2 which indicate poor fit and therefore such models have been excluded.

For easier interpretation the models have been combined into 20 profiles (Fig 23) in Aarhus workbench. Only a handful are presented in the result section, the rest can be found in appendix B and C. The profiles are visualised as a composite of both smooth and layered models, because they have different strengths and weaknesses. Layered models are presented as vertical bars at each sounding location, while the smooth models have been interpolated to get a broader perspective of the profile. The lower limitations of the models have been marked with two dashed grey lines which represent the standard (lower line) and conservative (upper line) depth of investigation (DOI). All data above the conservative DOI are considered reliable, given that the data residual of the models are low. Data between the conservative and standard DOI, has reduced accuracy but can still hold valuable information. Below the standard DOI the electromagnetic signal is too weak to provide any reliable information and such data should not be used for any interpretation (pers. com. Foged, September 2016). All numbered profiles are visualised from north to south and the cross-cutting profiles (A, B, C and D) from west to east.

The profiles provide vertical cross-sections, which makes lateral comparison in the third dimension hard, and are therefore complemented by horizontal grids. Each grid represents the mean resistivity of a 10/20 m vertical interval, which has been interpolated between the models using the kriging method. The data in the grids are blinded at the standard DOI to avoid any unreliable data. Due to the varying DOI in the models, the lower grids have patches with no data. Only intervals of interest and with adequate amount of data are presented in order to make the figures illustrative.

4.1 Area A

In the first area (A) of the fan the results consist of 53 layered models and 53 smooth models, after the exclu-
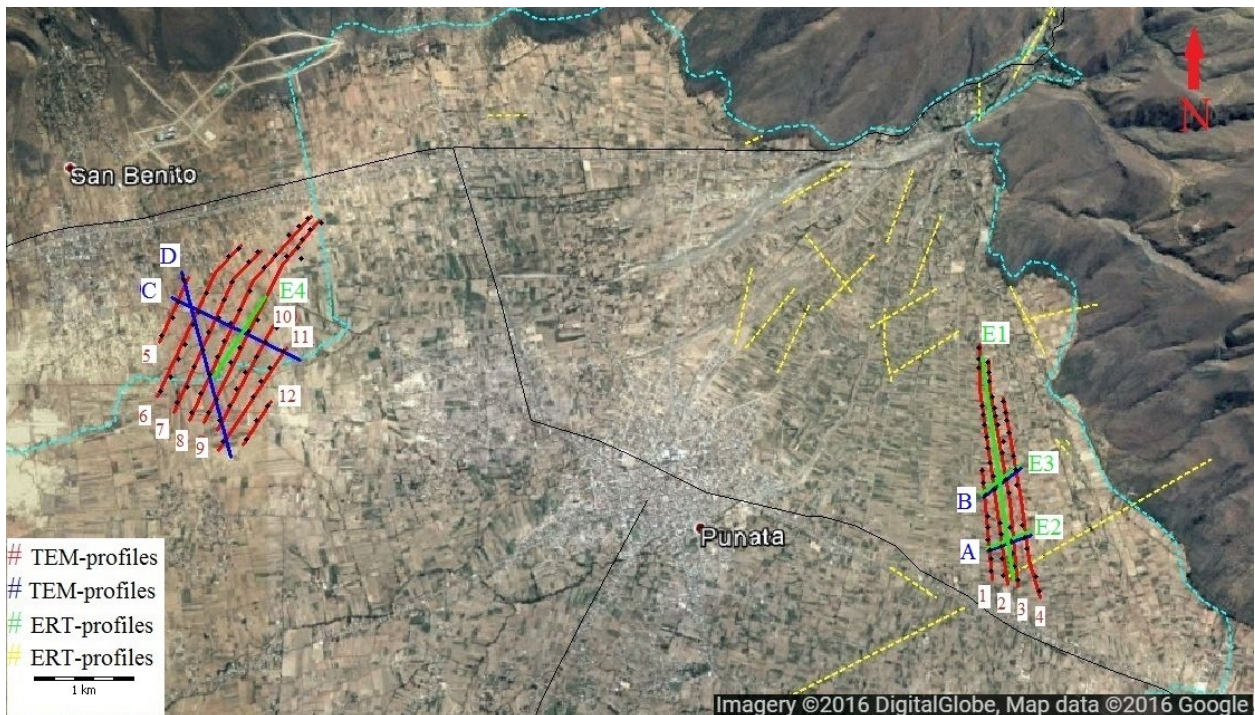

Fig 23. The map shows the locations and direction of all profiles. Red lines are TEM-profiles in north-south direction. Blue lines are cross-cutting TEM-Profiles in west-east direction. Green line represents the new ERT-surveys and the yellow line are previous ERT-surveys.
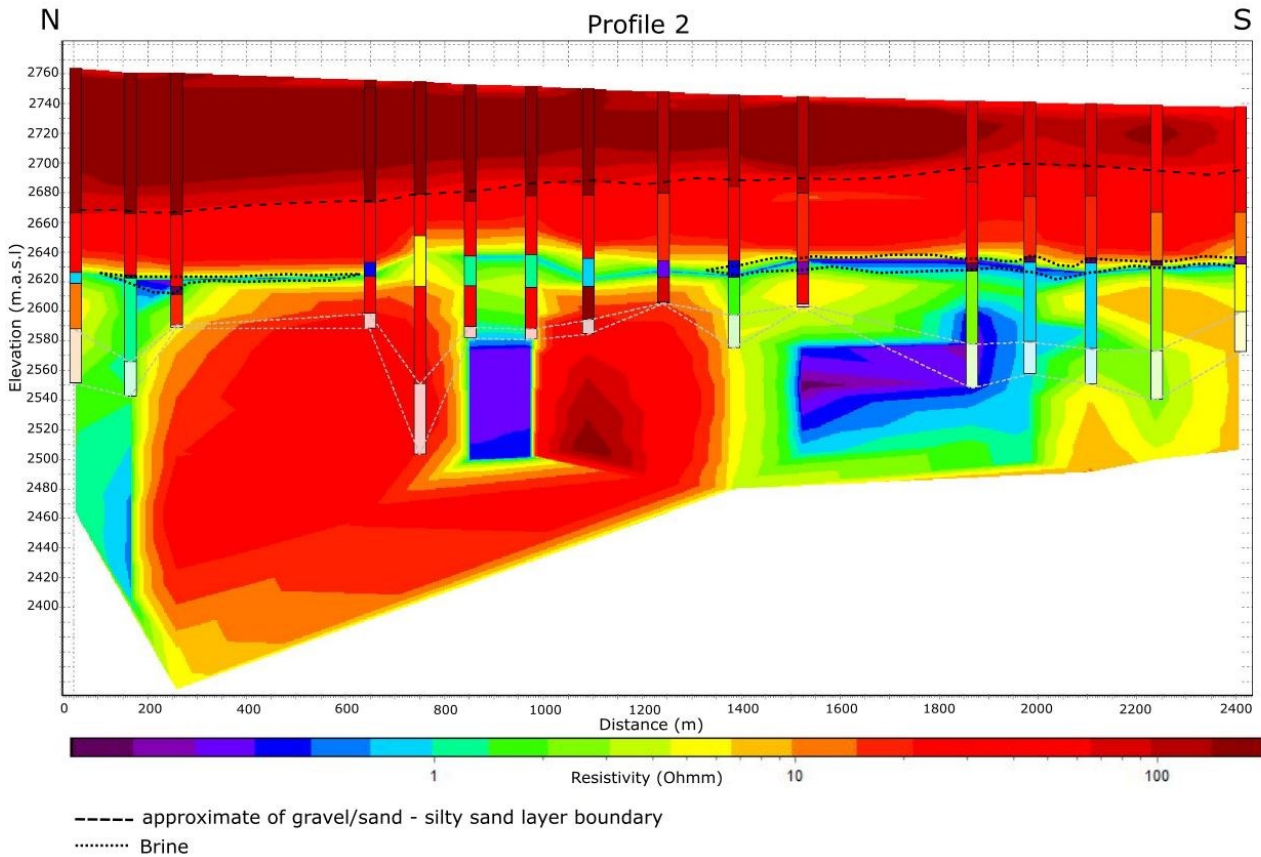
Fig 24. The vertical profile is a composite of layered models (bars) and interpolated smooth models (background). Profile 2 shows a distinct high resistivity layer with a lower boundary at ~2670 – 2780 m.a.s.l. The layer becomes less prominent in the south part of the profile. A distinct drop in resistivity at 2630 m.a.s.l is evident throughout the profile with some variance in the underlying strata. The dashed grey lines represent standard and conservative DOI under which the data is no longer reliable, and no interpretation should be made.
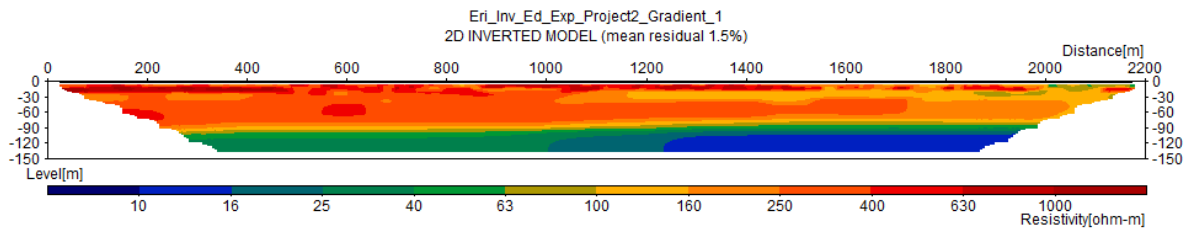
Fig 25. Profile E1. This profile runs along the same line as profile 2 for easy comparison. Note the shallower depth of penetration compared to the TEM-profile. They layer boundary corresponds to the upper layer boundary in profile 2. Note that all the ERT profiles in this paper have a different resistivity scale (Gonzales et al, 2017a).

sion of coupled data. There is a total of 6 profiles in the area. Profile 2 has been chosen to represent this part of the fan along with profiles A and B. The remaining profiles can be found in appendix B. There are also newly conducted ERT-surveys corresponding to the illustrated TEM-profiles. Data processing and inversion of the ERT results was carried out by Andres Gonzales and are also presented in Gonzales et al. (2016).

Profile 2 indicates a fairly homogenous resistivity distribution in the uppermost 100 – 120 m (2760 – 2640 m.a.s.l), with slightly reduced resistivity with depth (Fig 24). The sediments closest to the surface display a resistivity of 160 - 200 Ohmm which drops to 20 – 30 Ohmm at roughly 80 – 100 m depth (2670

m.a.s.l). This drop can be clearly distinguished in the layered models, while the smooth models have more minor variations. As the layered and smooth models have similar fit, the layered models represent the preferred interpretation in accordance with Occam's razor. The smooth models do however provide a slightly more nuanced distribution. At 2630 m.a.s.l there is an abrupt drop in resistivity, falling as low as 0.1 Ohmm in the beginning and end of the profile. This highly conductive layer is no more than 5- 10 m thick. Such thin formations are hard to model with smooth models as they have fixed layer thicknesses, whereby the layered models are more reliable. Recall that the smooth models in area A had better fit in the centre than in the north and south, where the low resistivity layer have
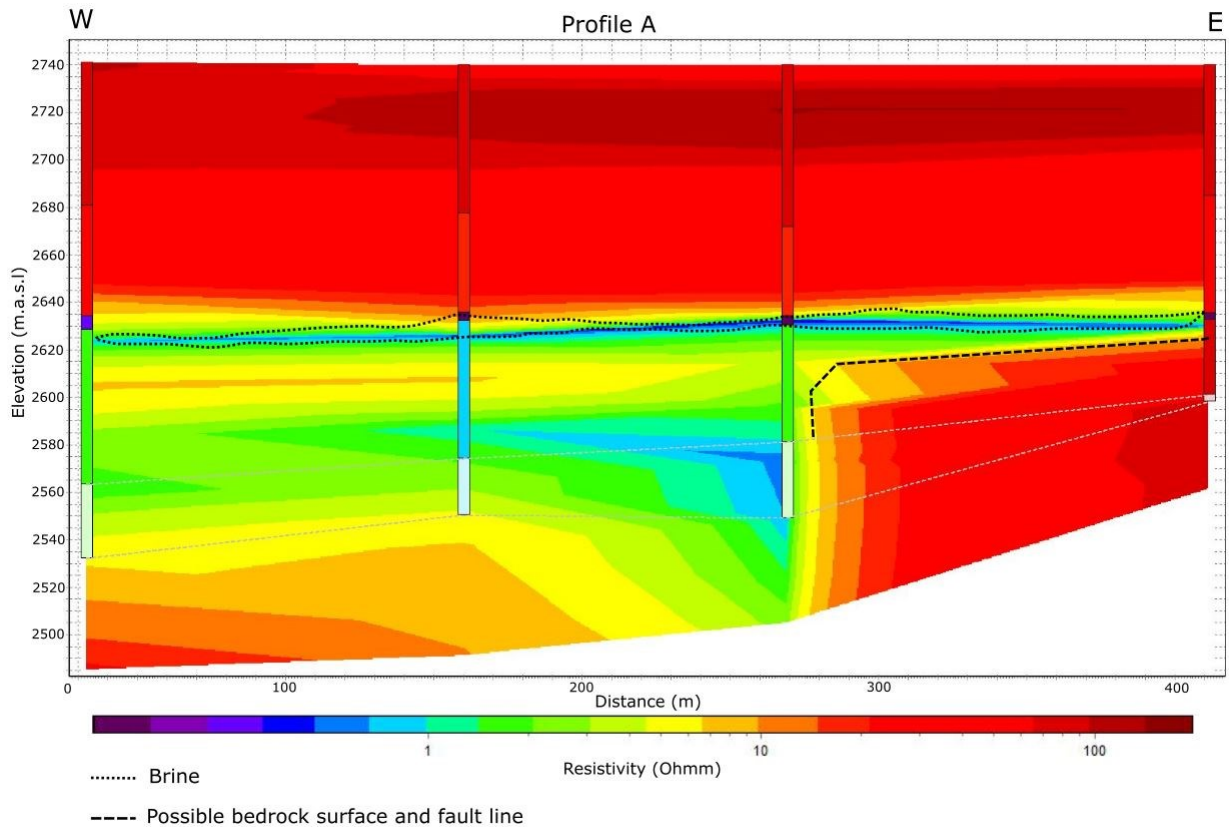
Fig 26. Profile A has an even low resistivity layer throughout the profile. The upper layer boundary is less prominent than in profile 2. There is also a discrepancy between the layered and smooth models in the second node from the west. Note the high resistivity feature at 2620 m.a.s.l in the east.
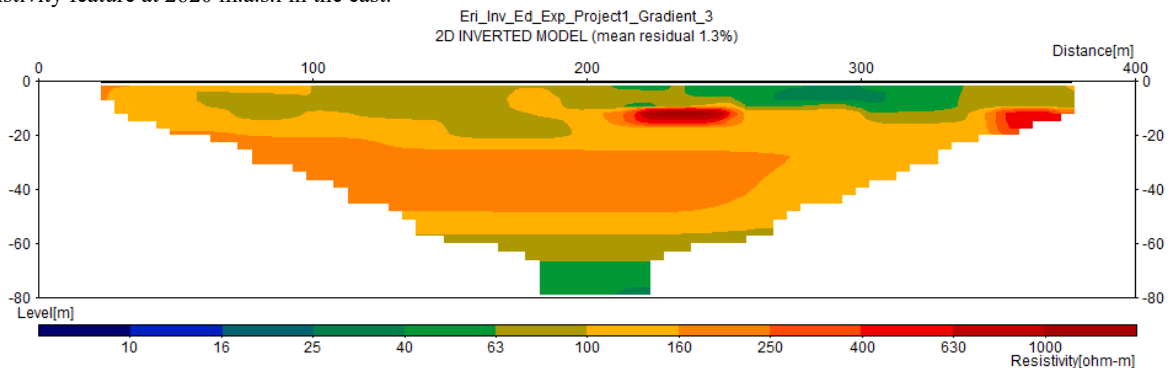

Fig 27. Profile E2 was performed long the same line as profile A for comparison. The depth of penetration in short ERT-lines are low compared to TEM (Gonzales et al. 2017a).

slightly greater thickness. Below the low resistivity layer, the ground is more heterogeneous with some parts increasing back up to 20 - 30 Ohmm while the southern part of the area experiences a less prominent increase in resistivity (~3 Ohmm). Unfortunately, the DOI is quite shallow (<200 m) which constrains further interpretations.

Profile 2 is complemented with an adjacent ERT-profile (Fig 25). The profile has a fixed depth of 140 m, regardless of signal strength. It displays a resistivity ranging from 100 – 400 Ohmm in the top 80 m, but it does not take topography into consideration and actual depth can vary a little. In the first 500 m of the profile the top 10 m are highly resistive (>630 Ohmm). Below 80 m the resistivity drops to 10 – 40 Ohmm. The dis-

tinct layer boundary is almost completely horizontal throughout the profile.

Profile A and B runs from west to east, cross-cutting profile 2. In profile A (Fig 26), the uppermost sediments have a resistivity of ~60 - 80 Ohmm, which makes the drop to ~30 Ohmm at 2680 – 2670 m.a.s.l, less prominent. The highly conductive layer at ~2630 m.a.s.l on the other hand is very well defined in both the layered and interpolated smooth models. Below this layer there is an interesting feature with higher resistivity in the east part (~80 Ohmm) while the western part of the profile continues to demonstrate low resistivities (1 – 5 Ohmm) until it reaches the DOI. A 400 m ERT- profile (Fig 27) was made along the same line as profile A. Because of its short measuring dis-
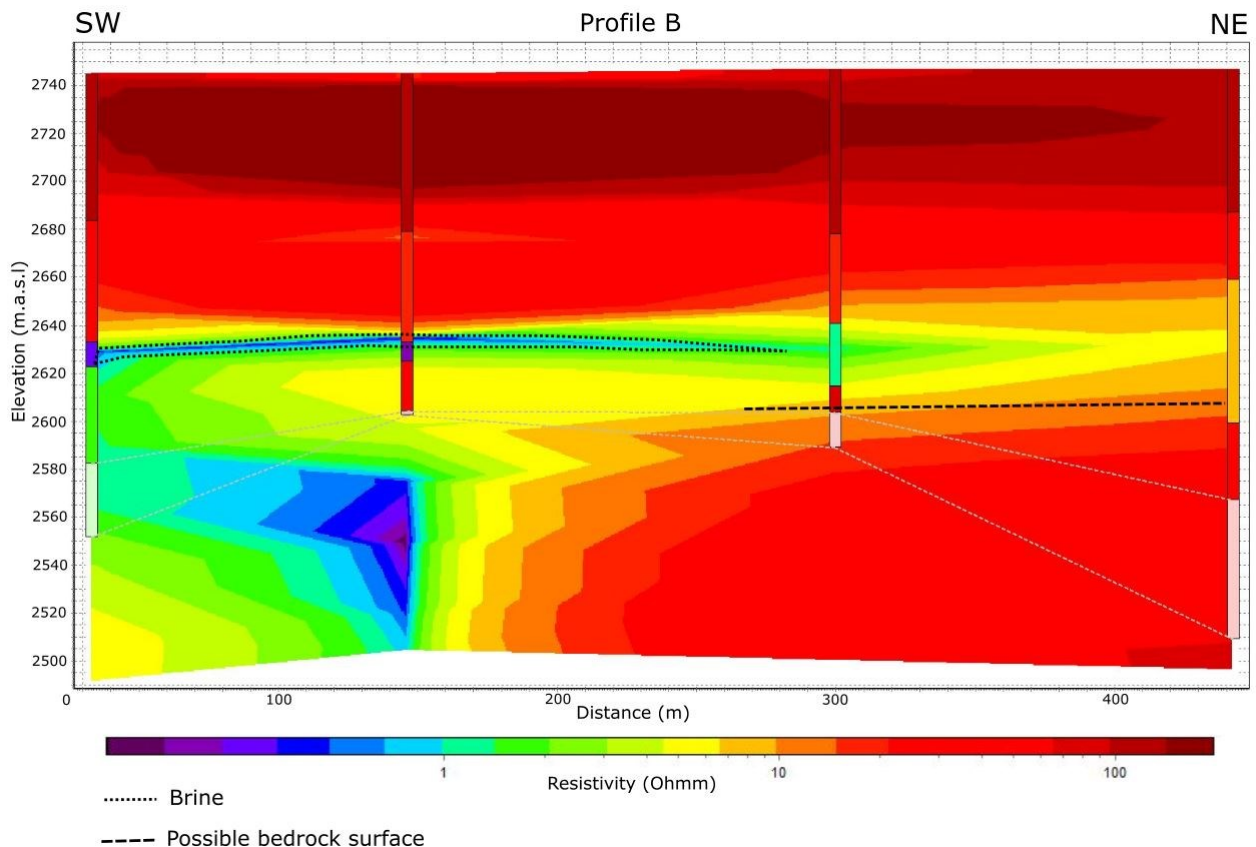
29

Fig 28. Profile B has no distinguished low resistivity layer in the east part of the profile. The upper boundary is prominent compared to profile A.
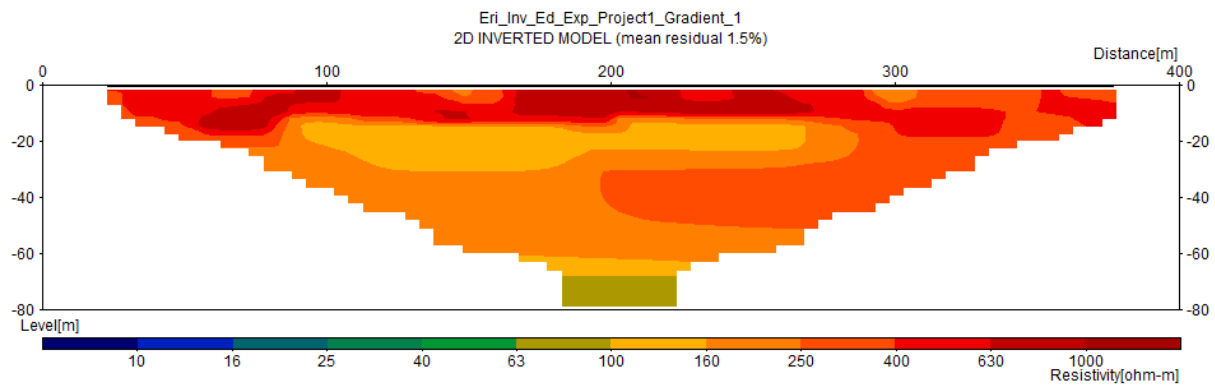

Fig 29. Profile E3 was made along the same line as Profile B. The high resistive layer in the top can be distinguished in both profiles, but E3 lack enough depth penetration to show the low resistive layers (Gonzales et al, 2017a).

tance, the depth of penetration is 80 m at best (centre of the profile), which restricts comparison. The profile indicates resistivities ranging from 60 – 200 Ohmm in the top layer and it just barely seems to reach slightly lower resistivity sediment (~40 Ohmm) in the middle.

Profile B (Fig 28) has a similar appearance to profile A, but with higher resistivity in the top 60 m (above 2685 m.a.s.l) just as profile 2. There is a sharp boundary with a drop from 100 - 120 Ohmm to ~20 Ohmm at 2685 m.a.s.l. The low resistivity layer is prominent in the western part of the profile and underlain by sediments with only slightly higher resistivity. Similar to profile A it demonstrates high resistivity just above the DOI in the eastern part. Profile B was

complemented by ERT-profile E3 (Fig 29), which is also 400 m long with a fixed depth of 80 m in the centre. It displays high resistivities of >400 Ohmm in the top 20 m, with lower resistivity (100 – 400 Ohmm) underneath. The depth of penetration is not great enough to distinguish any other layers, but there is an indication of a drop in resistivity (63 – 100 m) at 70 m depth in the centre of the profile.

Further illustrations from area A include two composites of horizontal maps at different depths (Fig 30). In this area each layer represents the mean resistivity over a 20 m depth interval. Note that the horizontal layers are not distributed to scale. The top layer is the mean resistivity between 2640 – 2660 m.a.s.l

30

(soundings performed at 2740 – 2765 m.a.s.l), where low resistivity (1 - 4 Ohmm) heterogeneities sits in sediments with resistivity >20 Ohmm. The heterogeneities are less prominent in the layered models, than in the smooth models, as they are less sensitive to minor vertical variations. In the second layer (2620 – 2640 m.a.s.l) there is a distinctive drop in resistivity, particularly in the southern part, which represents the low resistivity layer seen in profile 2, A and B. As the layers continue downwards the resistivity in the central part of the grids increases to 20 – 30 Ohmm, while the south-southwest corner continues to experience low resistivity values (1 – 3 Ohmm). The northern tip of the area has the same trend as the south-southwest corner with marginally higher resistivities.

4.2 Area B

After the exclusion of coupled soundings, area B yielded 62 layered models and 48 smooth models, which has been illustrated in 14 profiles, whereof two

are discussed in the results and the rest are found in appendix C. Horizontal grids as those in area A and a 1000 m ERT-survey were also produced to complement the TEM-profiles.

Profile 8 (Fig 31) was chosen to represent the north-south trend of area B, though the first 700 m of the profile do not have any smooth model data due to inadequate model fit in the north part. The topography in the area is almost constant at ~2715 m.a.s.l, which simplifies depth correlation. In the north part the first 50 – 60 m display a homogenous resistivity of 20 – 30 Ohmm, however this part does not have any smooth models in which heterogeneities are easier to identify. As the profile continues south a division in the top 60 m becomes more prominent with 20 – 30 Ohmm in the upper 30 m and 3 – 15 Ohmm in the lower 30 m. At 2650 m.a.s.l there is a 5 – 10 m thick layer with anomalously low resistivity, which is <0.1. Unfortunately, the DOI is very shallow (110 – 120 m) in this area which makes interpretations beneath the low resistivity
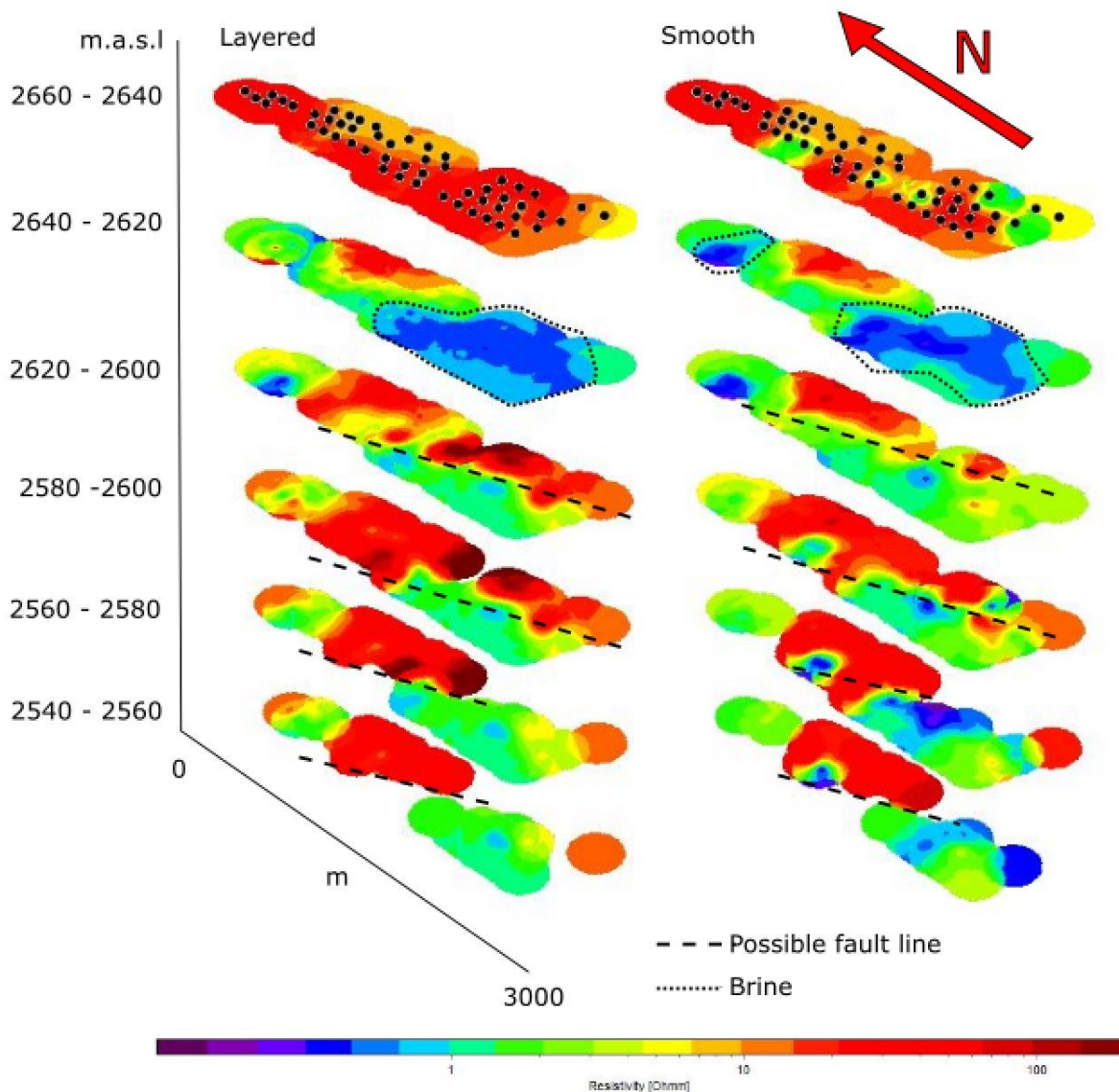

Fig 30. Horizontal maps of mean resistivity, based on the layered and smooth models respectively. Each layer represents an interval of 20 m. Note that the axes are not to scale. Both composite models display a distinct low resisitivity layer at 2640 – 2620
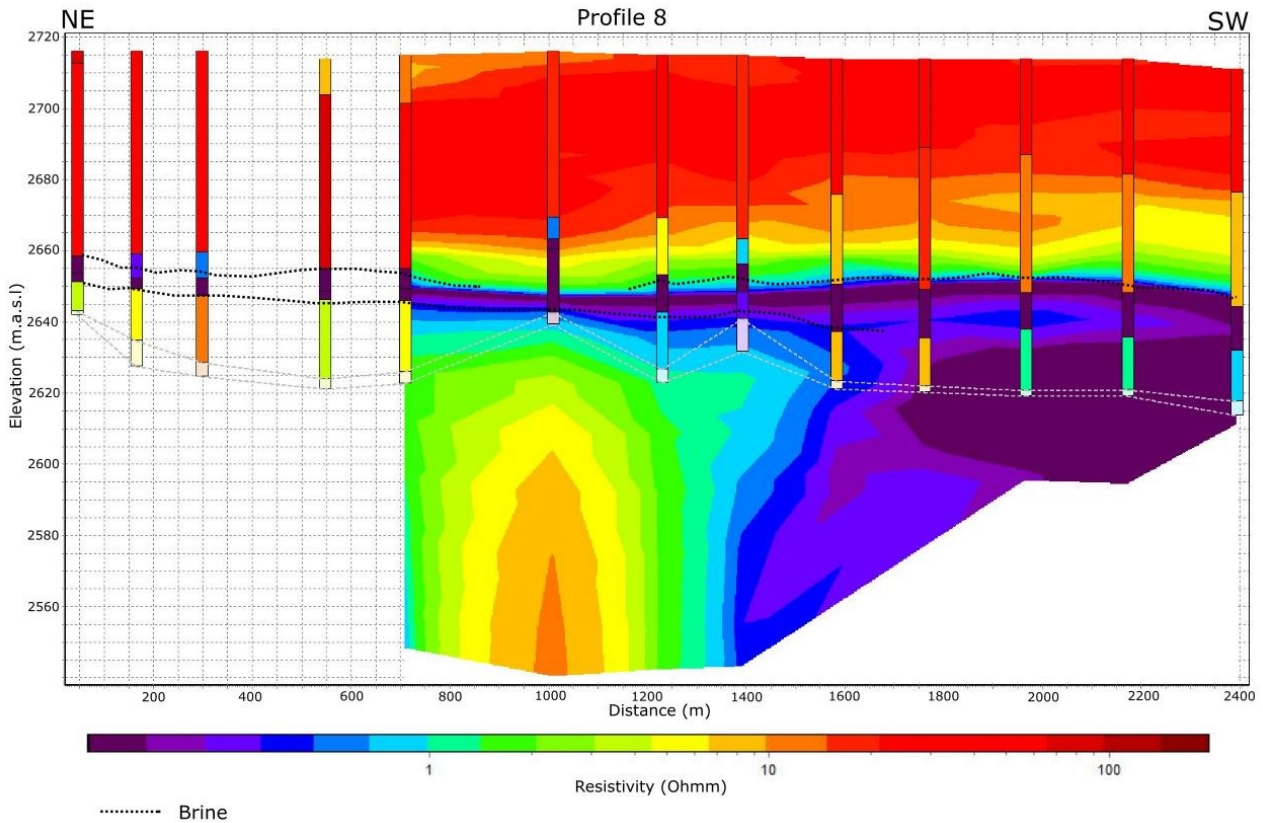
31

Fig 31. Profile 8 in area B. The northeast side do not have any smooth models with adequate fit (high data residual). There is a distinctive drop in resistivity at ~2660 m.a.s.l. In the south west there is a discrepancy between the layered and smooth models at ~2635 m.a.s.l.
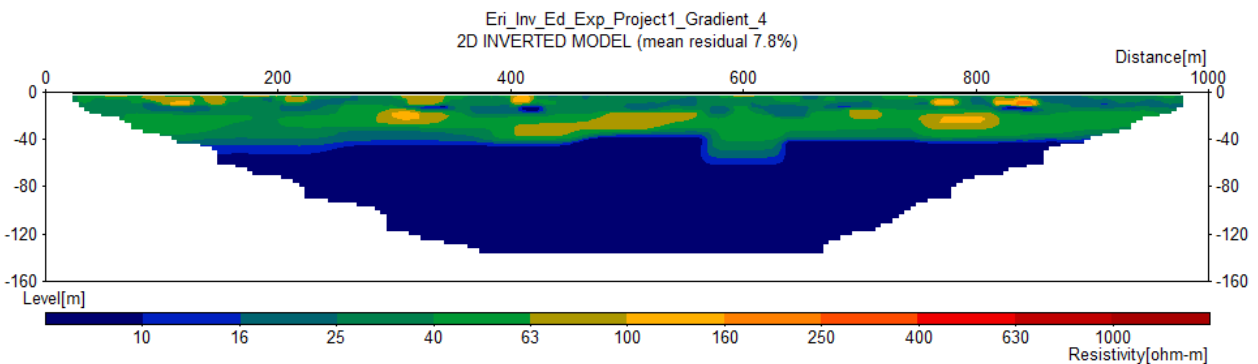

Fig 32. Profile E4 is almost parallel to profile 8 and can be used as comparison between TEM and ERT (Gonzales et al, 2017a)

layer difficult. There are however indications of slightly greater resistivity ranging from 1 – 10 Ohmm. ERT-profile E4 (Fig 32) was made along the same line, albeit shorter and only covers the central part of profile 8. This profile demonstrates resistivities ranging from 25 – 63 Ohmm, with local heterogeneities reaching 100 Ohmm and as low as 16 Ohmm. At 40 – 50 m depth there is a sharp boundary where the resistivity drops below 10 Ohmm. There are no apparent heterogeneities in this low resistivity layer.

Profile C runs perpendicular to profile 8 from west to east (Fig 33). It has similar characteristics as profile 8, but with the layers gently dipping towards the east. In the western part there is 25 m of sediment with 20 – 30 Ohmm resistivity that become successively thicker

towards the east, where they reach a thickness of ~45 m. The resistivity decreases with depth until 2660 m.a.s.l, where the values abruptly drop to <0.1. This low resistivity layer is no more than 10 m in the west and gently dips towards the east where it becomes slightly thicker. Below this horizon there is a marginal increase (~1 Ohmm) in resistivity before reaching the DOI.

The horizontal grids in this area are made in 10 m intervals due to the limited DOI (Fig 34). Unlike the grids in area A, these grids do not represent continuous intervals. The first two layers represent near surface sediments between 2705 – 2695 and 2685 – 2675 m.a.s.l. They indicate very little lateral variance in the resistivity, ranging from 20-30 Ohmm, even though
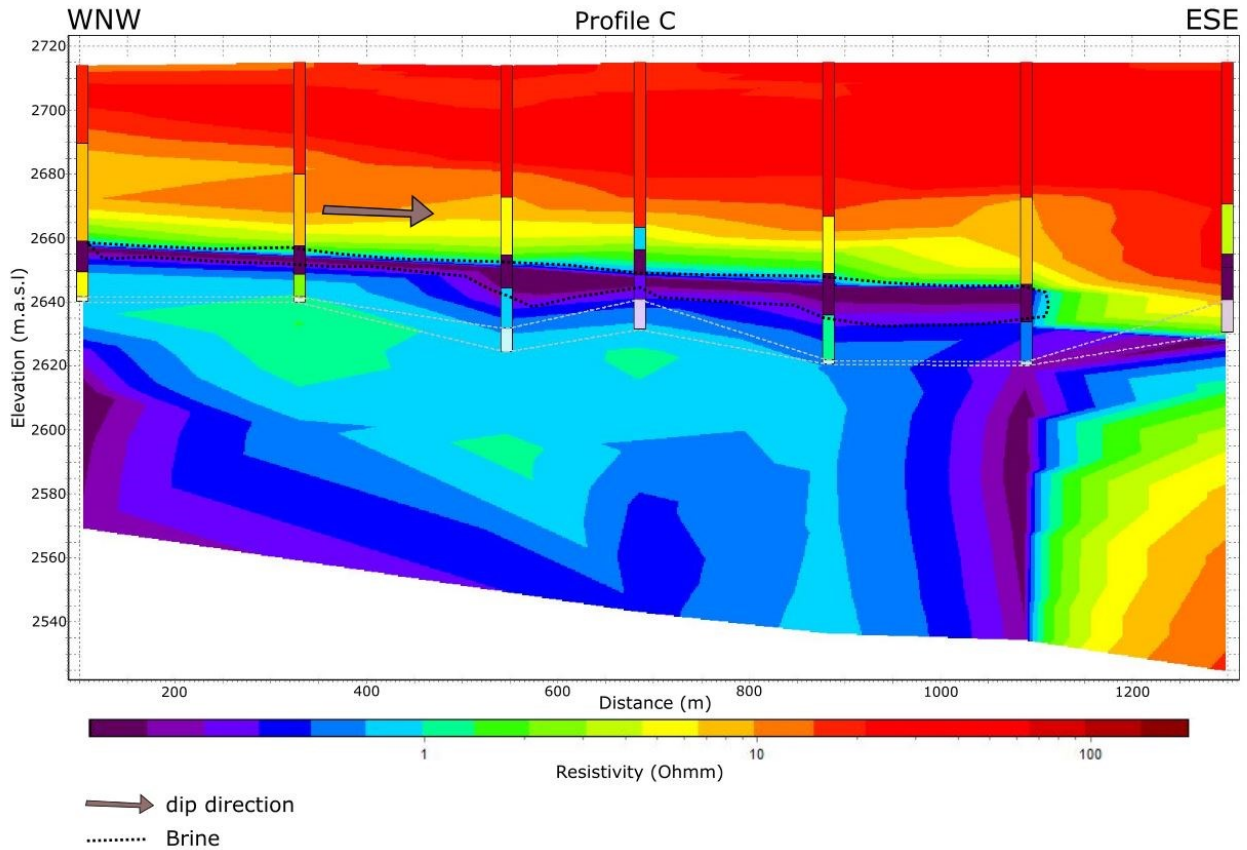
Fig 33. Profile C is drawn perpendicular to profile 8 and indicates a gentle eastward dip of the layer boundary.

there is a trend of slightly lower values in the west part of the second grid. In the third grid (2665 – 2655 m.a.s.l) there is a transition towards lower resistivity, with the lowest values in the west part of the area. Continuing downwards, the fourth grid (2655 – 2645 m.a.s.l) displays very low resistivity (<0.1) in most of the area. There is some discrepancy between the smooth models and the layered models, with the layered having slightly higher resistivity in the south corner and the smooth models having higher resistivity in the east corner. The two remaining layers (2645 – 2635 and 2635 – 2625 m.a.s.l) demonstrate a trend of slightly increasing resistivity spreading east-southeast from the west-northwest part of the area.

5 Discussion

The general trend of the study area has been interpreted as moderately resistive alluvium overlying a high conductive clay, with a thin layer of anomalously low resistivity separating them. Due to the highly conductive material the electromagnetic signal effectively disperses, in what is assumed to be the lacustrine clay, which restricts the depth of penetration. In areas with highly resistive formations the signal can propagate freely without dispersion, allowing it to reach greater depths. With a DOI ranging from 150 m to a best case scenario of 250 m in area A, and an average of 90 m in area B, there is no possibility of finding the general depth of the bedrock. There are however other aspects to be discussed in the results.

In both investigated areas there is a thin distinctive layer with very low resistivity which cannot be re-solved in the ERT-profiles. Profile E1 does not penetrate deep enough to reach the horizon, but in area B the reason it does not show in the profile E4 is that the vertical resolution of the method (with 10 m electrode spacing) is not good enough to separate thin (<10 m) formations, and signal from the layer has been added to a mean resistivity of the over and underlying strata. It is worth noting that there are discrepancies in the measured values between TEM and ERT, even though they display the same trends. For example, profile 2 and E1 indicate the same trend with higher surface resistivities in the north part of the area A, but the TEM indicates ~200 Ohmm while ERT indicate >630 Ohmm. In this particular case the ERT is most likely more reliable as TEM is optimal for finding low resistivity formation, and cannot distinguish between higher resistivities (>~250 Ohmm). However, when it is the opposite conditions TEM is most likely more reliable as it has higher sensitivity to variations within highly conductive material. In Area B the ERT indicates a completely homogenous formation with a resistivity <10 Ohmm below 40 – 50 m, while TEM distinguishes a layer with resistivity <0.1 Ohmm within highly conductive sediments both over and under said horizon. It is important to understand that the results for the smooth models are interpolated, and therefore the spatial distribution of the variations might not be completely accurate. When interpreting TEM results one must also keep the model equivalence problem in mind, as a data set can have equal fit to several models with slight variations. To illustrate the similar trends, but varying values, wire line resistivity logs from two wells (see P019 and P021 in fig 2), adjacent to the
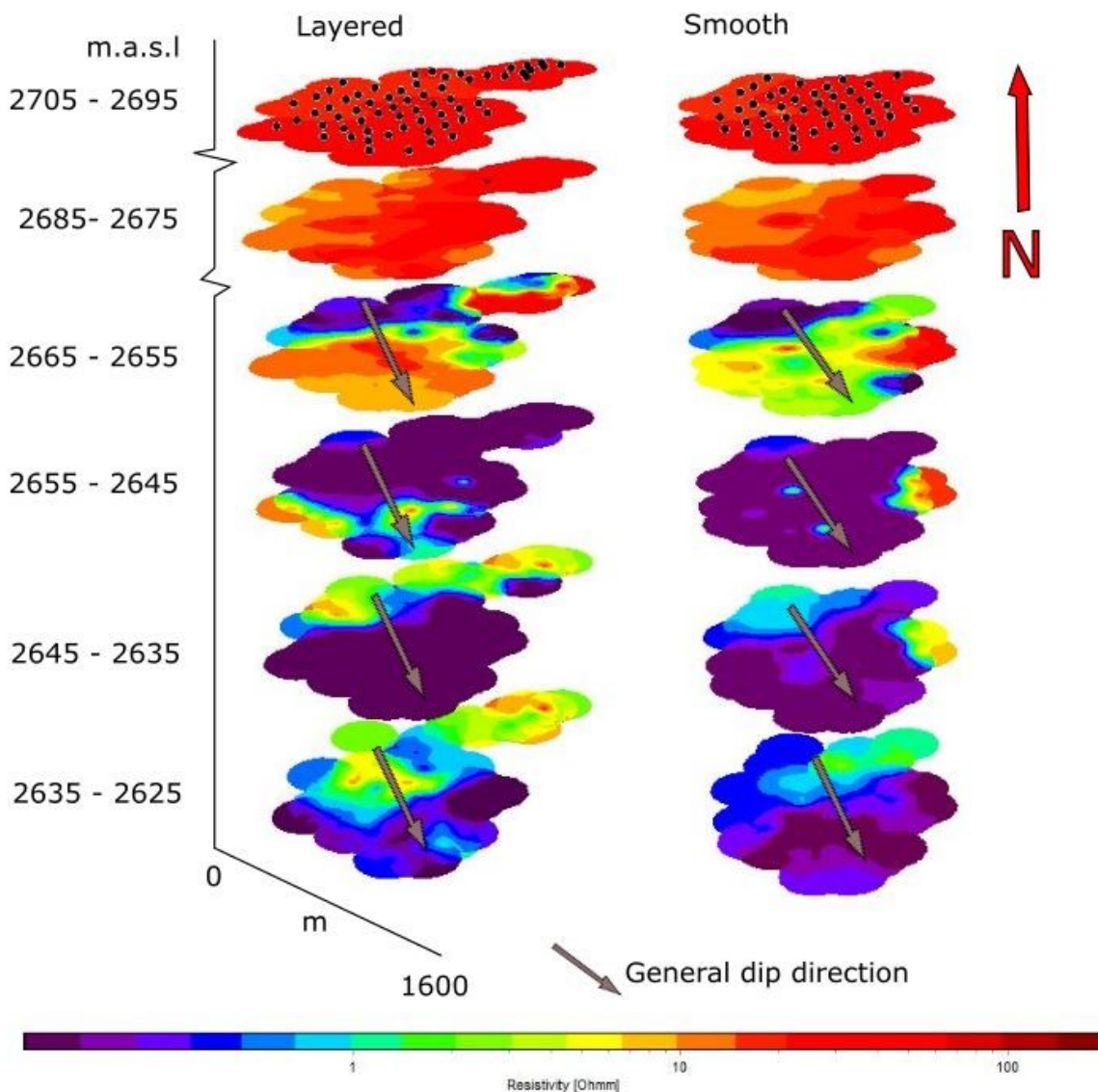
33

Fig 34. Horizontal maps of mean resistivity for the layered and smooth models respectively. Each layer represents an interval of 10 m. Note that the axes are not to scale and the layers are not in a continuous succession. At 2665 – 2655 m.a.s.l a very low resistivity feature becomes apparent in the northwest part, which propagate to SSE with increasing depth.

profiles in area A, are compared to the ERT and a TEM sounding in fig 35. It is evident that the ERT is less sensitive to very low resistivity values compared to TEM. The wire line log undoubtedly has the best vertical resolution, but it only shows the resistivity along the well walls. It is also a costly and time consuming method as deep wells needs to be drilled and logged before a well casing can be put in place.

There are only two types of geological formations that can yield resistivity lower than 0.1. One is massive sulphides with conductive metals, and the other is accumulation of brine (Unsworth, 2014). The former is not plausible in an alluvial fan setting, which leaves us with brine. This theory is on par with the general climatic and geological setting. Salinization of the surface occurs when the evaporation is high during the dry season, leading to accumulation of water soluble

salts such as chlorides, sulphates, sodium carbonates, magnesium and calcium (Metternicht & Zinck, 1996). During the rainy season these salts are dissolved and infiltrate the aquifer. Due to the higher density of saline water, these brines sink to the bottom of the aquifer where they accumulate on top of an aquiclude. Salinization of the surface can also be caused by anthropogenic factors such as deforestation or irrigation with brackish water (Metternicht & Zinck, 1996), but that is not a factor in the studied area. Water samples, analysed by Gonzales et al. (2017a), show there is an increased concentration of sodium and chloride in many parts of the Punata area, which further supports the conclusion.

Except for an indication of high salinity in the lower groundwater, the brine holds valuable information about the aquifer properties. In profile 2 there is a clear
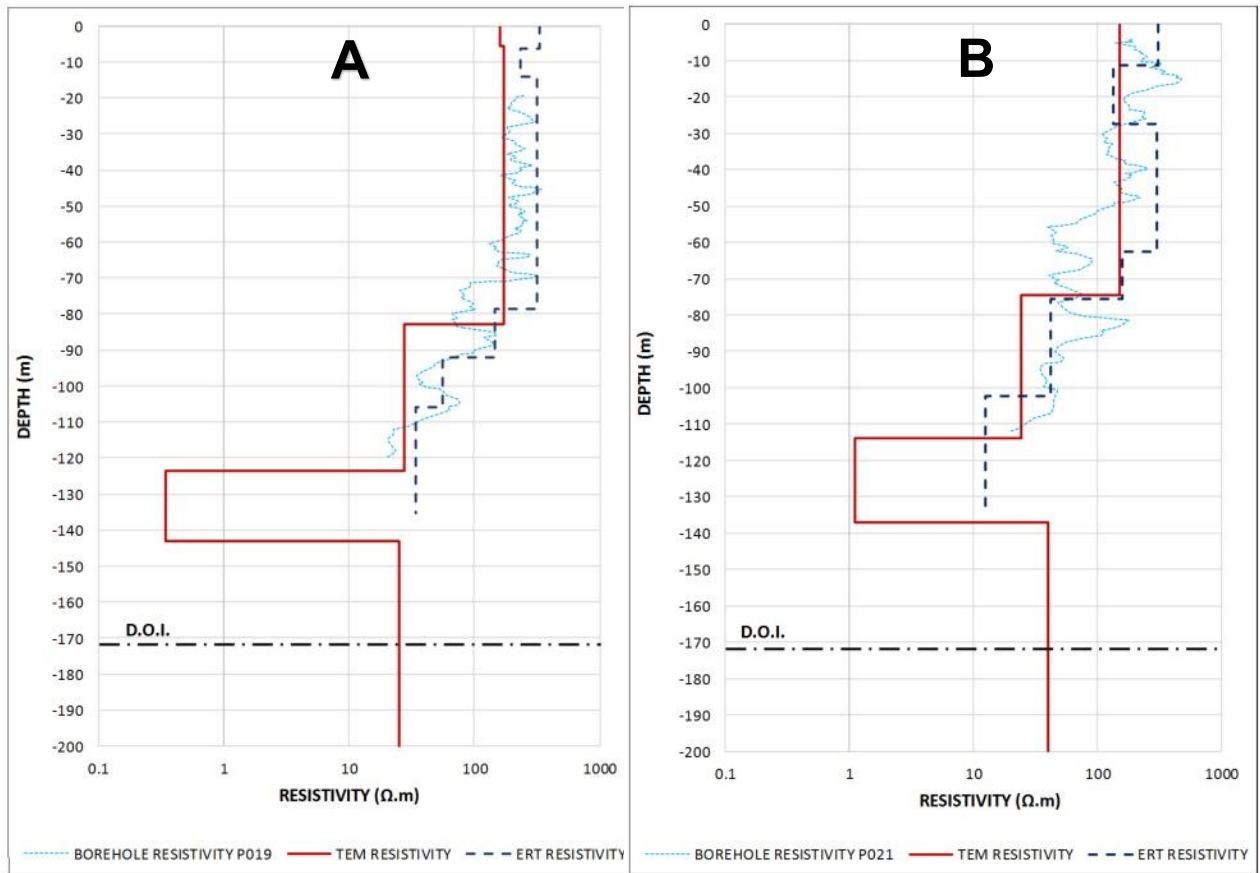
Fig 35. The graphs are composites of layered TEM models, ERT and measure wire line in adjacent wells. A is well P019 and B is well P021 (Gonzales et al. 2017b).
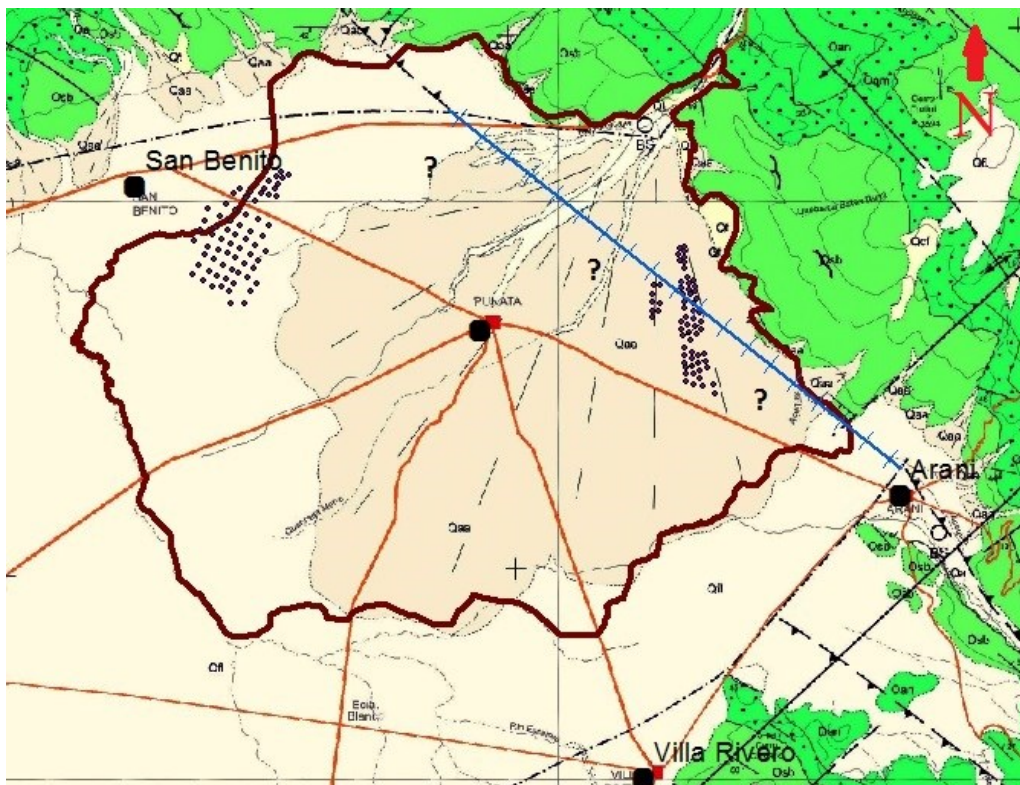

Fig 36. The extrapolated line (blue) between the faults to the northwest and southeast cuts through area A along the boundary between high and low resistivity. This could indicate a possible fault under the alluvial fan. (Based on map from SERGEOTECMIN, 2011)

drop from 160 – 200 Ohmm to 20 – 30 Ohm at 80 – 100 m depth. By correlating this with the Wasa Mayu borehole it is likely that the sudden drop in resistivity corresponds to the boundary at 100 m between the silty sand and clayey sand, which has previously been thought to be the bottom of the aquifer. The fact that the brines accumulate on what is then most likely the clay/silty clay boundary, at 150 m in the Wasa Mayu, it is safe to assume that the clayey sand is permeable/ semi-permeable and, at least to some extent, acts as groundwater depository.

The brine also leads to a few assumptions regarding the groundwater in area B. By looking at the horizontal maps of the area one can discern the eastward sloping trend, which is evident in profile C (Fig 33). In the third layer from the top there is brine in the west corner and as the depth increases the brine moves eastward and the resistivity in the western part increase slightly to represent the lacustrine clay. This suggests that there is a threshold west of the study area that prevents the brine from flowing out through the, now dry, springs that were mentioned in the background section, and thus has remained undetected until now.

There are some possible interpretations to be made from the horizontal maps in area A as well. In all layers except the top one there is a salient high resistive area in the centre of the model (Fig 30) which extends well below the brine layer. This could possibly represent the bedrock in the form of a fault in the San Benito Fm. The high resistivity indicates that it is not lacustrine clay as could be expected below the brine. This leaves the options of coarse grained sediment, as suggested in the conceptual model (Fig 8), or bedrock. With the newly discovered presence of the brine layer, it seems unlikely that it is coarse sediments because then the brine would continue to sink. The fact that it stays in place suggests that it impermeable bedrock. As previously mentioned the San Benito Fm. consists of mostly quarzitic sandstone and the measured resistivity (60 – 200 Ohmm) fits within the range of possible resistivities of such lithology. According to SER-GEOTECMIN (2011) there is a fault line that ends when it reaches a lineation northwest of the fan, as well as a fault line ending south east of the fan. If the fault line is extrapolated between the two lines, it cuts straight through the study area (Fig 36), with the same general angle as the southern limitation of the high resistive patches in the grids. However, it is not possible to draw any affirmative conclusions to corroborate the hypothesis without further investigations and an in depth analysis of the tectonic movements in the area.

6 Conclusions

♦ The main objective of the survey could not be conclusively achieved due to inadequate depth of investigation (DOI) in the soundings. In area A the DOI Varied between 150 m in the shallowest soundings to 250 m in the deepest, with an average of ~170 – 180 m. High resistivity allows the signal to propagate deeper than low resistive layers which disperses the signal. In area B the DOI was shallower still, with a consistent depth of ~90 m. The shallower depth in area B is attributed to a lesser amount of alluvium which makes the clay appear earlier in the strata.

♦ A brine layer on top of the lacustrine clay was identified. The brine is likely produced by resolution of water soluble salts that accumulate in the soils during the dry season, due to high evaporation. The brine infiltrates the unconfined aquifer and due to higher density than fresh water it sinks to the bottom of the aquifer.

♦ The position of the brine on top of the clay indicates that the clayey sand between 100 – 150 m in the Wasa Mayu borehole is at least semi-permeable and acts as a groundwater depository, not an aquiclude as previously thought.

♦ The eastwards sloping trend of the strata in area B keeps the brine from flowing out in through the former springs on the west side of the fan.

♦ The high resistivity feature extending below the brine layer in area A is likely to be bedrock as coarse grained sediment would allow water to infiltrate. By extrapolating the fault lines to the northwest and south east of the fan, a possible fault line cuts through the study area. Further investigations need to be performed in order to corroborate or discard the hypothesis.

8 References

Aarhus GeoSoftware. 2015: Getting started with ViewTEM. *Abem Instruments Ab,* 27 pp.

ABEM Instrument AB, 2014: WalkTEM User Guide. *Sundbyberg: ABEM Instrument AB.* Retrieved: 2016-04-27, from: http://www.guidelinegeo.com/support/resource-center/?qs_product=245&qs_types=44

CENTRO-AGUA, 2012. Desarrollo de capacidades y fortlecimiento organizativo para la gestión del agua en la Cuenca pedagógica Pucara. *Universidad Mayor de San Simon*, Cochabamba. 21 pp.

Christiansen, V. A., Auken, E., Sørensen, K. 2009: The transient electromagnetic method. *In:* R. Kirsch (ed.), *Groundwater geophysics a tool for hydrogeology.* p.179-225. Berlin: Springer (chapter in book)

Danielsen, J. E., Auken, E., Jørgensen, F., Sønder gaard, V. & Sørensen, K. I., 2003: The applica tion of the transient electromagnetic method in hydrogeophysical surveys. *Journal of Applied Geophysics 53*, 181-198. doi: http://dx.doi.org/10.1016/j.jappgeo.2003.08.004

GEOBOL, 1983: Estudio geologico de la hoja de pun ata cuadrangulo no 6441. GEOBOL, La Paz, Bolivia. 25 pp.

Gonzales, A. S., Dahlin, T., Barmen, G., Rosberg J-E. 2016a: Electrical Resistivity Tomography and Induced Polarization for Mapping the Subsur face of Alluvial Fans: A Case Study in Punata (Bolivia). *Geosciences, 6.* doi: 10.3390.geosciences6040051

Gonzales, A. S., 2017a: Analyzing the recharge pro cess and flow patterns in the semi-arid Punata alluvial fan (Bolivia) by hydrochemical and stable isotope data. *Applied Geochemistry*. [in prep]

Gonzales. A. S., 2017b: Delimiting a brackish? layer in a quaternary fluvial-alluvial deposit using Time Domain Electromagnetic [in prep, prelim inary title]

Huggett, R. J. 2011: *Fundamentals of Geomorphology 3rd edition*. Routledge, London and New York. 516 pp.

Loke, M.H., 2013. Tutorial 2-D and 3-D electrical imaging surveys. Dr. M.H. Loke. Retrieved: 2016-10-01, from: http://www.geotomosoft.com/coursenotes.zip. [pdf].

Mårdh, J. 2016: WalkTEM-undersökning vid Revinge hed provpumpningsanläggning. *Examensar beten i geologi vid Lunds Universitet 476*, 1 - 38

McNeill, D. J., 1980: Technical note TN-7 *Application of transient electromagnetic techniques.* Ontar io: Geonics Limited. Retrieved: 2016-05-06, from: http://geonics.com/html/technicalnotes.html

McNeill, D. J., 1980: Technical note TN-7 *Application of transient electromagnetic techniqies.* Ontar io: Geonics Limited. Retrieved: 2016-05-06, from: http://geonics.com/html/technicalnotes.html

Metternicht, G. & Zinck, J. A. 2010: Spatial discrimi nation of salt- and sodium-affected soil surfac es. *International Journal of Remote Sensing*, 18, 2571 – 2586. doi: http://dx.doi.org/10.1080/014311697217486

Montenegro, E. & Rojas, F. 2007: Potencial hidrico superficial y subterraneo del abanico de punata. Universidad Mayor de San Simon, Cochabam ba, Bolivia. 73 pp.

Nilsson, P. 2013: Grundvattenundersökningar i Skåne: Transient Elektromagnetisk Sondering. ISRN: LUTVDG/TVTG 5132/1-88/2013. Lund: Lunds Tekniska Högskola. 118 pp.

Renner, S. & Velasco, C. (CABAS). 2000: *Geology and Hydrogeology of Central Valley of Cocha bamba. Boletin del servicio nacional de geolog ica y mineria 34. 125 pp.*

Reynolds, J. M., 2011. *An Introduction to Applied and Enviromental Geophysics 2nd edition.* John Wiley & Sons Ltd., Essex. 696p.

Saldías, C., Speelman, S., Van Huylenbroeck, G. 2013: Access to Irrigation Water and Distribut ion of Water Rights in the Abanico Punata, Bolivia. *Society & Natural Resources*, 26, 1008 – 1021. DOI: http://dx.doi.org/10.1080/08941920.2012.7296 51

SERGEOTECMIN, 2011: Mapa geologico de Puna ta/geological map of Punata. Publicacion DGTM serie-i-cgb-65. 1:100 000. La Paz, Bo livia

UNDP-GEOBOL, 1978: Proyecto integrado de recur sos hidricos: Investigaciones de agues sub terráneas en las cuencas de Cochabamba. Co chabamba, Bolivia. 316 pp.

Unsworth, M. 2014. 2014: Geophysics 424 – Universi ty of Alberta. Retrieved: 2016-05-06, from https://www.ualberta.ca/~unsworth/UAclasses/ 424/notes424-2014.html

Personal communication

Auken, E. 2016: Professor with Special Responsibili ties, Department of Geoscience, Aarhus Univ ersity. [Personal communication], September

Foged, N. 2016: Academic staff, Department of Geo science, Aarhus University. [Personal commu nication], April, August and September

Sørensen, K. I. 2016: Professor Emeritus, Department of Geoscience, Aarhus University. [Personal communication], August

Lecture material

Jeppson, H. 2013: Electromagnetic waves, lecture ma terial. Lund University. [unpublished]

Appendix

There are four appendixes accompanying this paper.

App. A is a map with the spatial distribution of salinity/alkalinity in the top soils of Valle Alto. It is based on Landsat data from Metternicht & Zinck (2010).
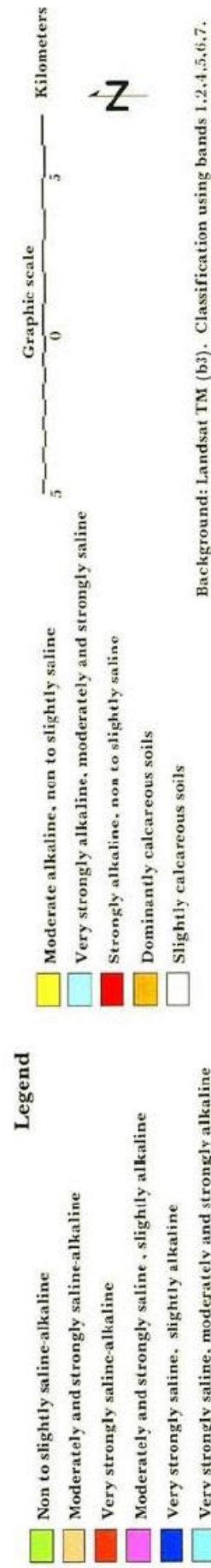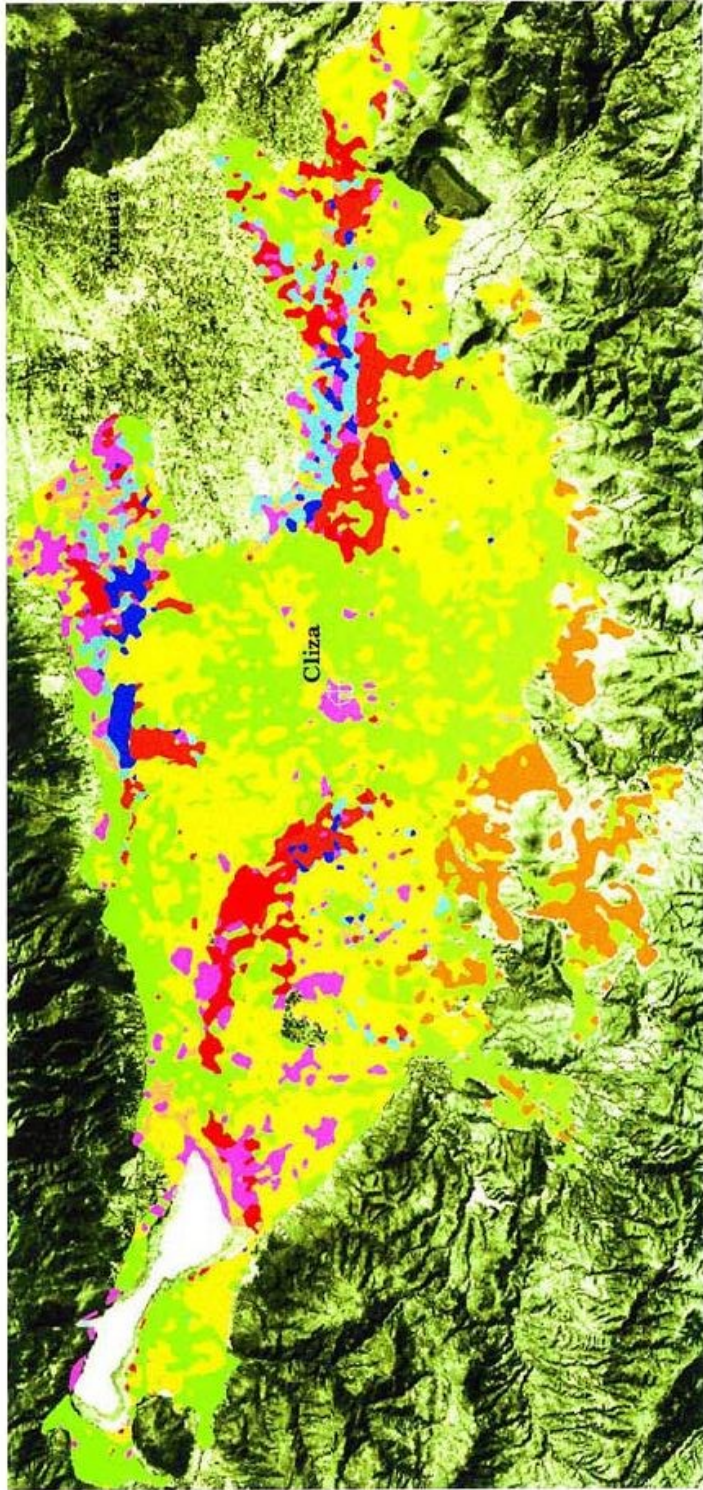
App. B contains the remaining vertical profiles in area A, with nr. 1 being the westernmost profile (see fig 23).

App. C contains the remaining profiles in area B. All the numbered profiles are NE—SW while profile D runs NW—SW.

App. D is the geologic map made by SERGE-OTECMIN (2011)

Appendix A

Landsat imaging of the salinity/alkalinity in the top soils in Valle Alto (Metternicht & Zinck, 2010).

Legend

- Non to slightly saline-alkaline
- Moderately and strongly saline-alkaline
- Very strongly saline-alkaline
- Moderately and strongly saline , slightly alkaline
- Very strongly saline , slightly alkaline
- Very strongly saline, moderately and strongly alkaline

- Moderate alkaline, non to slightly saline
- Very strongly alkaline, moderately and strongly saline
- Strongly alkaline, non to slightly saline
- Dominantly calcareous soils
- Slightly calcareous soils

Graphic scale

Kilometers

Background: Landsat TM (b3). Classification using bands 1,2,4,5,6,7.

Appendix B

This appendix contains the three reamining profiles made in area A.

Profile 3
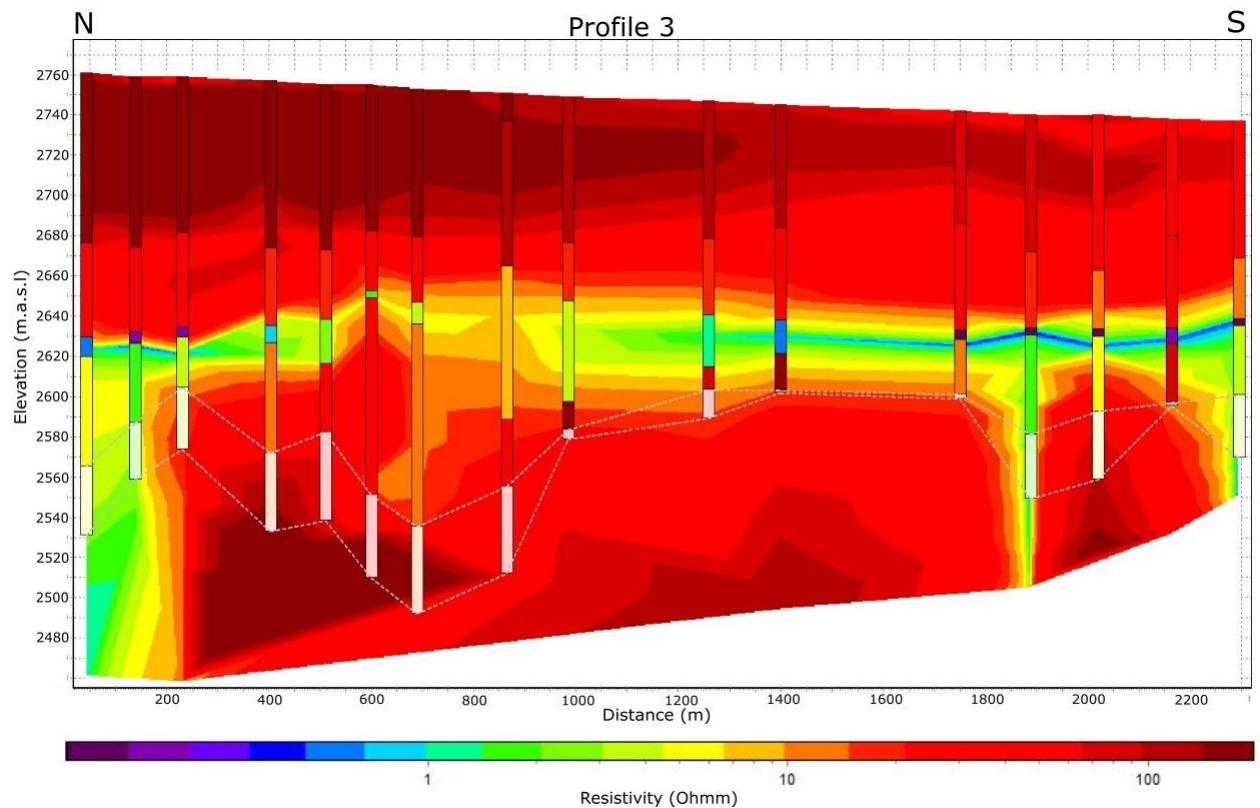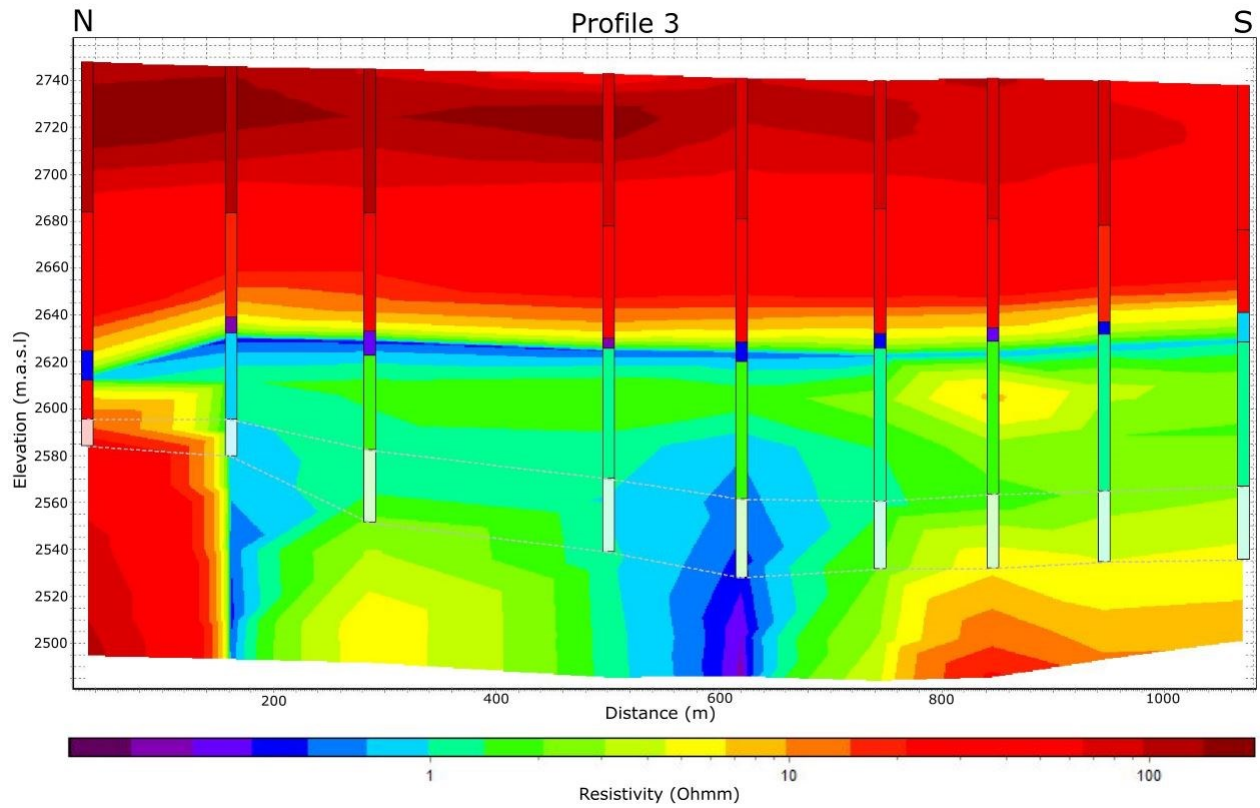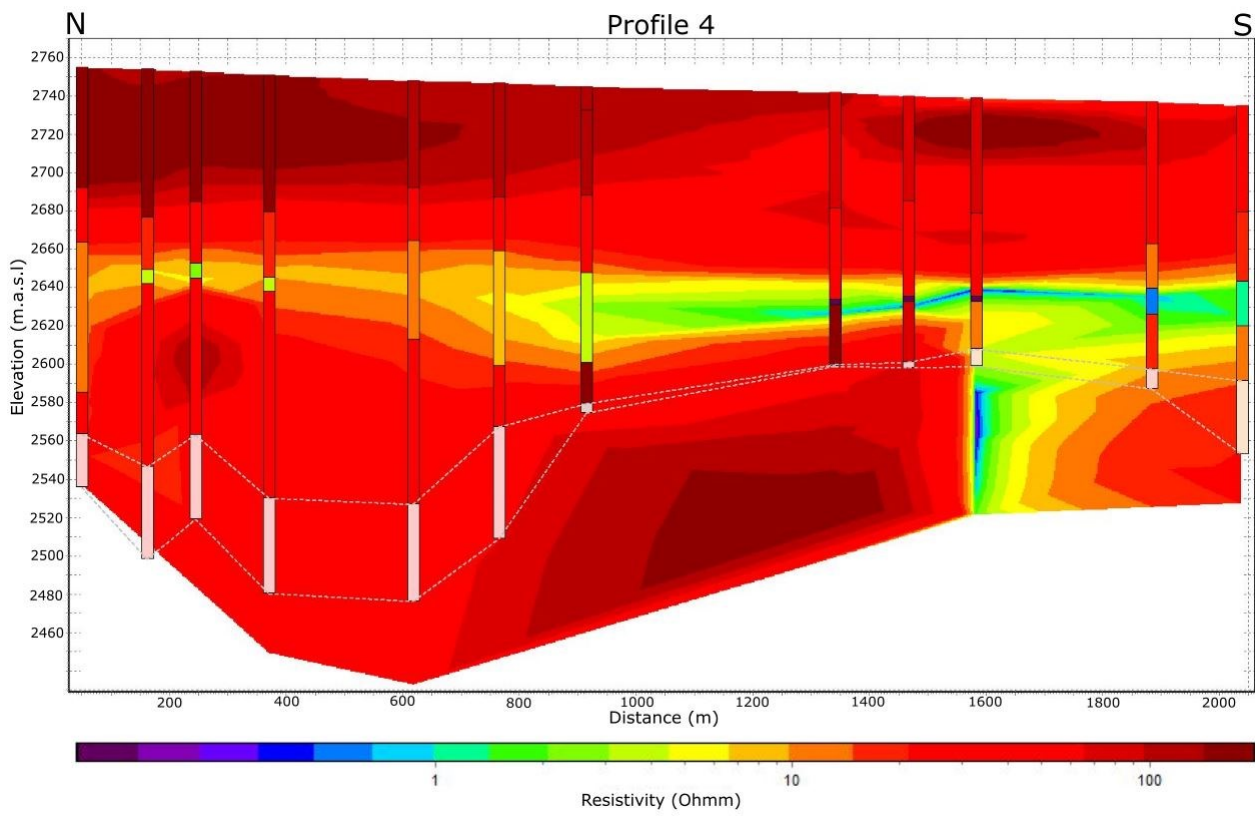
Profile 3

Profile 4

Appendix C

The eight remaining profiles from area B are simililar to profile 8 in most regards. Note that the last profile in this appandix do not follow the same geographical direction as the other profiles.

Profile 7

Profile 9

Profile 10

Profile 11

Profile 12

Profile D
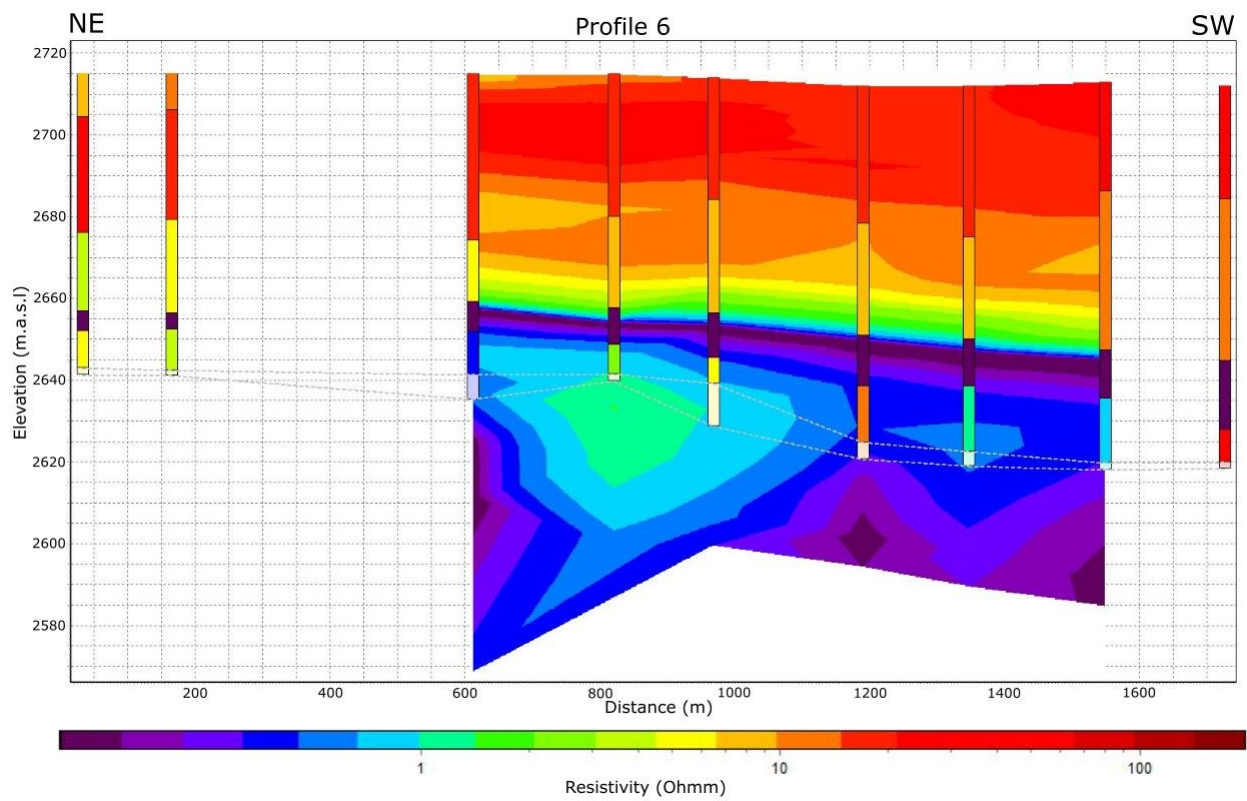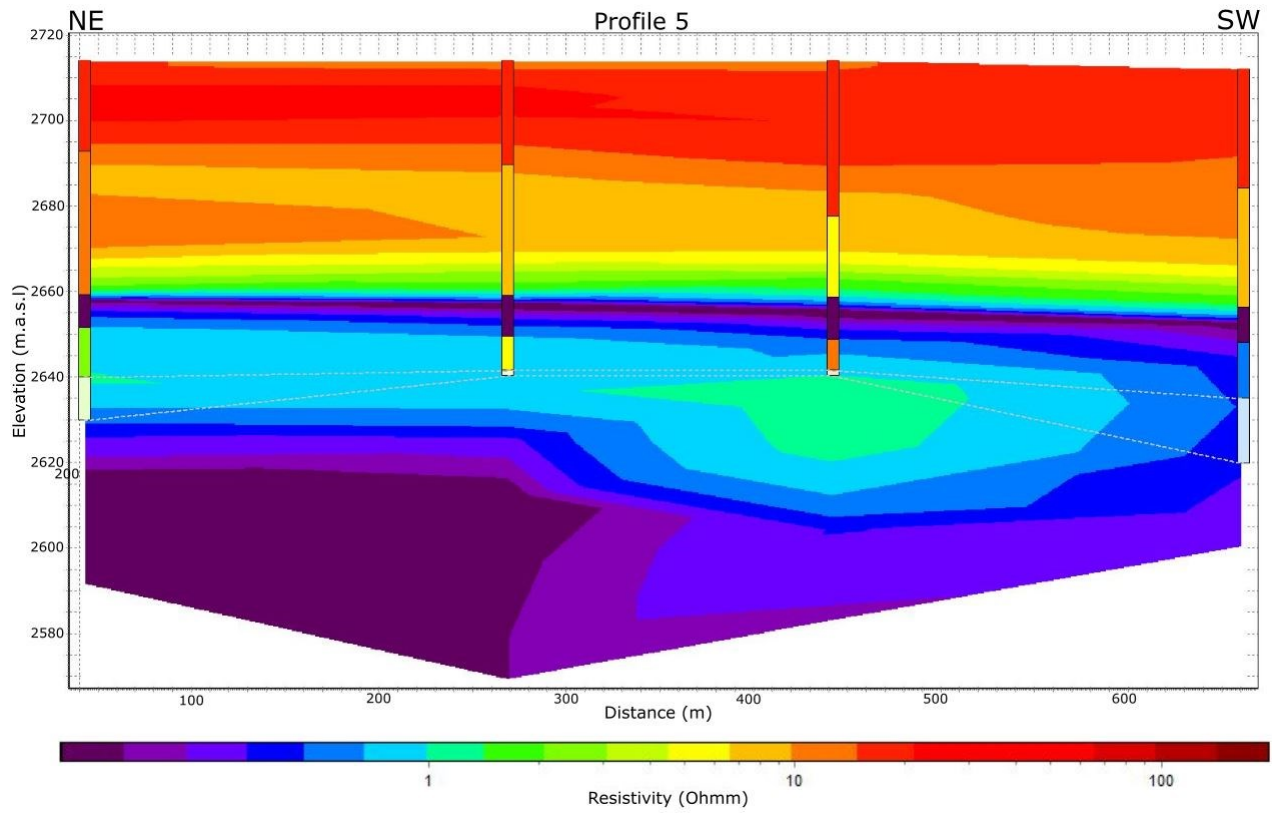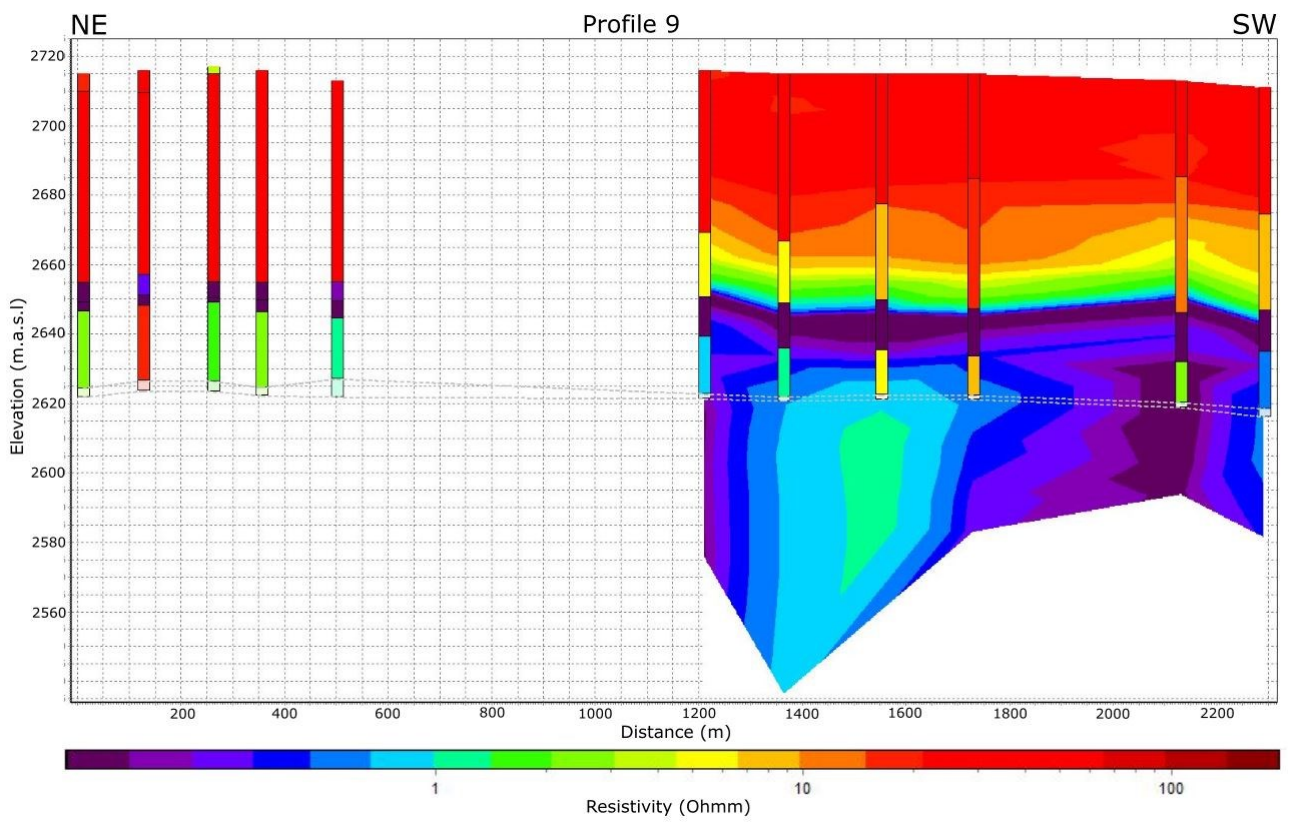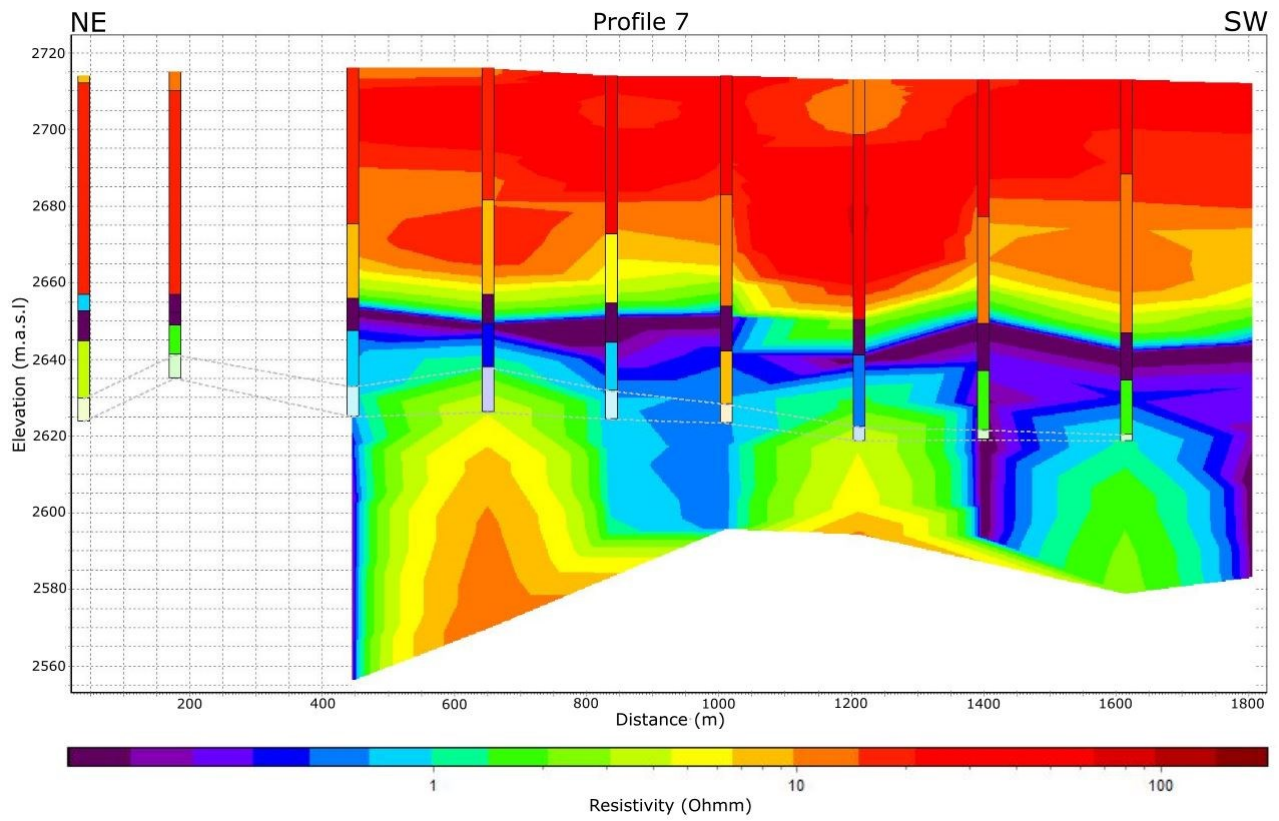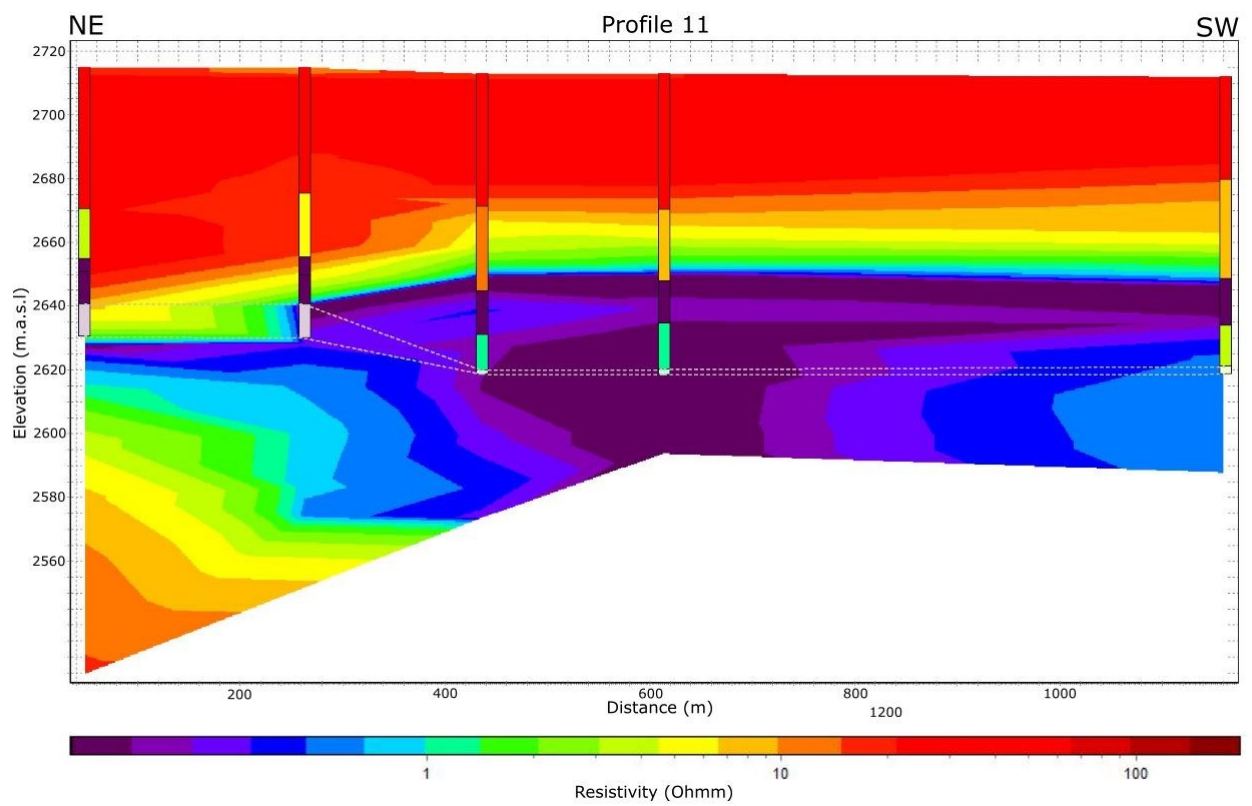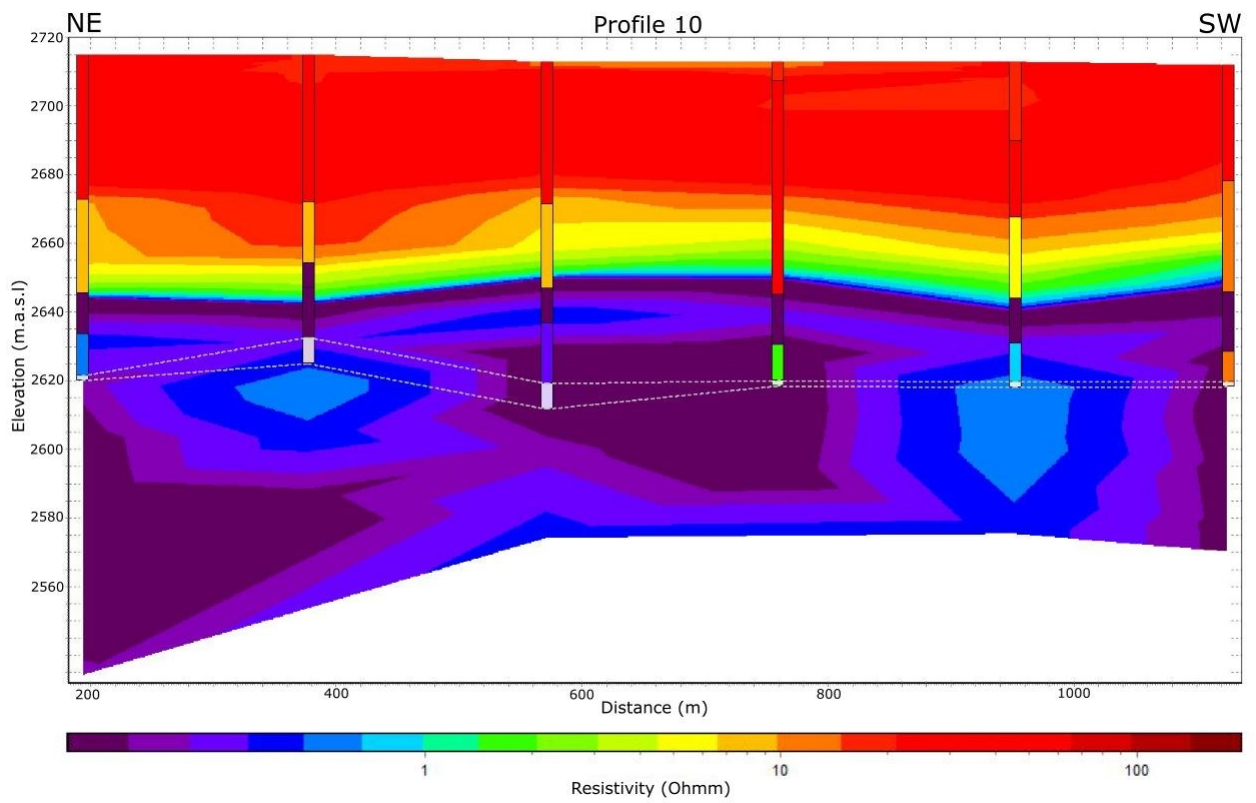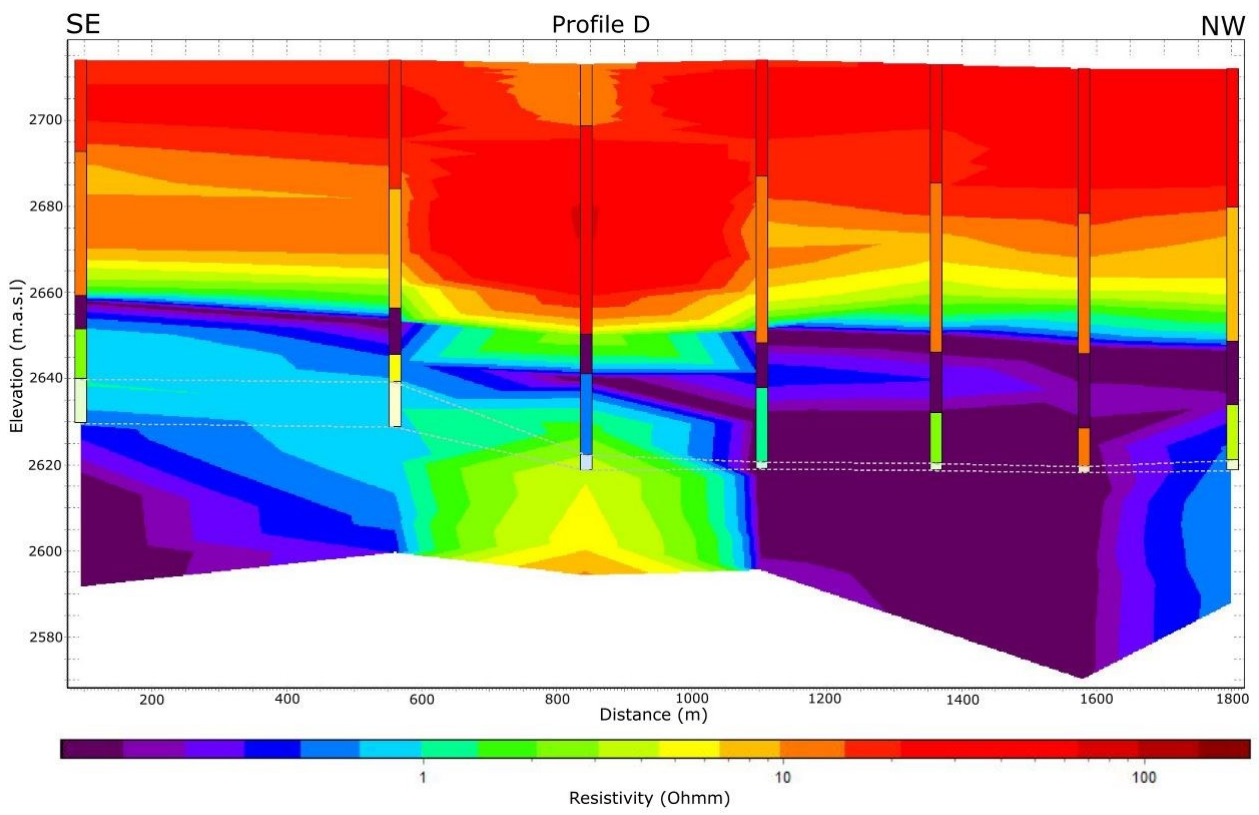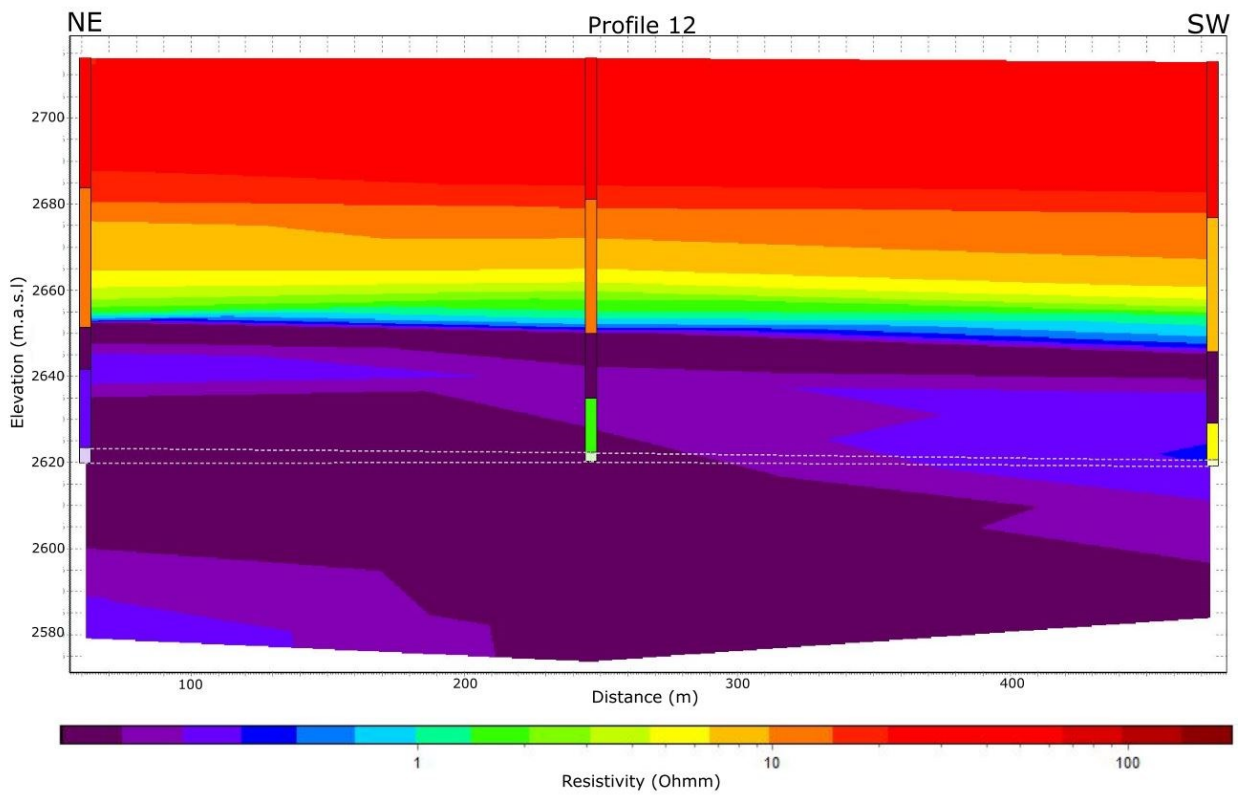
Appendix D

The geologic map from SERGEOTECMIN (2011) with the Puanata alluvial fan in the bottom left corner. Map legend can be found on the next page.

COLUMNA CRONO-ESTRATIGRAFICA
CHRONOSTRATIGRAPHIC COLUMN

	ERA	SISTEMA PERIODO	SERIE EPOCA	ORONGENIA

Chronostratigraphic column (left side):

- CENOZOICO
  - CUATERNARIO
    - PLEISTOCENO — HOLOCENO
  - NEOGENO
    - PLIOCENO
    - MIOCENO
  - PALEOGENO
    - OLIGOCENO
    - EOCENO
    - PALEOCENO
- MESOZOICO
  - CRETACICO (SUP. / INF.)
  - JURASICO (SUP. / MED. / INF.)
  - TRIASICO (SUP. / MED. / INF.)
- PALEOZOICO
  - PERMICO (SUP. / INF.)
  - CARBONIFERO (SUP. / MED. / INF.)
  - DEVONICO (SUP. / MED. / INF.)
  - SILURICO (SUP. / INF.)
  - ORDOVICICO (SUP. / INF.)

Orogenias: A N / D / I / N (ANDINA), A (ANDINA), HERCINICA, CALEDONICA

Ma scale values: 2,6 · 23,0 · 65,5 · 45,5 · 99,6 · 251,0 · 299,0 · 359,2 · 416,0 · 443,7 (approx)

Sin relación de escala
No scale proportion
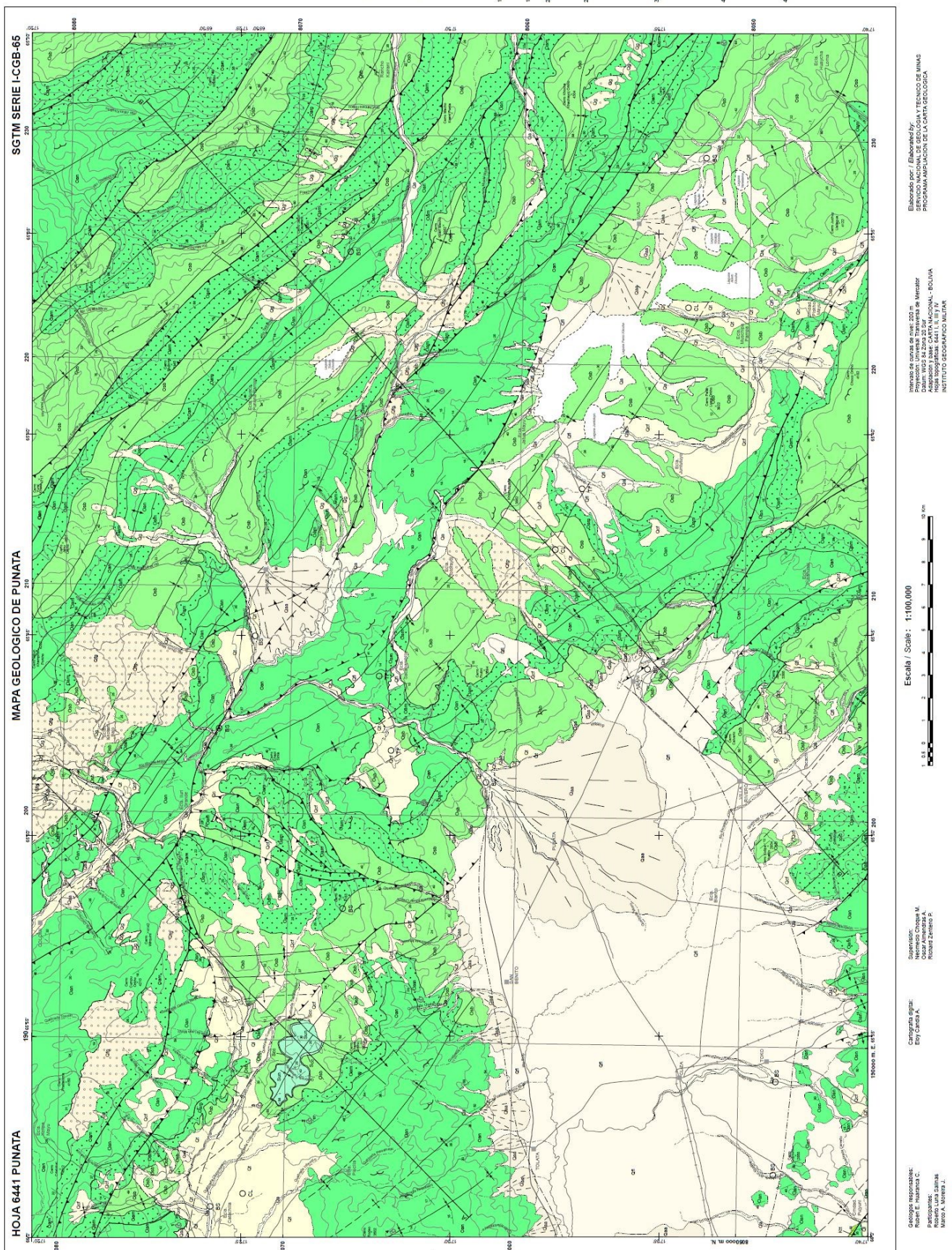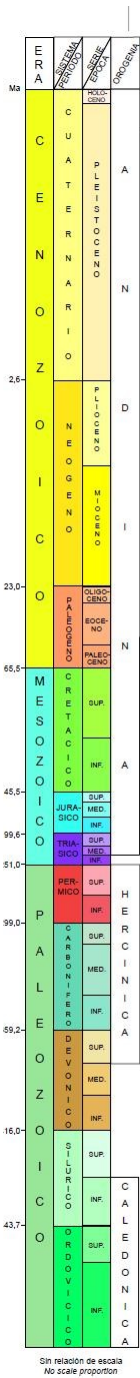
Symbol	Formation	Description
Qa	Dep. aluvial / *Aluvial dep.*	Cantos, gravas, arenas, limos y arcillas / *Pebbles, gravel, sand, silt and clay*
Qaa	Dep. de abanico aluvial / *Alluvial fan dep.*	Cantos, gravas, arenas(y limos / *Pebbles, gravel, sand and silt*
Qcf	Dep. coluvio-fluvial / *Coluvial-fluvial dep.*	Gravas, arenas, limos y arcillas / *Gravel, sand, silt and clay*
Qc	Dep. coluvial / *Coluvial dep.*	Bloques y gravas / *Boulders and gravel*
Qt	Dep. de terraza / *Terrace dep.*	Cantos, gravas, arenas, limos y arcillas / *Pebbles, gravel, sand, silt and clay*
Qfg	Dep. fluvio-glacial / *Fluvio-glacial dep.*	Gravas, arenas y arcillas / *Gravel, sand and clay*
Qg	Dep. glacial / *Glacial dep.*	Bloques, gravas y arcillas / *Boulders, gravel and clay*
Qfl	Dep. fluvio-lacustre / *Fluvio-lacustre dep.*	Gravas, arenas, limos y arcillas / *Gravel, sand, silt and clay*
Ql	Dep. lacustre / *Lacustrine dep.*	Limos, arcillas y arenas / *Silt, clay and sand*
Ktt	Fm. Toro Toro / *Toro Toro Fm.*	Conglomerados, areniscas limosas y limolitas rojizas. / *Reddish conglomerates, silt sandstones, and siltstones.*
Sun	Fm. Uncia / *Uncia Fm.*	Lutitas gris verdosas con niveles de areniscas y limolitas verde olivo / *Greenish-gray shales with beds of olive green sandstones and siltstones*
Soo	Fm. Cancañiri / *Cancañiri Fm.*	Diamictitas marrones a gris verdosas, areniscas y limolitas micáceas / *Brown to greenish-gray diamictites with sandstones and micaceous siltstones*
Osb	Fm. San Benito / *San Benito Fm.*	Cuarcitas gris claras, con capas delgadas de limolitas y lutitas / *Light gray quartzites with thin levels of siltstones and shales*
Oam	Fm. Amutara / *Amutara Fm.*	Areniscas silíceas, cuarcíticas y areniscas gris claras, con lutitas intercaladas / *Silicious sandstones, quartzites, and light gray sandstones, with intercalated shales*
Oan	Fm. Anzaldo / *Anzaldo Fm.*	Limolitas y niveles de areniscas gris verdosa a marrón claro / *Siltstones with levels of greenish-gray to light brown sandstones*

SIMBOLOS GEOLOGICOS
GEOLOGICAL SYMBOLS

Símbolo	Español	*English*
	Contacto geológico	*Geological contact*
	Inferido	*Inferred*
	Estrato conspicuo	*Conspicuous strata*
25°	Rumbo y buzamiento de estratos	*Strike and dip of bedding*
	Eje anticlinal	*Anticline axis*
	Inferido	*Inferred*
	Eje sinclinal	*Syncline axis*
	Inferido	*Inferred*
	Falla	*Fault*
	a) Inferida	*a) Inferred*
	b) inversa o de escurrimiento inferida: la dentadura indica el bloque elevado	*b) Inferred reverse or thrust: with teeth on uplifted block*
	c) lineamiento	*d) lineament*
	Fósiles	*Fossils*
	a) invertebrados	*a) Invertebrates*
	Linea de perfil geológico	*Geological cross section*

SIMBOLOS TOPOGRAFICOS
TOPOGRAPHIC SYMBOLS

Símbolo	Español	*English*
	Rio	*River*
	Rio intermitente	*Intermittent stream*
	Lago/laguna	*Lake*
3200	Curvas de nivel (con intervalo de 200 m)	*Contours (200 m interval)*
×3390	Altura o cota (m.s.n.m.)	*Elevation (m)*
	Población importante	*Village / town*
	Camino asfaltado	*Paved road*
	Camino de tierra	*Unpaved track*

LOCALIDADES FOSILIFERAS
FOSSIL LOCALITIES

SISTEMA / SYSTEM	ORDOVICICO *ORDOVICICO*		NÚMERO LOCALIDAD *LOCALITY NUMBER*							
FORMACION / *FORMATION*	Oan	Oam	1	2	3	4	5	6	7	8
FÓSILES / *FOSSILS*										
Skolithos? Isp.	x		1							
Brachiopoda Indet.	x			2						
Conularia qhichua Ulrich		x			3					
Lingula sp.	x					4				
Skolithos? Isp.	x						5			
Nautiloidea Indet.		x						6		
Lingula sp. cf. L. inomata	x								7	
Dravobinela? Sp. - Artropycus?	x									8

Oan = Fm. Anzaldo
Oam = Fm. Amutara

Fuente de información y consulta:
Source of Information and Consult

(1) HUARANCA R., J., 2011. Hoja Geológico 6441 Punata: Carta Geológica Nacional. Dirección Técnica de Geología, Servicio Nacional de Geología y Técnico de Minas.

(2) CHOQUE, N., 2010. Unidades Tectónicas de Bolivia. Dirección Técnica de Geología, Servicio Nacional de Geología y Técnico de Minas.

(3) SUÁREZ D. R. & Díaz Martínez E., 1996: Léxico Estratigráfico de Bolivia. Revista Técnica de Yacimientos Petrolíferos Fiscales Bolivianos, vol. 17.

(4) LEMA, J., & García, 1994. Hoja Geológico 6341 Cochabamba: Mapas Temáticos. Dirección Técnica de Geología, Servicio Nacional de Geología y Técnico de Minas.

(5) ORELLANA, J., PACHECO, J., Escabar, A., y Barriga, G., 1982. Mapa Geológico Punata Inédito por el Departamento de Recursos Naturales del Servicio Geológico de Bolivia GEOBOL.

(6) OLLER J. (1992): Cuadro Cronoestratigráfico de Bolivia. YPFB, Santa Cruz, Bol.

(7) SEMPERE, T., 1986. Contribución a la estratigrafía del Mesozoico boliviano en el dominio andino. Publicación Misión ORSTOM en Bolivia, La Paz.

Tidigare skrifter i serien
"Examensarbeten i Geologi vid Lunds
universitet":

446. Stevic, Marijana, 2015: Identification and environmental interpretation of microtextures on quartz grains from aeolian sediments - Brattforsheden and Vittskövle, Sweden. (15 hp)
447. Johansson, Ida, 2015: Is there an influence of solar activity on the North Atlantic Oscillation? A literature study of the forcing factors behind the North Atlantic Oscillation. (15 hp)
448. Halling, Jenny, 2015: Inventering av sprickmineraliseringar i en del av Sorgenfrei-Tornquistzonen, Dalby stenbrott, Skåne. (15 hp)
449. Nordas, Johan, 2015: A palynological study across the Ordovician Kinnekulle. (15 hp)
450. Åhlén, Alexandra, 2015: Carbonatites at the Alnö complex, Sweden and along the East African Rift: a literature review. (15 hp)
451. Andersson, Klara, 2015: Undersökning av slugtestsmetodik. (15 hp)
452. Ivarsson, Filip, 2015: Hur bildades Bushveldkomplexet? (15 hp)
453. Glommé, Alexandra, 2015: $^{87}Sr/^{86}Sr$ in plagioclase, evidence for a crustal origin of the Hakefjorden Complex, SW Sweden. (45 hp)
454. Kullberg, Sara, 2015: Using Fe-Ti oxides and trace element analysis to determine crystallization sequence of an anorthosite-norite intrusion, Älgön SW Sweden. (45 hp)
455. Gustafsson, Jon, 2015: När började plattektoniken? Bevis för plattektoniska processer i geologisk tid. (15 hp)
456. Bergqvist, Martina, 2015: Kan Ölands grundvatten öka vid en uppdämning av de utgrävda dikena genom strandvallarna på Ölands östkust? (15 hp)
457. Larsson, Emilie, 2015: U-Pb baddeleyite dating of intrusions in the south-easternmost Kaapvaal Craton (South Africa): revealing multiple events of dyke emplacement. (45 hp)
458. Zaman, Patrik, 2015: LiDAR mapping of presumed rock-cored drumlins in the Lake Åsnen area, Småland, South Sweden. (15 hp)
459. Aguilera Pradenas, Ariam, 2015: The formation mechanisms of Polycrystalline diamonds: diamondites and carbonados. (15 hp)
460. Viehweger, Bernhard, 2015: Sources and effects of short-term environmental changes in Gullmar Fjord, Sweden, inferred from the composition of sedimentary organic matter. (45 hp)
461. Bokhari Friberg, Yasmin, 2015: The paleoceanography of Kattegat during the last deglaciation from benthic foraminiferal stable isotopes. (45 hp)
462. Lundberg, Frans, 2016: Cambrian stratigraphy and depositional dynamics based on the Tomten-1 drill core, Falbygden, Västergötland, Sweden. (45 hp)
463. Flindt, Anne-Cécile, 2016: A pre-LGM sandur deposit at Fiskarheden, NW Dalarna - sedimentology and glaciotectonic deformation. (45 hp)
464. Karlatou-Charalampopoulou, Artemis, 2016: Vegetation responses to Late Glacial climate shifts as reflected in a high resolution pollen record from Blekinge, south-eastern Sweden, compared with responses of other climate proxies. (45 hp)
465. Hajny, Casandra, 2016: Sedimentological study of the Jurassic and Cretaceous sequence in the Revinge-1 core, Scania. (45 hp)
466. Linders, Wictor, 2016: U-Pb geochronology and geochemistry of host rocks to the Bastnäs-type REE mineralization in the Riddarhyttan area, west central Berglsagen, Sweden. (45 hp)
467. Olsson, Andreas, 2016: Metamorphic record of monazite in aluminous migmatitic gneisses at Stensjöstrand, Sveconorwegian orogen. (45 hp)
468. Liesirova, Tina, 2016: Oxygen and its impact on nitrification rates in aquatic sediments. (15 hp)
469. Perneby Molin, Susanna, 2016: Embryologi och tidig ontogeni hos mesozoiska fisködlor (Ichthyopterygia). (15 hp)
470. Benavides Höglund, Nikolas, 2016: Digitization and interpretation of vintage 2D seismic reflection data from Hanö Bay, Sweden. (15 hp)
471. Malmgren, Johan, 2016: De mellankambriska oelandicuslagren på Öland - stratigrafi och faciestyper. (15 hp)
472. Fouskopoulos Larsson, Anna, 2016: XRF-studie av sedimentära borrkärnor - en metodikstudie av programvarorna Q-spec och Tray-sum. (15 hp)
473. Jansson, Robin, 2016: Är ERT och

Tidsdomän IP potentiella karteringsverktyg inom miljögeologi? (15 hp)

474. Heger, Katja, 2016: Makrofossilanalys av sediment från det tidig-holocena undervattenslandskapet vid Haväng, östra Skåne. (15 hp)

475. Swierz, Pia, 2016: Utvärdering av vattenkemisk data från Borgholm kommun och dess relation till geologiska förhållanden och markanvändning. (15 hp)

476. Mårdh, Joakim, 2016: WalkTEM-undersökning vid Revingehed provpumpningsanläggning. (15 hp)

477. Rydberg, Elaine, 2016: Gummigranulat - En litteraturstudie över miljö- och hälsopåverkan vid användandet av gummigranulat. (15 hp)

478. Björnfors, Mark, 2016: Kusterosion och äldre kustdyners morfologi i Skälderviken. (15 hp)

479. Ringholm, Martin, 2016: Klimatutlöst matbrist i tidiga medeltida Europa, en jämförande studie mellan historiska dokument och paleoklimatarkiv. (15 hp)

480. Teilmann, Kim, 2016: Paleomagnetic dating of a mysterious lake record from the Kerguelen archipelago by matching to paleomagnetic field models. (15 hp)

481. Schönström, Jonas, 2016: Resistivitets- och markradarmätning i Ängelholmsområdet - undersökning av korrosiva markstrukturer kring vattenledningar. (15 hp)

482. Martell, Josefin, 2016: A study of shock-metamorphic features in zircon from the Siljan impact structure, Sweden. (15 hp)

483. Rosvall, Markus, 2016: Spår av himlakroppskollisioner - bergarter i nedslagskratrar med fokus på Mien, Småland. (15 hp)

484. Olausson, My, 2016: Resistivitets- och IP-mätningar på den nedlagda deponin Gustavsfält i Halmstad. (30 hp)

485. Plan, Anders, 2016: Markradar- och resistivitetsmätningar – undersökningar utav korrosionsförhöjande markegenskaper kring fjärrvärmeledningar i Ängelholm. (15 hp)

486. Jennerheim, Jessica, 2016: Evaluation of methods to characterise the geochemistry of limestone and its fracturing in connection to heating. (45 hp)

487. Olsson, Pontus, 2016: Ekologiskt vatten från Lilla Klåveröd: en riskinventering för skydd av grundvatten. (15 hp)

488. Henriksson, Oskar, 2016: The Dynamics of Beryllium 10 transport and deposition in lake sediments. (15 hp)

489. Brådenmark, Niklas, 2016: Lower to Middle Ordovician carbonate sedimentology and stratigraphy of the Pakri peninsula, north-western Estonia. (45 hp)

490. Karlsson, Michelle, 2016: Utvärdering av metoderna DCIP och CSIA för identifiering av nedbrytningszoner för klorerade lösningsmedel: En studie av Färgaren 3 i Kristianstad. (45 hp)

491. Elali, Mohammed, 2016: Flygsanddyners inre uppbyggnad – georadarundersökning. (15 hp)

492. Preis-Bergdahl, Daniel, 2016: Evaluation of DC Resistivity and Time-Domain IP Tomography for Bedrock Characterisation at Önneslöv, Southern Sweden. (45 hp)

493. Kristensson, Johan, 2016: Formation evaluation of the Jurassic Stø and Nordmela formations in exploration well 7220/8-1, Barents Sea, Norway. (45 hp)

494. Larsson, Måns, 2016: TEM investigation on Challapampa aquifer, Oruro Bolivia. (45 hp)

495. Nylén, Fredrik, 2017: Utvärdering av borrhålskartering avseende kalksten för industriella ändamål, File Hajdarbrottet, Slite, Gotland. (45 hp)

496. Mårdh, Joakim, 2017: A geophysical survey (TEM; ERT) of the Punata alluvial fan, Bolivia. (45 hp)